Title:

Homotopic classification of band structures: Stable, fragile, delicate, and stable representation-protected topology

+

Author(s):

Piet W. Brouwer and Vatsal Dwivedi

Document type: Preprint

Homotopic classification of band structures: Stable, fragile, delicate, and stable representation-protected topology

Piet W. Brouwer and Vatsal Dwivedi

Dahlem Center for Complex Quantum Systems and Physics Department,
Freie Universität Berlin, Arnimallee 14, 14195 Berlin, Germany

(Dated: July 26, 2023)

The topological classification of gapped band structures depends on the particular definition of topological equivalence. For translation-invariant systems, stable equivalence is defined by a lack of restrictions on the numbers of occupied and unoccupied bands, while imposing restrictions on one or both leads to "fragile" and "delicate" topology, respectively. In this article, we describe a homotopic classification of band structures — which captures the topology beyond the stable equivalence — in the presence of additional lattice symmetries. As examples, we present complete homotopic classifications for spinless band structures with twofold rotation, fourfold rotation and fourfold dihedral symmetries, both in presence and absence of time-reversal symmetry. Whereas the rules of delicate and fragile topology do not admit a bulk-boundary correspondence, we identify a version of stable topology, which restricts the representations of bands, but not their numbers, which does allow for anomalous states at symmetry-preserving boundaries, which are associated with nontrivial bulk topology.

I. INTRODUCTION

The concept of topological equivalence, combined with symmetry constraints, has been an important tool to classify gapped band structures of non-interacting fermions [1–4]. Topological gapped band structures include the quantized Hall effect, the quantum spin-Hall effect, topological insulators, and, if crystalline symmetries are imposed, topological crystalline insulators. A nontrivial topology of the band structure implies the existence of anomalous, gapless states on the sample boundary and vice versa, provided the boundary respects the symmetry constraints that are imposed on the bulk.

Various notions of topological equivalence of band structures have been employed in the literature, which differ in the possible transformations that are allowed to deform two topologically equivalent Hamiltonians into each other. The standard definition in condensed matter physics has been the "stable equivalence" [5], which allows addition of an arbitrary number of "trivial" bands which respect the symmetry requirements. This definition ensures that the topology realized in mathematical models, often consisting of only a few bands, is realized in physical systems consisting of atoms with infinitely many orbitals. Indeed, a plethora of stable topological phases [1–4], that were originally discovered theoretically, have been realized experimentally, such as the quantum Hall effect, the quantum spin Hall insulator and the three dimensional topological insulators.

A conceptually simpler, although physically less useful, definition of topological equivalence does away with the freedom to add of extra bands, resulting in "delicate" topology [6, 7]. The paradigmatic example of such a band structure is the so-called Hopf insulator [6, 8–10], realized by two-band models in three dimensions without any additional symmetries. A third intermediate possibility, which involves the freedom to add unoccupied bands while keeping the occupied subspace unchanged, results in "fragile" topology [11–14]. Nontrivial fragile topology has been invoked to explain, *e.g.*, the obstruction to the construction of real-space models for the lowest two bands of magic-angle twisted bilayer graphene [15–19]. In general, topology that is trivial according to the rules of stable topology, but nontrivial following the delicate or fragile schemes is referred to as "unstable'

The classification of stable topological phases with only local symmetries leads to the well-known "periodic table of topological insulators and superconductors" [5, 20, 21]. Stable stable topological insulators with additional crystalline symmetries have been comprehensively classified for many crystalline symmetries [22–26]. However, delicate and fragile band structures have only been identified systematically in the absence of crystalline symmetries [27] or, with crystalline symetries, using partial classifications or symmetry-specific arguments [11–14, 28–31].

In this article, we show how delicate band structures can be classified systematically using the theory of homotopy on CW complexes [32]. Similar techniques have previously been used by Moore and Balents to rederive the quantum spin Hall effect and to obtain the classification of topological insulators in three dimensions [33]. Our classification procedure is defined for a fixed number of occupied and empty bands, thereby yielding the classification of delicate topological phases. Classifications for the stable and fragile equivalence schemes naturally follow by taking the limit of a large number of conduction and/or valence bands. We illustrate the classification procedure by (re)deriving delicate classifications of spinless band structures in two and three dimensions without crystalline symmetry, and with C_2T, C_2, C_4, and D_4 symmetries, where C_n and D_n refer to n-fold rotation and dihedral symmetries and T is time-reversal. Band structures with C_2T, C_2, and C_4 symmetry have been used as paradigmatic examples of unstable topology protected by crystalline symmetries [6, 28–31, 34–37], which are systematized by our classification.

Stable topology is an essential prerequisite for the existence of anomalous gapless boundary states. This follows from elementary considerations: As the rules of fragile and delicate topology restrict the number of occupied and/or unoccupied bands, the size of the unit cell must be fixed, which requires the existence of a discrete translation symmetry in all spatial directions. Since a boundary necessarily breaks the translation symmetry, it follows that anomalous boundary states cannot exist without stable protection [38]. A more subtle route to protected gapless boundary states beyond conventional stable topology was pointed out by Song *et al.* [30], Alexandradinata *et al.* [37], and Kobayashi and Furusaki [31] for a C_4-symmetric lattice model originally proposed by Fu [39]. In this case, anomalous surface states are protected by topology that remains stable under addition of bands that are not only constrained by a symmetry, but also by its particular representation (*i.e.*, the types of orbitals). We term this *representation-protected* stable topology. Following our systematic classification, we identify such phases and the associated anomalous boundary states not only for C_4-symmetric band structures, but also for C_2 and D_4 symmetries. For the latter, the representation-protected phase is intimately linked to the existence of a two-dimensional irreducible representation of the discrete nonabelian group D_4.

Despite the absence of anomalous boundary states, unstable topology has physical relevance, first and foremost, because it may signal an obstruction to the construction of a real-space basis with localized orbitals within the available number of bands, as in the case for magic-angle twisted bilayer graphene [15–19]. Unstable topology has been shown to affect bulk physics, such as the appearance of Bloch oscillations with an extended period [40] and connected, unbounded Hofstadter butterflies in the presence of a magnetic field [41–43]. Various *boundary signatures* beyond anomalous gapless boundary states have also been proposed [44], such as a nonzero Chern number for the surface bands in the case of Hopf insulators[45, 46], boundary states for a pre-defined crystal termination [7], gap closing under twisted boundary condition [29, 47], and fractional corner charges [18, 48]. In this article, we do not venture into such manifestations of unstable topology and focus exclusively on the classification problem and the anomalous boundary states associated with various forms of stable topology.

The remainder of this article is organized as follows: In Sec. II, we describe the general classification procedure and the required mathematical background. In Sec. III we apply the classification procedure to band structures without crystalline symmetries. Section IV contains general observations concerning the classification of band structures with crystalline symmetries, which is followed by specific examples of increasing complexity: Band structures with C_2T symmetry in Sec. V, with C_2 symmetry in Sec. VI, with C_4 symmetry in Sec. VII, and with D_4 symmetry in Sec. VIII. We conclude with a discussion in Sec. IX. Various technical details of the classi-

fication procedure have been relegated to the appendices.

II. CLASSIFICATION STRATEGY

In this section, we describe the homoptopic classification for band structures with arbitrary lattice symmetries, which is based on well-established methods of algebraic topology for CW complexes. Our classification procedure is applicable to all ten Altland-Zirnbuaer classes [49]; however, to avoid overburdenening the present exposition, we restrict the explicit discussion to Bloch Hamiltonians without antisymmetry requirements, corresponding to the Altland-Zirnbauer classes A, AI, and AII. These classes include all topological crystalline insulators, but not topological superconductors or lattice models with a sublattice symmetry. In the examples of Secs. III-VIII we further restrict to symmetry classes A and AI, describing insulators with spin-rotation symmetry with and without time-reversal symmetry.

A. Stable, fragile, delicate, and representation protected topologies

We begin with some general remarks on various notions of topological equivalence for translation invariant systems, which are completely described by a finite-dimensional Bloch Hamiltonian $H(\mathbf{k})$. Two Bloch Hamiltonians $H_{1,2}$ are considered *homotopically* equivalent,

$$H_1 \sim H_2, \qquad (1)$$

if H_1 can be continuously deformed to H_2 without closing the gap or violating the symmetry constraints imposed on $H_{1,2}$. A looser notion is that of *stable* equivalence, whereby two Bloch Hamiltonians $H_{1,2}$ are considered topologically equivalent if there exists a gapped Bloch Hamiltonian H, subject to the same symmetry constraints as $H_{1,2}$, so that

$$H_1 \oplus H \sim H_2 \oplus H \qquad (2)$$

in the homotopic sense [50]. Finally, *fragile* equivalence is defined by Eq. (2) with the further constraint on H that it consist only of unoccupied bands. In mathematical terms, the problem of fragile and stable classification can be expressed as the computation of equivalence classes of vector bundles, with the equivalence being isomorphism [6, 51, 52] for the former case and isomorphism *up to Whitney sums* for the latter, which falls under the purview of topological K-theory [5]. Given a choice of a reference band structure H_{ref}, a Bloch Hamiltonian H is said to have "stable topology" if it is not equivalent to H_{ref} under stable equivalence. If H and H_{ref} are topologically equivalent under stable equivalence, but not under homotopic equivalence or vector bundle isomorphism, then H is said to possess "unstable" topology. The space of stably equivalent band structures can be endowed with

a group structure, the group operation corresponding to the direct sum of the Bloch Hamiltonians [53]. As this group operation is incompatible with the restrictions imposed by fragile and delicate topology, they do not have a similar group structure.

The rules of topological classification can be generalized by *a priori* limiting the types of orbitals and Wyckoff positions allowed, *i.e.*, restricting the band representations. Such *representation-protected* phases have been previously investigated in Refs. [30, 31, 39], whereby C_4-symmetric band structures were shown to exhibit a topological phase for arbitrary number of bands, provided one only allows p-orbitals. As in the unrestricted case, one may have delicate, fragile, and stable versions of representation-protected topological classifications. All of these are sometimes referred to in the literature as "fragile" [30, 31]; however, stable representation-protected topology exhibits many of the characteristics of conventional stable topology, such as a group structure and the existence of anomalous states at boundaries that respect the symmetry restrictions imposed on the bulk.

Our classification procedure starts by fixing the numbers n_o and n_e of occupied and unoccupied bands and thus naturally identifies all possible delicate topological phases. The fragile classification is obtained by taking the limit $n_\mathrm{e} \to \infty$ for a fixed n_o, while the stable classification is obtained when we take $n_\mathrm{o,e} \to \infty$. As our goal is to obtain a full homotopic classification, we respect symmetry-imposed obstructions between atomic-limit phases and do not follow the sometimes-used custom [54–56] to refer to all band structures that are homotopically equivalent to an atomic-limit as "trivial". To infer whether a certain homotopic equivalence class corresponds to an atomic-limit phase, one has to compare the topological invariants to the topological invariants of atomic limit phases. An exhaustive listing of atomic-limit phases for all crystalline symmetry groups has been obtained in Ref. [54] in the framework of "topological quantum chemistry".

B. Lattice symmetries and the Bloch Hamiltonian

We consider a $n \times n$ Bloch Hamiltonian $H(\mathbf{k})$ in the basis of Bloch states $|\mathbf{k}, \alpha\rangle$, which are defined as

$$|\mathbf{k}, \alpha\rangle = \sum_{\mathbf{R}} e^{i\mathbf{k}\cdot(\mathbf{R}+\mathbf{r}_\alpha)} |\mathbf{R}, \alpha\rangle. \tag{3}$$

Here, $|\mathbf{R}, \alpha\rangle$ denote the position-space basis states, with $\mathbf{R} \in \mathbb{Z}^d$ the center of the unit cell and $\alpha = 1, \ldots, n$ an index labeling a set of n orbitals at positions $\mathbf{r}_\alpha \in (-1/2, 1/2]^d$ inside the unit cell. The lattice symmetries impose constraints on $H(\mathbf{k})$, which are encoded by a representation $C(g)$ of the *reciprocal-space group* G_Λ [35] as

$$H(g\mathbf{k}) = C^\dagger(g)H(\mathbf{k})C(g), \quad g \in G_\Lambda. \tag{4}$$

The reciprocal-space group is generated by the point group and translations by reciprocal lattice vectors. The latter act nontrivially on $H(\mathbf{k})$, since our gauge choice for the Bloch states — made to ensure that the matrices $C(g)$ representing the reciprocal-space group are independent of $\mathbf{k}$ — yields a Bloch Hamiltonian that is not periodic under reciprocal lattice translations. Instead, it satisfies

$$H(\mathbf{k} + 2\pi\mathbf{e}_a) = \Lambda_a^\dagger H(\mathbf{k})\Lambda_a, \tag{5}$$

where $a \in \{x, y, z\}$ and we have set $\Lambda_a \equiv C(g_a)$, where g_a denotes translation by a reciprocal unit vector along the a-direction. Antiunitary symmetries, if present, are also included in G_Λ; however, for an antiunitary $\bar{g} \in G_\Lambda$, Eq. (4) must be replaced with

$$H(\bar{g}\mathbf{k}) = C^\dagger(\bar{g})H^*(\mathbf{k})C(\bar{g}), \quad \bar{g} \in G_\Lambda. \tag{6}$$

The precise form of the representation matrices $C(g)$ depends on which orbitals are present. The relevant information is encoded in the Wyckoff positions of the orbitals and their representations under the relevant point group symmetries, which must be considered "input data" for the homotopic classification.

In view of the symmetry constraints (4) and (6), the Bloch Hamiltonian $H(\mathbf{k})$ for all $\mathbf{k}$ can be derived from its knowledge over a subset of the full reciprocal space. Such a subset is referred to as the "irreducible Brillouin zone", the "effective Brillouin zone" [33], or the "fundamental domain" corresponding to the reciprocal-space group G_Λ [57]. By construction, no two momenta in the fundamental domain are related by a symmetry operation in G_Λ, so that, within the fundamental domain, all symmetry restrictions on $H(\mathbf{k})$ are local in $\mathbf{k}$.

Fundamental domain as a CW complex

The fundamental domain for a d-dimensional system with a given group of symmetries G_Λ can be naturally constructed in terms of "p-cells", which are homotopically equivalent to the p-dimensional cube $(0,1)^p$ for $p \geq 1$ and points for $p = 0$. Starting from a disjoint union of p-cells with $0 \leq p \leq d$, one recovers the structure of the fundamental domain by imposing a set of *gluing maps*. For each p-cell, these maps assign to its boundary a closed loop formed by q-cells of lower dimensions, which may include multiple copies of a given q-cell related by symmetry operations in G_Λ. This construction endows the fundamental domain with the structure of a *CW complex* [58] — a construct well known in the field of algebraic topology [32].

For example, in $d = 1$ with inversion symmetry, we can take the set $[0, \pi]$ as the fundamental domain, which can be constructed by gluing the two 0-cells Γ and M, which consists of the points $k = 0$ and $k = \pi$, respectively, to the ends of the 1-cell $(0, \pi)$. Further examples of the fundamental domain and its decomposition into various p-cells are shown in Fig. 1 for a three-dimensional band structure without additional crystalline symmetries and
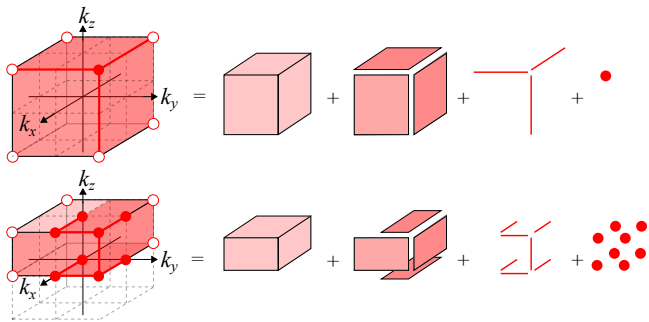
FIG. 1. Fundamental domain $\mathbb{D}$ for a three-dimensional band structure on a simple cubic lattice without (top) and with (bottom) time-reversal symmetry. Knowledge of the Bloch Hamiltonian on the fundamental domain is sufficient to determine it everywhere in the reciprocal space. Also shown is the decomposition of the fundamental domain into p-cells with $p = 0, 1, 2, 3$ (red dots, line segments, rectangles, and cuboid), endowing it with the structure of a "CW complex". Copies of 0-cells on the boundary $\partial\mathbb{D}$ that are obtained by a reciprocal lattice transformation are shown using open dots.

without (top) and with (bottom) time-reversal symmetry. For the fundamental domain shown in Fig. 1 (top), the gluing condition identifies the boundary $\partial\mathbb{D}_3$ of the 3-cell with the three 2-cells, the three 1-cells, and the single 0-cell, with each of them occuring two, four and eight times on the boundary, respectively. Similarly, in the presence of time-reversal symmetry, the boundary $\partial\mathbb{D}_3$ of the 3-cell in Fig. 1 (bottom) is identified with the four 2-cells, seven 1-cells, and eight 0-cells and with their images under translation with a reciprocal wavevector and/or time-reversal, which sends $\mathbf{k} \to -\mathbf{k}$.

We hereafter denote the fundamental domain with this additional structure by $\mathbb{D}$ and its p-dimensional subset by $\mathbb{D}_p$. The action of the reciprocal-space group G_Λ on $\mathbb{D}$ has two aspects:

1. A given p-cell α may be left invariant by a subgroup $G_\alpha \subset G_\Lambda$, which is termed its *little group*. These must be compatible with the gluing maps, in that the little groups of the q-cells $\beta \in \partial\alpha$ satisfy $G_\beta \supseteq G_\alpha$. Cells with $G_\alpha \neq 1$ are usually referred to as high-symmetry points/lines/planes.

2. If multiple copies of a q-cell β exist in the boundary $\partial\alpha$, then these copies are related by an element of the reciprocal-space group G_Λ, which is unique up to elements of the little group G_β.

Both aspects are evident in Fig. 1 (bottom): All 0-cells have a nontrivial little group isomorphic to $\mathbb{Z}_2$, generated by a combination of time-reversal and a translation by a reciprocal lattice vector, while the 1-cells have trivial little groups. Furthermore, in defining the boundary of the 2-cells, five of the seven 1-cells occur four times, whereas two of the 1-cells occur twice, with copies related by time-reversal and/or a reciprocal lattice translation. A G_Λ-symmetric Bloch Hamiltonian H can be defined abstractly as a map $H : \mathbb{D} \to \mathcal{X}$, where the target space

$\mathcal{X}$ consists of all gapped Hermitian $n \times n$ matrices. This map consists of a collection of maps $H_\alpha \colon \alpha \to \mathcal{X}_\alpha$ for each p-cell α, which are constrained by the CW-complex structure of $\mathbb{D}$. Explicitly, these maps must be compatible with the gluing map, *i.e.*, if $\beta \in \partial\alpha$, then the restriction of H_α to β is equal to H_β. Since α is an open set, we assume that the maps H_α can be continuously extended to its boundary. For instance, in Fig. 1 (top), the gluing condition implies that the maps H_β for the three 2-cells β as well as their images under a reciprocal lattice translation must coincide with H_α defined on the 3-cell α, as one approaches the respective boundaries of α.

The maps constituting the Bloch Hamiltonian satisfy further constraints, which descend from the corresponding constraints on the p-cells:

1′. The target space $\mathcal{X}_\alpha \subseteq \mathcal{X}$ consists of matrices that are invariant under the action of the little group $G_\alpha \subset G_\Lambda$, see Eqs. (4) and (6). (This property assumes a representation of G_Λ on $\mathcal{X}$, see Subsec. II B.) Consequently, the eigenstates of H_α can be labeled by the irreps of G_α. For $\beta \in \partial\alpha$, the relation between little groups $G_\beta \supseteq G_\alpha$ implies that $\mathcal{X}_\beta \subseteq \mathcal{X}_\alpha$.

2′. If two copies of β in $\partial\alpha$ are related by $g \in G_\Lambda$, then the Hamiltonian on those two copies is related by the symmetry transformation of Eq. (4) or (6).

C. Homotopic classification

We have reduced the classification problem of band structures with a given lattice symmetry to the classification of maps from a CW complex $\mathbb{D}$ to certain target spaces. The latter can be performed using the cellular decomposition of $\mathbb{D}$, starting at 0-cells and inductively working our way up to the d-cells. We refer to the classification of H_α defined on p-cells α as the "level-p topological classification". As shown below, classifications at different levels are interlinked in both directions:

1. The precise value of the topological invariants of levels $< p$ determines the allowed types of level-p topological invariants, and

2. The consideration of level-p topology yields compatibility relations constraining the topological invariants associated with all levels $\leq p$.

1. Topology at level-0: Symmetry indicators

We begin with a classification of zero-dimensional Hamiltonians, *viz*, the restriction H_S of the Bloch Hamiltonian H to the 0-cell S. H_S can be block diagonalized, with blocks corresponding to the irreps of the little group G_S. Since there are no further constraints within each block, their topological class is completely determined by

$n^S_{\mathrm{o/e},\rho} \geq 0$, the number of occupied/empty orbitals of ir-rep ρ. This can be generalized to any p-cell α, where the numbers of occupied/empty orbitals $n^\alpha_{\mathrm{o/e},\rho} \geq 0$ are well-defined for the restriction of H to α. If G_α has a single irrep, then the corresponding level-0 invariants are simply the total number of occupied/empty bands $n_{\mathrm{o/e}}$.

Together, the natural numbers $n^\alpha_{\mathrm{o/e},\rho}$ constitute the level-0 invariants, which form the semigroup $\prod_\alpha \mathbb{N}^{\nu_\alpha}$, where ν_α is the number of irreps of G_α. For a given p-cell α, if two q-cells $\beta, \beta' \in \partial\alpha$, then $\mathcal{X}_\beta, \mathcal{X}_{\beta'} \subseteq \mathcal{X}_\alpha$ and H_β and $H_{\beta'}$ are homotopically equivalent within $\mathcal{X}_\alpha$. Put differently, H_β and $H_{\beta'}$ are homotopically equivalent, when we lift the symmetry restrictions on them to G_α for any cell α connecting them. This property constrains the values level-0 invariants can take [54, 55, 59]. In particular, since all p-cells α with $p < d$ lie on the boundary of $\mathbb{D}$, the corresponding level-0 invariants satisfy

$$n_{\mathrm{o/e}} = \sum_{\rho=1}^{\nu_\alpha} \dim(\rho)\, n^\alpha_{\mathrm{o/e},\rho}, \tag{7}$$

where ν_α is the number of irreps of G_α and $\dim(\rho)$ is the dimension of the irrep ρ. Physically, this constraint expresses that the number of occupied/empty bands $n_{\mathrm{o/e}}$ must be the same throughout reciprocal space for gapped band structures. This constraint is an example of a *level-0 compatibility condition*. There may be further constraints on the level-0 invariants of a q-cell by their inclusion in a p-cells for $p < d$, which we discuss as required.

For a given band, the set of representations of the little groups G_α define a *band representation*. An arbitrary band representation can be decomposed into a direct sum of *elementary band representations* (EBRs), which can be enumerated by considering all possible orbital types localized at high-symmetry points of the lattice. A systematic study of possible band representations has been central to the partial classifications based on "symmetry-based indicators" [55, 59–63] and "topological quantum chemistry" [54, 64–66]. The full homotopic classification is thus an extension of these partial classifications.

2. Topology at levels $p > 0$

We now turn to topology associated with the p-cells for $p > 0$. We start with two observations:

- The topological class of H is always determined relative to a reference H_{ref}. The classification thus addresses *pairs* of Bloch Hamiltonians (H, H_{ref}).

- If H and H_{ref} have different invariants on level-q for any $q < p$, then they are topologicaly inequivalent. Thus, for classification on p-cells, we may assume that H and H_{ref} have identical invariants up to level $p-1$.

The latter observation implies that for a p-cell α, the restrictions of H and H_{ref} to $\partial\alpha$ can be smoothly deformed
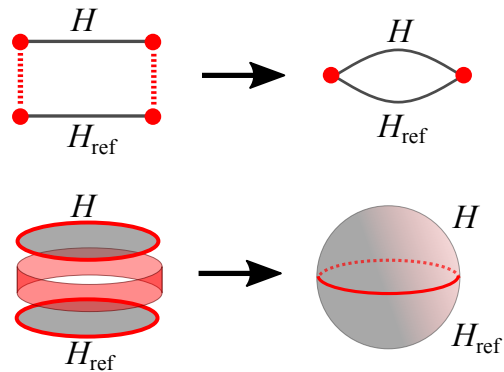

FIG. 2. For two Hamiltonians H and H_{ref} whose topological invariants on the boundary of a q-cell are identical, we can define a boundary deformations (shown in gray) that renders the two Hamiltonians equal at the boundary. One thereby obtains a Bloch Hamiltonian defined on a q-sphere, which can be classified by a homotopy group. The figure shows this procedure for $q = 1$ (top) and $q = 2$ (bottom).

into each other, and, furthermore, that this deformation can be done simultaneously for all p-cells. Choosing such a smooth deformation, the "difference" between H and H_{ref} then defines a map from the p-sphere S^p to $\mathcal{X}_\alpha$ for each p-cell α. This is illustrated in Fig. 2 for the cases $p = 1$ and $p = 2$. Such maps are classified by the homotopy spaces $K_\alpha \equiv \pi_p[\mathcal{X}_\alpha]$, which we term the *parent classification set* of the p-cell α. The full level-p parent classification set then reads

$$K_p = \prod_\alpha K_\alpha; \quad K_\alpha = \pi_p\left[\mathcal{X}_\alpha\right]. \tag{8}$$

The parent classification set K_p is, however, not the actual classifying set for equivalence classes of Bloch Hamiltonians H, because a given pair (H, H_{ref}) can yield different elements in K_p, depending on the deformation used to achieve equality of H and H_{ref} on $\partial\mathbb{D}_p$. Such elements of K_p must be identified to get a true descriptor of homotopic equivalence classes. Explicitly, any deformation used to achieve equality of H and H_{ref} on $\partial\mathbb{D}_p$ can be written as a p-dimensional "Bloch Hamiltonian" $H_\partial(\mathbf{k}_\partial, t)$, where $\mathbf{k}_\partial \in \partial\mathbb{D}_p$, $t \in [0, 1]$, and H_∂ satisfies

$$H_\partial(\mathbf{k}_\partial, 0) = H(\mathbf{k}_\partial), \quad H_\partial(\mathbf{k}_\partial, 1) = H_{\mathrm{ref}}(\mathbf{k}_\partial), \tag{9}$$

as well as symmetry constraints for each q-cell in $\partial\mathbb{D}_p$ for any t. The "difference" of two boundary deformations transforming H to H_{ref} on $\partial\mathbb{D}_p$ can be viewed as a boundary deformation that connects H_{ref} to itself, *i.e.*, with

$$H_\partial(\mathbf{k}_\partial, 0) = H_\partial(\mathbf{k}_\partial, 1) = H_{\mathrm{ref}}(\mathbf{k}_\partial). \tag{10}$$

These "boundary deformations" can be visualized as in Fig. 3, whereby one imagines that $H_\partial(\mathbf{k}_\partial, t)$ is continuously "grown" onto the band structure defined by H on α for each p-cell $\alpha \in \mathbb{D}_p$. The level-p topological invariants
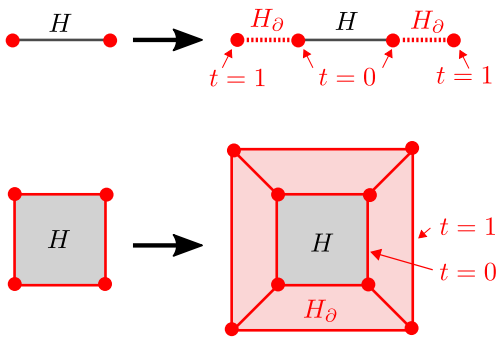
FIG. 3. Boundary deformation of a band structure $H(\mathbf{k})$ defined on a 1-cell (top) and on a 2-cell (bottom). A boundary deformation $H_\partial(\mathbf{k}_\partial, t)$, $0 \leq t \leq 1$, is continously added onto $H(\mathbf{k})$ at the boundary of the cell, such that $H(\mathbf{k})$ coincides with the reference band structure $H_{\mathrm{ref}}(\mathbf{k})$ on the cell boundary $\partial\mathbb{D}_m$ for $t = 0$ and $t = 1$ and $H(\mathbf{k})$ satisfies all symmetry constraints at each point in the transformation.

are then obtained from K_p by identification of elements related by deformations of this type.

To determine the action of boundary deformations H_∂ on the elements of K_p, it is sufficient to consider at least one boundary deformation from each topological equivalence class of boundary deformations. Considering multiple boundary deformations from the same topological class is unproblematic, because they have the same action on K_p and therefore lead to identification of the same elements. Since the domain $\partial\mathbb{D}_p \times [0, 1]$ of a boundary deformation is again a CW complex, these topological equivalence classes can be determined in the same manner as described above. It is, in fact, sufficient to only determine the corresponding parent classification set

$$K_p^\partial = \prod_{\alpha \in \partial\mathbb{D}_p} \pi_{r_\alpha}[\mathcal{X}_\alpha], \qquad (11)$$

where $r_\alpha = \dim \alpha + 1$. This is because the parent classification set K_p^∂ is "overcomplete", so that considering one boundary deformation from each class in K_p^∂ ensures that *at least* one boundary transformation from each (true) topological class is considered. Only having to determine K_p^∂ leads to a substantial simplification by avoiding having to deal with "boundary transformations of boundary transformations". For the reader that is nevertheless interested in obtaining the exact boundary classification set, we review a recursive procedure in Appendix C.

There are additional constraints on the (parent) topological invariants, which arise from the fact that the individual cells are contractible. For any $(p + 1)$-cell α with $1 \leq p \leq d - 1$, the boundary $\partial\alpha$ can thus be continuously deformed to a point within α. Consequently, the topology of any Bloch Hamiltonian H restricted to $\partial\alpha$, evaluated with respect the (larger) target space $\mathcal{X}_\alpha \supseteq \mathcal{X}_\beta$ for $\beta \in \partial\alpha$, must be trivial. This implies that the "sum" of level-p invariants for p-cells $\beta \in \partial\alpha$ must vanish. We term these conditions — one for each $(p + 1)$-cell — the

level-p compatibility conditions. Since this sum over level-p invariants may also depend on topological invariants at levels $q < p$, the level-p compatibility conditions may affect invariants at all levels $q \leq p$. The compatibility condition equally apply to the boundary deformations and their parent classification K_p^∂.

To summarize, the topological invariants at all levels $0 \leq p \leq d$, modulo the ambiguities associated with boundary deformations, and constrained by the compatibility relations at all levels, constitute the complete classification of the d-dimensional systems. The compatibility relations ensure that for each set of topological invariants there is a gapped band structure with these invariants, while the robustness to boundary deformations ensures that the topological invariants can be uniquely associated with a gapped band structure. The classification naturally has a hierarchical reciprocal-space structure [6], since the classification at level-p depends on the invariants at all lower level, starting with the symmetry based indicators at level-0.

D. Target spaces

We now discuss the various target spaces $\mathcal{X}$ that arise in the classification for symmetry classess A, AI, and AII and describe their homotopy groups.

1. Grassmannians and their topology

We are interested in the space of $n \times n$ Hermitian matrices with a fixed number of occupied and empty bands (*i.e.*, negative and positive eigenvalues) $n_{\mathrm{o/e}}$ satisfying

$$n = n_{\mathrm{o}} + n_{\mathrm{e}}. \qquad (12)$$

For a topological classification, $H(\mathbf{k})$ may be replaced by a Hermitian matrix with a "flattened spectrum" by deforming all positive/negative eigenvalues to ± 1, so that $H(k)$ is unitarily equivalent to $\mathrm{diag}\{\mathbb{1}_{n_{\mathrm{e}}}, -\mathbb{1}_{n_{\mathrm{o}}}\}$. The space of such Hamiltonians is the *complex Grassmannian* $\mathrm{Gr}_{\mathbb{C}}(n_{\mathrm{o}}, n_{\mathrm{e}})$, which is a manifold that parametrizes n_{o}-dimensional (or equivalently, n_{e}-dimensional) complex planes in $\mathbb{C}^n$ (see App. D for more details). We also encounter Bloch Hamiltonians $H(\mathbf{k})$ with real ($\mathbb{R}$) or quaternion ($\mathbb{H}$) entries, for which the target space is the corresponding Grassmannian $\mathrm{Gr}_{\mathbb{R}}(n_{\mathrm{o}}, n_{\mathrm{e}})$ or $\mathrm{Gr}_{\mathbb{H}}(n_{\mathrm{o}}, n_{\mathrm{e}})$, respectively. These three spaces constitute the top-level target spaces $\mathcal{X}$ for the symmetries considered here.

For a p-cell α with a nontrivial little group G_α, the target spaces $\mathcal{X}_\alpha \subseteq \mathcal{X}$ can be written as a product of Grassmannians. This is because the eigenstates of H restricted to α can be labeled with irreps ρ of G_α, so that after a spectral flattening, we get

$$\mathcal{X}_\alpha = \prod_\rho \mathrm{Gr}_{\mathbb{F}_\rho}\left(n_{\mathrm{o},\rho}^\alpha, n_{\mathrm{e},\rho}^\alpha\right), \qquad (13)$$

where ρ runs over the irreps of G_α and $\mathbb{F}_\rho$ is a number field, which, depending on ρ, may be $\mathbb{C}$, $\mathbb{R}$, or $\mathbb{H}$. The latter two occur only if G_α contains antiunitary symmetries. Since we are interested in $\pi_p[\mathcal{X}_\alpha]$ and the homotopy of a product of spaces satisfies

$$\pi_k\Big[\prod_\alpha X_\alpha\Big] = \prod_\alpha \pi_k[X_\alpha], \qquad (14)$$

we only need to compute $\pi_p[\mathrm{Gr}_\mathbb{F}(n_\mathrm{o}, n_\mathrm{e})]$.

Homotopy groups of Grassmannians have been extensively studied in the mathematical literature. Their computation is briefly outlined in Appendix D. We, however, make two general observations here:

- $\pi_p[\mathrm{Gr}_\mathbb{F}(n_\mathrm{o}, n_\mathrm{e})] = 0$ for all $p > 0$ if $n_\mathrm{o} = 0$ or $n_\mathrm{e} = 0$, since in that case, $\mathrm{Gr}_\mathbb{F}(n_\mathrm{o}, n_\mathrm{e})$ degenerates to a single point.

- $\pi_p[\mathrm{Gr}_\mathbb{F}(n_\mathrm{o}, n_\mathrm{e})]$ becomes independent of n_o and n_e ("stabilizes") once n_o and n_e are large enough, which typically means $n_\mathrm{o/e} \gtrsim p$.

As to the former observation, while $n_\mathrm{o,e} > 0$ for gapped band structure, $\mathrm{Gr}_\mathbb{F}(n_\mathrm{o}, n_\mathrm{e})$ with $n_\mathrm{o} = 0$ or $n_\mathrm{e} = 0$ may occur in individual symmetry sectors at high-symmetry manifolds. The latter observation forms the basis for the classification of "stable" topology.

The homotopy invariants of Grassmannians can often be expressed in terms of Wilson lines or loops [67, 68]. Given a path γ in the reciprocal space, the Wilson line $W^{\mathrm{o/e}}(\gamma) \in \mathrm{U}(n)$ can be associated with the occupied/empty bands and encodes the evolution of the corresponding subspaces under parallel transport along γ. Wilson lines are not gauge invariant, since they depend on the choice of basis at the end points of γ. They are unambiguously defined only if there are additional constraints on the end points of γ that fix the basis or if the path γ is a closed loop. A local-in-$\mathbf{k}$ symmetry on $H(\mathbf{k})$ implies a restriction on Wilson lines/loops; in particular, if the Hamiltonian is restricted by symmetries to be real- or quaternion-valued, then they are restricted to $\mathrm{O}(n)$, $\mathrm{Sp}(n) \subset \mathrm{U}(n)$, respectively.

2. Topological invariants for complex Grassmannians

We now discuss the nontrivial topological invariants associated with complex Grassmannians, which are summarized in Table. I.

$\pi_2[\mathrm{Gr}_\mathbb{C}(n_\mathrm{o}, n_\mathrm{e})]$ — These stabilize to $\mathbb{Z}$ for all $n_\mathrm{o/e} > 0$, with the corresponding invariant being the Chern number C. For a complex Hamiltonian, $\det W^{\mathrm{o/e}}(\gamma)$ is a phase factor, *i.e.*, it is defined on the unit circle. To define the Chern number, we take a family of Wilson loops $W^{\mathrm{o/e}}(\gamma_t)$ with $t \in [0, 1]$ and $\gamma_0 = \gamma_1$ so that the γ_t cover the two-sphere S^2 precisely once, in a manner compatible with the orientation of S^2. The Chern number C is then equal to the winding number of $\det(W^{\mathrm{o}}(\gamma_t))$ for $0 \le t \le 1$. As

d	Bands	Topological Invariant	
1	—		—
2	—	$\mathbb{Z}$	Chern number C
3	$n_\mathrm{o}, n_\mathrm{e} = 1$	$\mathbb{Z}$	Hopf invariant H
	$n_\mathrm{o} + n_\mathrm{e} > 2$		—

TABLE I. Topological invariants associated with complex Grassmannians $\mathrm{Gr}_\mathbb{C}(n_\mathrm{o}, n_\mathrm{e}) \cong \mathrm{Gr}_\mathbb{C}(n_\mathrm{e}, n_\mathrm{o})$.

the total Chern number of a set of bands must vanish, the Chern number of the unoccupied bands equals $-$C.

$\pi_3[\mathrm{Gr}_\mathbb{C}(n_\mathrm{o}, n_\mathrm{e})]$ — The only nontrivial case occurs for $n_\mathrm{o} = n_\mathrm{e} = 1$, with the topological invariant being the $\mathbb{Z}$-valued Hopf invariant. This arises from the fact that $\mathrm{Gr}_\mathbb{C}(1, 1) \cong S^2$, so that its third homotopy group $\pi_3(S^2) \cong \mathbb{Z}$ is generated by the Hopf map. We refer to App. E for more details.

3. Topological invariants for real Grassmannians

The nontrivial topological invariants associated with real Grassmannians are summarized in Table. II. These exhibit multiple low-dimensional exceptions.

$\pi_1[\mathrm{Gr}_\mathbb{R}(n_\mathrm{o}, n_\mathrm{e})]$ — These groups stabilize to $\mathbb{Z}_2$ for $n_\mathrm{o/e} > 1$, with the corresponding topological invariant being the *first Stiefel-Whitney invariant* SW_1. To define this invariant, we note that the Wilson loops are orthogonal matrices if the Hamiltonian is real, so that $\det W^{\mathrm{o/e}}(\gamma) \in \{\pm 1\}$ for any closed loop γ. The first Stiefel-Whitney invariant is defined as [69]

$$\mathrm{SW}_1 \equiv \mathrm{sgn}\left(\det W^{\mathrm{o/e}}(\gamma)\right). \qquad (15)$$

As the total set of bands must be topologically trivial, SW_1 may be calculated either from the occupied or from the empty bands. Since $W^{\mathrm{o/e}}(\gamma) \in \mathrm{O}(n_\mathrm{o/e})$ encodes the basis transformation of the occupied/empty subspace under parallel transport along γ, a nontrivial SW_1 represents an obstruction to defining an orientation of these subspaces continuously along γ.

For $n_\mathrm{o} = n_\mathrm{e} = 1$, this $\mathbb{Z}_2$ classification can be refined to a $\mathbb{Z}$ classification. To see this, we note that after flattening the spectrum, a gapped real 2×2 Hamiltonian can be written as

$$H(\mathbf{k}) = \cos\theta_\mathbf{k}\, \sigma_1 + \sin\theta_\mathbf{k}\, \sigma_3, \qquad (16)$$

where σ_j are the Pauli matrices. Thus, for any closed path in the reciprocal space, $\mathbf{k} \mapsto \theta_\mathbf{k}$ defines a map from S^1 to S^1. Such maps are classified by a winding number $\mathrm{Eu}_1 \in \pi_1[S^1] \cong \mathbb{Z}$, termed the *first Euler class*. The sign of the Euler class depends on a choice of orientation for $\mathrm{Gr}_\mathbb{R}(1, 1)$, since a unitary transformation can flip the sign of σ_1, thereby flipping the sign of Eu_1 [28]. Thus, in

d			Topological invariant(s)	
1	$n_\mathrm{o}, n_\mathrm{e} = 1$	$\mathbb{Z}$	1st Euler invariant Eu_1	
	$n_\mathrm{o}, n_\mathrm{e} > 1$	$\mathbb{Z}_2$	1st Stiefel-Whitney invariant SW_1	
2	$n_\mathrm{o}, n_\mathrm{e} = 1$	—	—	
	$n_\mathrm{o} = 1,$ $n_\mathrm{e} = 2$	$2\mathbb{Z}$	2nd Euler invariant Eu_2^o	
	$n_\mathrm{o} = 2,$ $n_\mathrm{e} = 1$	$2\mathbb{Z}$	2nd Euler invariant Eu_2^e	
	$n_\mathrm{o}, n_\mathrm{e} = 2$	$\mathbb{Z}^2\vert_\mathrm{p}$	2nd Euler invariants $(\mathrm{Eu}_2^\mathrm{o}, \mathrm{Eu}_2^\mathrm{e})$ satisfying $\mathrm{Eu}_2^\mathrm{o} + \mathrm{Eu}_2^\mathrm{e} = 0 \mod 2$	
	$n_\mathrm{o} = 2,$ $n_\mathrm{e} > 2$	$\mathbb{Z}$	2nd Euler invariant Eu_2^o	
	$n_\mathrm{o} > 2,$ $n_\mathrm{e} = 2$	$\mathbb{Z}$	2nd Euler invariant Eu_2^e	
	$n_\mathrm{o}, n_\mathrm{e} > 2$	$\mathbb{Z}_2$	2nd Stiefel-Whitney invariant SW_2	

TABLE II. Topological invariants associated with real Grassmannians $\mathrm{Gr}_\mathbb{R}(n_\mathrm{o}, n_\mathrm{e}) \cong \mathrm{Gr}_\mathbb{R}(n_\mathrm{e}, n_\mathrm{o})$. The $\mathbb{Z}$-valued invariants are defined only up to a sign ambiguity if the Grassmannian does not have a preferred orientation. The set $\mathbb{Z}^2\vert_\mathrm{p}$ consists of all ordered integer pairs (p, q) with $p = q \mod 2$.

absence of a preferred orientation, Eu_1 is defined only up to a sign, so that the space of topological invariants is $\mathbb{N}$ (instead of $\mathbb{Z}$). The first Euler invariant is related to the first Stiefel-Whitney invariant as

$$\mathrm{SW}_1 = \mathrm{Eu}_1 \mod 2. \tag{17}$$

$\pi_2[\mathrm{Gr}_\mathbb{R}(n_\mathrm{o}, n_\mathrm{e})]$ — These groups stabilize to $\mathbb{Z}_2$ for $n_\mathrm{o/e} > 2$, with the corresponding topological invariant being the *second Stiefel-Whitney invariant* SW_2. If $n_\mathrm{o/e} = 2$, the corresponding invariants are the *second Euler invariants* $\mathrm{Eu}_2^\mathrm{o/e}$. To define these invariants, we consider a one-parameter family of Wilson loops $W^\mathrm{o/e}(\gamma_t) \in \mathrm{O}(n_\mathrm{o/e})$, where $t \in [0, 1]$ such that $\gamma_0 = \gamma_1$ and the γ_t cover the two-sphere S^2 precisely once, in a matter compatible with its orientation. Such a family of Wilson loops defines a closed curve in $\mathrm{O}(n_\mathrm{o/e})$. For $n_\mathrm{o/e} = 2$, one associates an integer-valued winding number $\mathrm{Eu}_2^\mathrm{o/e}$ with such a closed loop, since 2×2 orthogonal matrices are parameterized by a single phase variable. For $n_\mathrm{o/e} > 2$ the winding number is only defined mod 2, with the parity being the $\mathbb{Z}_2$-valued second Stiefel-Whitney number $\mathrm{SW}_2^\mathrm{o/e}$ [69].

Since the combination of all bands must be topologically trivial, one has $\mathrm{SW}_2^\mathrm{o} = \mathrm{SW}_2^\mathrm{e}$, so that one may write SW_2 instead of SW_2^o and SW_2^e. The second Euler and Stiefel-Whitney invariants (if defined) further satisfy the parity constraint

$$\mathrm{Eu}_2^\mathrm{o} = \mathrm{Eu}_2^\mathrm{e} = \mathrm{SW}_2 \mod 2, \tag{18}$$

If $n_\mathrm{o} = 1$ or $n_\mathrm{e} = 1$, continuity enforces that $W^\mathrm{o}(\gamma_t) = 1$ or $W^\mathrm{e}(\gamma_t) = 1$ for all $t \in [0, 1]$, respectively, so that SW_2

must be trivial and Eu_2^e or Eu_2^o, if defined, must be even. The sign of Eu_2^o and Eu_2^e depends on the orientation of the basis of $\mathrm{Gr}_\mathbb{R}(n_\mathrm{o}, n_\mathrm{e})$. If this orientation is not fixed, then Eu_2^o and Eu_2^e have a sign ambiguity, which is a joint sign ambiguity if both Eu_2^o and Eu_2^e are defined. In this case the classifying space reduces to $\mathbb{N}$ and $\mathbb{N} \times \mathbb{Z}\vert_\mathrm{p}$, respectively, where $\mathbb{N} \times \mathbb{Z}\vert_\mathrm{p}$ consists of all ordered integer pairs (p, q) with $p \geq 0$ and $p = q \mod 2$.

4. Topological invariants for symplectic Grassmannians

The first two homotopy groups of the symplectic Grassmannians are trivial,

$$\pi_1[\mathrm{Gr}_\mathbb{H}(n_\mathrm{o}, n_\mathrm{e})] = \pi_2[\mathrm{Gr}_\mathbb{H}(n_\mathrm{o}, n_\mathrm{e})] = 0. \tag{19}$$

E. Topology and bulk-boundary correspondence

Band structures with nontrivial stable topology in d dimensions exhibit anomalous gapless boundary states on $(d-1)$-dimensional boundaries that respect all symmetries — a phenomenon known as the "bulk-boudary correspondence" [1–4]. In this context, a boundary mode is called "anomalous" if it cannot be realized by any $(d-1)$-dimensional lattice model that respects all the symmetries. Of the three types of topological classification — based on delicate, fragile, and stable equivalence — only the first allows for anomalous boundary states as a signature of the bulk topology. This, however, also includes the representation protected topological phases (defined in Sec. II A), provided the boundary respects the symmetry as well as the representation constraints.

Our classification procedure can also be used to classify anomalous gapless states at a symmetry-preserving boundary. To this end, we first enumerate the possible gapless phases consistent with given symmetries by looking for all possible violations of the compatibility conditions in $d - 1$ dimensions. Such violations indicate gapless phases, since a level-p compatibility condition follows from the contractibility of a $(p + 1)$-cell α, so that its a violation implies that $H_\alpha : \alpha \to \mathcal{X}_\alpha$ is defined only for a noncontractible subset of α, *i.e.*, the Bloch Hamiltonian is gapless somewhere on α. A gapless $(d-1)$-dimensional Bloch Hamiltonian H is anomalous if it necessarily violates a constraint imposed on the topological invariants by a gluing condition or by symmetry. We illustrate this classification scheme for anomalous boundary states by deriving some well known examples in the next section.

III. CLASSIFICATION WITHOUT CRYSTALLINE SYMMETRIES

We first apply our classification strategy to band structures without additional crystalline symmetries. Since
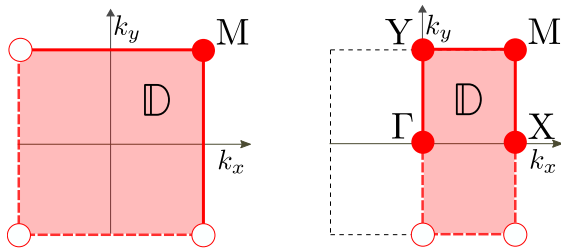
FIG. 4. Fundamental domain of a band structure on a square lattice, without (left) or with (right) time-reversal symmetry, but without additional crystalline symmetries. In the latter case, two of the 0-cells and all 1-cells occur twice in $\partial \mathbb{D}$.
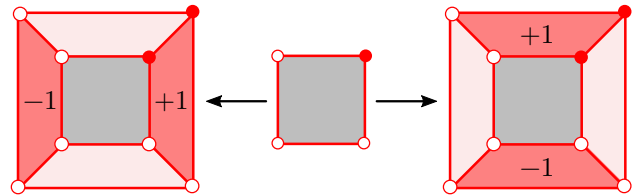

FIG. 5. Generators of the boundary deformations at the boundary of a 2-cell for a band structure without time-reversal symmetry and without additional crystalline symmetries. Periodicity of the Bloch Hamiltonian in reciprocal space forces that the net Chern number associated with the boundary deformation is zero. Hence, a boundary deformation cannot change the Chern number associated with the 2-cell.

these classification results are well known, this section mainly serves as an illustration of our classification scheme following the more abstract discussion of Sec. II.

A. Classification without time-reversal symmetry

In the absence of time-reversal symmetry (symmetry class A), the fundamental domain is the entire Brillouin zone, which can be decomposed into cells as shown in the left column of Fig. 4 and Fig. 1 in two and three dimensions, respectively. The topological invariants for the unique 0-cell are the numbers of occupied and unoccupied bands $n_{o/e}$. The level-0 topological invariant is thus the pair $(n_o, n_e) \in \mathbb{N}^2$. The target space $\mathcal{X}$ for all cells is

$$\mathcal{X} = \text{Gr}_{\mathbb{C}}(n_o, n_e). \tag{20}$$

We can now read off the parent topological invariants from Tab. I.

There are no level-1 invariants, since the first homotopy group of complex Grassmannians is always trivial. At level-2, the parent classification set is $K_1 = \pi_2[\mathcal{X}] \cong \mathbb{Z}$ and the corresponding topological invariant is the $\mathbb{Z}$-valued Chern number C. To get the true topological invariant, however, we need to check if it is robust to deformations at the boundary of a 2-cell. As discussed in Sec. II C, the parent classification set of boundary deformations K_2^∂ is generated by deformations along the 0-cells and the 1-cells, whose equivalence classes are parametrized by $\pi_1[\mathcal{X}] = 0$ and $\pi_2[\mathcal{X}] \cong K_2 \cong \mathbb{Z}$, respectively. Thus, boundary deformations may carry a nonzero Chern number along a 1-cell on $\partial \mathbb{D}$. However, since each 1-cell occurs twice in $\partial \mathbb{D}$ and the corresponding deformations carry opposite Chern numbers (see Fig. 5), the net Chern number of any boundary deformation is zero, rendering the parent Chern number robust. This argument applies for each 2-cell in the fundamental domain, so that the level-2 invariants are the single Chern number C in 2d and three Chern numbers $C_{x,y,z}$ in 3d.

At level-3, the parent invariant is the $\mathbb{Z}$-valued Hopf invariant H if $n_o = n_e = 1$ [8]. The boundary deformations in K_3^∂ depend on the three level-2 invariants

	Bands	Topological invariant
Level 1	—	—
Level 2	—	$C_x, C_y, C_z \in \mathbb{Z}$
Level-3	$n_o = n_e = 1$	if $C_x = C_y = C_z = 0$, then $H \in \mathbb{Z}$ else: $H \in \mathbb{Z}_{2C}$, where $C \equiv \gcd(C_x, C_y, C_z)$
	$n_o + n_e > 2$	—

TABLE III. Homotopic classification of gapped band structures with broken time-reversal symmetry and no additional crystalline symmetries.

$C_{x,y,z}$ [10]. There are six generators of the boundary deformations: Three carry unit Chern number associated with segments along one of the three 1-cells and its three images under translation by a reciprocal lattice vector and three carry unit Hopf number associated with segments along one of the three 2-cells and its image under translation by a reciprocal lattice vector. Because of the periodicity constraint in reciprocal space, the latter leave the Hopf number H invariant, while the former change H by $2C_\alpha$, $\alpha = x, y, z$ (see App. E for details). The minimum change to H one may thus obtain is $2\gcd(C_x, C_y, C_z)$, where "gcd" denotes the greatest common divisor. Hence, H is well defined up to multiples of $2\gcd(C_x, C_y, C_z)$, so that the level-3 invariant is $\mathbb{Z}$–valued if $C_x = C_y = C_z = 0$ and $\mathbb{Z}_{2C}$–valued otherwise, where $C \equiv \gcd(C_x, C_y, C_z)$.

These classification results are summarized in Tab. III.

B. Classification with time-reversal symmetry

1. Symmetry class AI (spinless fermions)

In the presence of time-reversal and spin-rotation symmetry, the Bloch Hamiltonian satisfies

$$H(\mathbf{k}) = H^*(-\mathbf{k}). \tag{21}$$

The fundamental domain is half the Brillouin zone, which can be decomposed as shown in Fig. 4 and Fig. 1 for two and three dimensions, respectively. The level-0 invariants are given by the number of occupied/empty bands $n^S_{\mathrm{o/e}}$ for each 0-cell S. Since $n_{\mathrm{o/e}}$ must be constant throughout the Brillouin zone for a gapped Hamiltonian, one has $n^S_{\mathrm{o/e}} = n_{\mathrm{o/e}}$ for all S, leading to a single pair of level-0 invariants $(n_{\mathrm{o}}, n_{\mathrm{e}}) \in \mathbb{N}^2$. At the 0-cells S, time-reversal symmetry constraints the Hamiltonian H_S to be real-valued, so that the corresponding target spaces are

$$\mathcal{X}_S = \mathrm{Gr}_{\mathbb{R}}(n_{\mathrm{o}}, n_{\mathrm{e}}), \tag{22}$$

For the p-cells with $p > 0$, we have $\mathcal{X} = \mathrm{Gr}_{\mathbb{C}}(n_{\mathrm{o}}, n_{\mathrm{e}})$. Thus, beyond level-0, the *parent topological invariant* for individual p-cells are identical to the symmtry class A, *i.e.*, no invariants at level 1, a $\mathbb{Z}$-valued Chern number for each 2-cell at level-2 and a $\mathbb{Z}$-valued Hopf invariant at level-3 if $n_{\mathrm{o}} = n_{\mathrm{e}} = 1$.

At level-2, the parent classification set of boundary deformations K^{∂}_2 consists of a copy of $\pi_1[\mathcal{X}_S]$ for each 0-cell and $\pi_2[\mathcal{X}] = \mathbb{Z}$ for the 1-cells. The former homotopy set is nontrivial for each 0-cell, and since the 0-cells Γ and X occur only once in $\partial\mathbb{D}$, a boundary deformation that is topologically nontrivial at one of these can change the Chern number by an arbitrary integer. In App. F, we construct such a deformation explicitly as well as present another argument for the existence of such a boundary deformation. Thus, in contrast to symmetry class A, there are no level-2 topological invariants for symmetry class AI. Similarly, at level-3, there exists a boundary deformation that changes the Hopf number H of the parent classification by one, as shown in Appendix E, rendering the level-3 invariant trivial.

2. Symmetry class AII (spinful fermions)

In the presence of time-reversal symmetry without spin-rotation symmetry, the Hamiltonian satisfies

$$H(\mathbf{k}) = \Sigma_2 H^*(-\mathbf{k})\Sigma_2, \tag{23}$$

where $\Sigma_2 = \mathbb{1}_n \otimes \sigma_2$ is the time-reversal operator and $2n$ is the total number of bands. Kramers degeneracy implies that the number of occupied and unoccupied bands must be even, so that the level-0 invariants $(n^S_{\mathrm{o}}, n^S_{\mathrm{e}})$ are *half* the number of occupied/empty bands. The level-0 compatibility condition is $n_{\mathrm{o/e}} = n^S_{\mathrm{o/e}}$, where $2n_{\mathrm{o/e}}$ are the total number of filled/empty bands.

To derive the target space $\mathcal{X}_S$, we note that at the high symmetry points, time-reversal implies that the Hamiltonian can be written as

$$H_S = h_0 \otimes \sigma^0 + h_j \otimes \mathrm{i}\sigma^j, \tag{24}$$

where h_0 and h_j are real-valued $n \times n$ symmetric and antisymmetric matrices, respectively. Since the set of 2×2
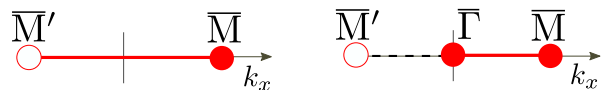

FIG. 6. Fundamental domain of a one-dimensional band structure, without (left) or with (right) time-reversal symmetry, and without additional crystalline symmetries.

conplex matrices $\{\sigma^0, \mathrm{i}\sigma^1, \mathrm{i}\sigma^2, \mathrm{i}\sigma^3\}$ constitute a representation of the quaternion algebra, H_S in Eq. (24) can be interpreted as a quaternion-valued matrix. The target space $\mathcal{X}_S$ is thus a quaternionic Grassmannian

$$\mathcal{X}_S = \mathrm{Gr}_{\mathbb{H}}(n_{\mathrm{o}}, n_{\mathrm{e}}). \tag{25}$$

For p-cells with $p > 0$, we have $\mathcal{X} = \mathrm{Gr}_{\mathbb{C}}(2n_{\mathrm{o}}, 2n_{\mathrm{e}})$.

The topological classification proceeds as for the symmetry class AI, with one important difference: While considering the boundary deformations to level-2 invariants, $\pi_1[\mathcal{X}_S] = 0$ for the quaternionic Grassmannian, so that there are no nontrivial deformations at the 0-cells. The boundary deformations at 1-cells can carry a Chern number. These cancel for the two copies of YM, but add up for the two copies of ΓY and MX, so that boundary deformations may add an even integer to the Chern number of the 2-cell. This renders the level-2 invariant $\mathbb{Z}_2$-valued. Thus, at level-2, we get one and four $\mathbb{Z}_2$-valued invariants for $d = 2$ and $d = 3$, respectively [33]. These are the well-known classifications of the quantum spin-Hall effect and of three-dimensional topological insulators [33, 70–73].

C. Anomalous boundary states

In the symmetry class A, anomalous boundary states are associated with a nontrivial value of the only stable invariant, *viz*, the Chern number. In two dimensions, these are the chiral edge states of the quantum Hall effect, while in three dimensions, these are chiral surface states of a weak Chern insulator. We now derive these invariants from a boundary perspective.

Consider a 1d Bloch Hamiltonian in symmetry class A, whose fundamental domain is the entire 1d Brillouin zone, as shown in Fig. 6 (left). We assume that H is gapped at the 0-cells, so that the level-0 invariants $n^{\bar{S}}_{\mathrm{o/e}}$ are well defined for $\bar{S} \in \{\overline{\mathrm{M}}, \overline{\mathrm{M}}'\}$. The presence of a chiral state crossing the Fermi level implies that the level-0 invariants $n^{\overline{\mathrm{M}}}_{\mathrm{o/e}} \neq n^{\overline{\mathrm{M}}'}_{\mathrm{o/e}}$, which violates both the compatibility condition and the gluing condition. The former violation signifies that a band structure with a chiral state crossing the Fermi level is necessarilty gapless, while the latter violation signals that such a band structure is anomalous, *i.e.*, it can not be realized in a one-dimensional lattice model [74]. An analogous argument holds for a chiral band crossing the Fermi energy in 2d.

In symmetry class AI, there is no nontrivial bulk topology and, hence, there are no associated anomalous

boundary states. The same conclusion can be obtained from a boundary perspective. To wit, the fundamental domain of a 1d Bloch Hamiltonian in symmetry class AI is half the 1d Brillouin zone, as shown in Fig. 6 (right). A band crossing between $\overline{\Gamma}$ amd $\overline{M}$ violates the level-0 compatibility condition for the $n_{o/e}^{\bar{S}}$ for $\bar{S} \in \{\overline{\Gamma}, \overline{M}\}$ — signalling a gapless phase — but it does not imply the violation of a gluing condition, so that such a band crossing is not anomalous. Instead, time-reveral symmetry imposes the presence of two opposite crossings of the Fermi energy in the full boundary Brillouin zone, which can be realized in a 1d lattice model and which may deformed to a gapped Hamiltonian. Thus, there are no anomalous boundary modes in symmetry class AI.

In symmetry class AII, anomalous boundary modes are associated with the $\mathbb{Z}_2$-valued stable invariant. In two dimensions, these are the helical edge states of the quantum spin Hall effect, while in three dimensions, these are the surface Dirac cones of a strong topological insulator. In this case, the fundamental domain is identical to that of symmetry class AI (Fig. 6), but the level-0 invariants $n_{o/e}^{\bar{S}}$ are *half* the number of occupied/unoccupied bands. Thus, if a chiral mode crosses the Fermi level between $\overline{\Gamma}$ and $\overline{M}$, then the total number of occupied/empty bands differ by an odd integer, which is incompatible with the level-0 invariants being integers, rendering such crossings anomalous. Application of a similar arguments to any pair of high-symmetry points in the surface Brillouin zone indicates the existence of anomalous surface states for 3d topological insulators [33, 72, 73].

IV. CLASSIFICATION IN THREE DIMENSIONS WITH CRYSTALLINE SYMMETRIES: GENERAL REMARKS

In the next sections, we apply the classification strategy of Sec. II to band structures with C_2T, C_2, C_4, and D_4 symmetries. Since these symmetries are all two-dimensional and include a rotation, in two dimensions they do not exhibit a boundary that is invariant under the symmetries; however, they all exhibit invariant planes in three dimensions, which may host anomalous boundary states. We thus consider a simple-cubic lattice with unit lattice constant, with the rotation axis (and mirror planes for D_4) parallel to the z-axis. For the crystalline symmetries considered in this article, this simplification does not affect our conclusions. Since C_2 is an element of all of these groups, for the time-reversal-symmetric case, we choose a basis such that C_2T is represented by the identity matrix, so that

$$H(k_x, k_y, k_z) = H^*(k_x, k_y, -k_z). \qquad (26)$$

For $k_z = 0, \pi$ (and for 2d systems), this reduces to a reality condition on $H(\mathbf{k})$.

The fundamental domain in all such cases is a prism with the two-dimensional fundamental domain as the

base and $k_z \in (-\pi, \pi]$ without and $k_z \in [0, \pi]$ with time-reversal symmetry. (See Fig. 1 for the fundamental domains without crystalline symmetries.) The "vertical" faces are formed by extruding the 1-cells of the fundamental domain $\mathbb{D}_2$ along z, so that the vertical faces and edges inherit the little groups of the 1- and 0-cells of which they are an extrusion. The "horizontal" faces at $k_z = \pm\pi$ for the time-reversal broken case and $k_z = 0, \pi$ for the time-reversal-symmetric case are copies of $\mathbb{D}_2$, and thus satisfy the corresponding constraints.

The classification on the horizontal faces depends on the details of the symmetry in question, but that on the vertical faces can be described more generally. Since time-reversal (if present) does not impose any additional constraints on the side faces for a two-dimensional symmetry, the target space for the vertical 1- and 2-cells is always the complex Grassmannian. Thus, there are no level-1 invariants for the vertical 1-cells, while the level-2 parent invariants are given by a set of Chern numbers, one for each irrep on the 1-cells of $\mathbb{D}_2$. The various Chern numbers satisfy a compatibility constraint arising from the fact that taken together, the 2-cells form the boundary of the 3-cell.

The parent classification set on the 3-cell is identical to that obtained without additional symmetries, *i.e.*, the $\mathbb{Z}$-valued Hopf invariant H only if $n_o = n_e = 1$. Interestingly, it is robust even if the vertical 2-cells possess nonzero Chern numbers, as shown in App. E. This can alternatively be seen by extending the calculation of the Hopf invariant to the full Brillouin zone, for which the C_2 or C_4 symmetry rules out a nonzero Chern number associated with the vertical faces of the full Brillouin zone. However, if a cross section of the fundamental domain $\mathbb{D}$ at constant k_z has a nonzero Chern number C, then the Hopf invariant reduces to a $\mathbb{Z}_{2C}$-valued invariant, owing to a deformation along the vertical faces that changes H by an even multiple of C (see App. E).

V. C_2T SYMMETRY

As a first application with crystalline symmetries, we obtain the homotopic classification of two- and three-dimensional band structures with only a combined C_2T symmetry. In two dimensions, C_2T-symmetric Bloch Hamiltonians are real and the corresponding topological invariants are formulated in terms of the Euler class and the Stiefel-Whitney invariants (see Sec. II D 3).

A stable classification of C_2T-symmetric topological insulators was first given by Fang and Fu [34]. Delicate and fragile classifications for the two-dimensional case were obtained by Kennedy and Guggenheim [6] and by Bouhon, Bzdusek, and Slager [28]. These authors showed that level-2 classification spaces for delicate and fragile topology depends on the values of the level-1 invariants. Our discussion below shows that the topological classification may also depend on the number of orbitals present at each Wyckoff position. To expose this feature, we be-

FIG. 7. Special Wyckoff positions (left) and fundamental domain of a one-dimensional IT symmetric band structure.

gin with the analogous case in one dimension, where the combination of inversion (I) and time-reversal imposes a reality condition on $H(k)$.

A. IT symmetry in one-dimension

1. Wyckoff positions and the fundamental domain

A lattice with IT symmetry has two special Wyckoff positions "a" and "b" at $x = 0$ and $x = 1/2$ (shown in Fig. 7) as well as one generic Wyckoff position pair "g" at $x = \pm a$. Denoting the number of orbitals at Wyckoff position α by n_α, the total number of orbitals n is

$$n = n_a + n_b + 2n_g. \tag{27}$$

With a suitable choice of the basis orbitals at the Wyckoff positions a, b, and g, the constraint on $H(\mathbf{k})$ imposed by IT symmetry can be cast in a form that is the same for all Wyckoff positions,

$$H(k) = H^*(k). \tag{28}$$

The symmetry relation (5) for translations by reciprocal lattice vectors, however, bears reference to the Wyckoff positions:

$$H(k + 2\pi) = \Lambda_x^\dagger H(k)\Lambda_x, \tag{29}$$

with

$$\Lambda_x = \text{diag}\left\{\mathbb{1}_{n_a}, -\mathbb{1}_{n_b}, \mathbb{1}_{n_g} \otimes e^{2\pi i a \sigma_2}\right\}. \tag{30}$$

Since a pair of orbitals at the generic Wyckoff position can always be moved to one of the special Wyckoff positions, we may without loss of generality assume that all orbitals are at the Wyckoff positions a and b.

In reciprocal space, the fundamental domain $\mathbb{D}$ consists of (two copies of) one 0-cell M, corresponding to $k = \pi$, and one 1-cell MM', corresponding to $-\pi < k < \pi$, as depicted in Fig. 7. The Hamiltonians at M and M' are related by Eq. (29).

2. Homotopic classification

The level-0 invariants are given by the number of occupied/empty bands $n_{o/e}$. For fixed level-0 invariants, the target space for all p-cells is

$$\mathcal{X} = \text{Gr}_\mathbb{R}(n_o, n_e). \tag{31}$$

	Condition(s)	Invariants
$n_o = n_e = 1$	Identical WPs	$\text{Eu}_1 \in \mathbb{Z}$
	Distinct WPs	$\text{Eu}_1 \mod 2 \in \mathbb{Z}_2$
$n_o + n_e > 2$	—	$\text{SW}_1 \in \mathbb{Z}_2$

TABLE IV. Homotopic classification of gapped band structures with IT symmetry in one dimension. The classification for $n_o = n_e = 1$ depends on the Wyckoff positions (WPs) in the lattice model.

At level-1, the parent classification set is $K_1 = \mathbb{Z}$ when $n_o = n_e = 1$ and $\mathbb{Z}_2$ otherwise, the corresponding topological invariants being the first Euler number Eu_1 and the first Stiefel-Whitney invariant SW_1, respectively (see Sec. II D for more details).

The parent classification set for the boundary deformations K_1^∂ consists of a copy of $\pi_1[\mathcal{X}] \cong K_1$ for each end point $k = \pm\pi$. The deformations at these two points are related by Eq. (29) as

$$H_\partial(-\pi; t) = \Lambda_x H_\partial(\pi, t)\Lambda_x^\dagger. \tag{32}$$

Since Λ_x depends on the Wyckoff positions occupied, so does the effect of deformations on the 1d invariants. We now discuss the effect of boundary deformations on the Euler and Stiefel-Whitney invariant separately.

First Euler invariant — In this case, $n_e = n_o = 1$ and Λ_x is proportional to σ^0 or σ^3, depending on whether the two Wyckoff positions involved are identical or distinct. In the former case, the windings of $H_\partial(\pm\pi; t)$ are equal and opposite and thus cancel each other, rendering Eu_1 a robust topological invariant. In the latter case, the winding numbers associated with $H_\partial(\pm\pi; t)$ add up, so that the boundary deformation can add an even integer to Eu_1. In this case, the true topological invariant is $\mathbb{Z}_2$ valued and is given by $\text{Eu}_1 \mod 2$.

Interestingly, in the latter case, the two topological classes are both homotopic to atomic limits, *i.e.*, Bloch Hamiltonians in either of these classes can be continuously deformed to k-independent Hamiltonians. To see how an atomic limit Hamiltonian can be assigned a nontrivial Euler invariant, we set $\Lambda_x = \sigma^3$ and (arbitrarily) take $H_{\text{ref}} = -\sigma^3$, corresponding to Wyckoff position "a" being occupied. With respect to this reference Hamiltonian, $H(k) = \sigma^3$ — corresponding to Wyckoff position "b" being occupied — carries a nontrivial level-1 invariant. This is precisely the invariant carried by the boundary deformation, which must rotate σ^3 to $-\sigma^3$ in opposite senses for $k = \pm\pi$.

First Stiefel-Whitney invariant — This invariant is given by $\text{SW}_1 = \text{sgn}(\det W^{o/e})$, see Eq (15). The Wilson lines associated with the deformations at $\pm\pi$ are related as

$$W_\partial^{o/e}(\pi) = \Lambda_x^{o/e} W_\partial^{o/e}(-\pi)\Lambda_x^{o/e\dagger}. \tag{33}$$

where $\Lambda_x^{o/e}$ denotes the projection of Λ_x onto the occu-

	Bands	Additional condition(s)	Topological invariant
Level 1	$n_{\rm o} = n_{\rm e} = 1$	Identical Wyckoff positions	$\mathrm{Eu}_{1,x}, \mathrm{Eu}_{1,y} \in \mathbb{Z}$
		Distinct Wyckoff positions	$\mathrm{SW}_1 \in \mathbb{Z}_2$
	$n_{\rm o} \geq 1, n_{\rm e} > 1$ or $n_{\rm o} > 1, n_{\rm e} \geq 1$	—	$\mathrm{SW}_{1,x}, \mathrm{SW}_{1,y} \in \mathbb{Z}$
Level 2	$n_{\rm o} = n_{\rm e} = 1$		——
	$n_{\rm o} = 1, n_{\rm e} = 2$	if $\mathcal{Q}^{\rm e}$	$\mathrm{Eu}_2^{\rm e} \in 2\mathbb{N}$
		if not $\mathcal{Q}^{\rm e}$	$\mathrm{SW}_2^{\rm e} \in \mathbb{Z}_2$
	$n_{\rm o} = 1, n_{\rm e} > 2$		——
	$n_{\rm o} = n_{\rm e} = 2$	if $\mathcal{Q}^{\rm o}$ and $\mathcal{Q}^{\rm e}$	$(\mathrm{Eu}_2^{\rm o}, \mathrm{Eu}_2^{\rm e}) \in \mathbb{N} \times \mathbb{Z}|_{\rm p}$
		if $\mathcal{Q}^{\rm o}$, but not $\mathcal{Q}^{\rm e}$	$\mathrm{Eu}_2^{\rm o} \in \mathbb{N}$
		if $\mathcal{Q}^{\rm e}$, but not $\mathcal{Q}^{\rm o}$	$\mathrm{Eu}_2^{\rm e} \in \mathbb{N}$
		if not $\mathcal{Q}^{\rm o}$ and not $\mathcal{Q}^{\rm e}$	$\mathrm{SW}_2 \in \mathbb{Z}_2$
	$n_{\rm o} = 2, n_{\rm e} > 2$	if $\mathcal{Q}^{\rm o}$	$\mathrm{Eu}_2^{\rm o} \in \mathbb{N}$
		if not $\mathcal{Q}^{\rm o}$	$\mathrm{SW}_2 \in \mathbb{Z}_2$
	$n_{\rm o}, n_{\rm e} > 2$	—	$\mathrm{SW}_2 \in \mathbb{Z}_2$

TABLE V. Homotopic classification of gapped band structures with $\mathrm{C}_2\mathrm{T}$ symmetry in two dimensions. The classification for $n_{\rm o} = n_{\rm e} = 1$ depends on the Wyckoff positions of the two sites. The symbol $\mathcal{Q}^{\rm o/e}$ refers to the condition $\mathcal{Q}_2^{a,{\rm o/e}}$ of Eq. (36) being met for $a = x$ and for $a = y$. The set $\mathbb{N} \times \mathbb{Z}_{\rm p}$ consists of all ordered integer pairs (p, q) with $p \geq 0$ and $p = q \mod 2$.

pied/empty subspaces. Thus,

$$\det W_\partial^{\rm o/e}(\pi) = \det W_\partial^{\rm o/e}(-\pi) \in \{\pm 1\},$$

so that $\det W^{\rm o/e}$ for the entire loop remains unchanged under boundary deformation. The first Stiefel-Whitney invariant is thus robust under boundary deformations.

These classification results are summarized in Tab. IV.

B. $\mathrm{C}_2\mathrm{T}$ symmetry in two dimensions

1. Wyckoff positions and the fundamental domain

In two dimensions, there are four special Wyckoff positions "a", "b", "c", and "d", as shown in Fig. 8, and one pair of generic Wyckoff positions "g" at coordinates (a_x, a_y). Denoting the number of orbitals at the Wyckoff position α by n_α, the total number of orbitals is

$$n = n_{\rm a} + n_{\rm b} + n_{\rm c} + n_{\rm d} + 2n_{\rm g}. \tag{34}$$

We choose the basis vectors that are invariant under $\mathrm{C}_2\mathrm{T}$ (see Appendix A 2), so that the Bloch Hamiltonian satisfies $H^*(\mathbf{k}) = H(\mathbf{k})$. The reciprocal-space group G_Λ is generated by the two reciprocal lattice translations. We denote the corresponding representation matrices (see Eq. (4)) by $\Lambda_{x/y}$, which are explicitly given by

$$\Lambda_x = \mathrm{diag}\left\{ \mathbb{1}_{n_{\rm a}}, \mathbb{1}_{n_{\rm b}}, -\mathbb{1}_{n_{\rm c}}, -\mathbb{1}_{n_{\rm d}}, \mathbb{1}_{n_g} e^{2\pi i a_x \sigma_2} \right\},$$
$$\Lambda_y = \mathrm{diag}\left\{ \mathbb{1}_{n_{\rm a}}, -\mathbb{1}_{n_{\rm b}}, -\mathbb{1}_{n_{\rm c}}, \mathbb{1}_{n_{\rm d}}, \mathbb{1}_{n_g} e^{2\pi i a_y \sigma_2} \right\}. \tag{35}$$

For the purpose of classifying topological phases, we may continuously shift any orbitals at the Wyckoff position

"g" to the special Wyckoff position "a" and use the corresponding expressions for $\Lambda_{x/y}$. The fundamental domain is the same as symmetry class A, as depicted in Fig. 4.

2. Homotopic classification

The level-0 invariants are given by the number of occupied/empty bands $n_{\rm o/e}$. The target space for all cells is again the real Grassmannian $\mathcal{X} = \mathrm{Gr}_\mathbb{R}(n_{\rm o}, n_{\rm e})$. The level-1 classification is similar to the one-dimensional case discussed above: each of the two 1-cells contribute the $\mathbb{Z}$-valued first Euler classes $\mathrm{Eu}_{1,x/y}$ if $n_{\rm o} = n_{\rm e} = 1$ and $\mathbb{Z}_2$-valued Stiefel-Whitney invariants $\mathrm{SW}_{1,x/y}$ otherwise. The latter are robust to boundary deformations, while the former are robust only if both orbitals lie at Wyckoff position with the same x/y coordinate, and reduce to a $\mathbb{Z}_2$ invariant otherwise.

The level-1 invariants are further constrained by compatibility relations. Since the boundary of the 2-cell consists of two copies of each 1-cell, the $\mathbb{Z}_2$-valued SW_1 always add up to 0, so that there are no additional restrictions on $\mathrm{SW}_{1,x/y}$. There are nontrivial compatibility constraints on $\mathrm{Eu}_{1,x/y}$, however, that depend on the reciprocal-space translation operators $\Lambda_{x/y}$. If the two orbitals are at the same Wyckoff position, such that $\Lambda_{x/y} \propto \sigma^0$, then there are no additional constraints on $\mathrm{Eu}_{1,x/y}$, so that the level-1 classification set is $\mathbb{Z}^2$. If only one of the translation operators (Λ_x, say) is proportional to σ^3, then $\mathrm{Eu}_{1,x}$ is only defined modulo 2, while $\mathrm{Eu}_{1,y}$ adds up for the two copies of the 1-cell along y, so that the compatibility constraint requires $2\,\mathrm{Eu}_{1,y} = 0$. This leaves only one $\mathbb{Z}_2$-valued invariant, viz, $\mathrm{SW}_1 \equiv \mathrm{Eu}_{1,x}$

mod 2. On the other hand, if both $\Lambda_{x/y} \propto \sigma^3$ (such as when the two orbitals are at Wyckoff positions "a" and "d"), then the compatibility condition reads

$$2\,\mathrm{Eu}_{1,x} - 2\,\mathrm{Eu}_{1,y} = 0 \implies \mathrm{Eu}_{1,x} = \mathrm{Eu}_{1,y} \equiv \mathrm{Eu}_1.$$

Furthermore, the boundary deformations (described for the 1d case) simultaneously changes both $\mathrm{Eu}_{1,x}$ and $\mathrm{Eu}_{1,y}$ by an even integer. Thus, we are again left with only one $\mathbb{Z}_2$-valued invariant Eu_1.

At level-2, $K_2 = \pi_2[\mathcal{X}]$ depends on $n_{\mathrm{o/e}}$ (see Tab. II), and the corresponding invariants can be derived from the winding number $\mathrm{Eu}_2^{\mathrm{o/e}}$ of a family of Wilson loops. These are the $\mathbb{Z}$-valued second Euler invariant (up to a parity constraint, see Tab. II) when $n_{\mathrm{o/e}} = 2$, while for $n_{\mathrm{o/e}} > 2$, we get the $\mathbb{Z}_2$-valued second Stiefel-Whitney invariant $\mathrm{SW}_2 \equiv \mathrm{Eu}_2^{\mathrm{o/e}} \mod 2$. For the boundary deformations, K_2^{∂} consists of a copy of $\pi_1[\mathcal{X}]$ for the 0-cell and $\pi_2[\mathcal{X}] \cong K_2$ for each of the 1-cells. We now discuss their effect on the Euler and Stiefel-Whitney invariant separately.

Second Euler invariant — Since these invariants are defined only when $n_{\mathrm{o}} = 2$ or $n_{\mathrm{e}} = 2$, the contribution of the 0-cell to K_2^{∂} is $\pi_1[\mathcal{X}] = \mathbb{Z}_2$. We first consider deformations that are trivial on the 0-cell. Nontrivial deformation along each 1-cell can carry a second Euler invariant given by the winding number of the Wilson loops in SO(2) (see Sec. II D 3). However, each 1-cell occurs twice in $\partial\mathbb{D}$, and the corresponding windings cancel each other, unless the orientation of the basis states is changed while going from one copy of the 1-cell to the other. This change of orientation can originate from either a reciprocal space translation operator or a nontrivial first Stiefel-Whitney invariant. Explicitly, denoting the 1-cells along x and y by α_x and α_y, respectively, the windings on two copies of α_x cancel if either $\det\Lambda_y = -1$ or $\mathrm{SW}_{1,y} = 1$. Thus, Eu_2 is robust to boundary deformations only if

$$\mathcal{Q}_{2,a}^{\mathrm{o/e}} : \quad (-1)^{\mathrm{SW}_{1,a}} \det\Lambda_a^{\mathrm{o/e}} = 1. \tag{36}$$

for $a = x, y$. Note that while $\mathrm{SW}_{1,a}$ and $\det\Lambda_{x/y}^{\mathrm{o/e}}$ both depend on the choice of the reference Hamiltonian H_{ref}, this condition does not. If this condition is obeyed, then $\mathrm{Eu}_2^{\mathrm{o/e}}$ is robust to boundary deformations, while if it is violated, the boundary deformations can change it by even integers, rendering the level-2 invariant $\mathbb{Z}_2$-valued.

A boundary deformation that is nontrivial at a 0-cell changes the sign of $\mathrm{Eu}_2^{\mathrm{o}}$ and $\mathrm{Eu}_2^{\mathrm{e}}$ simultaneously, since it changes the orientation of the bases for both the occupied and the unoccupied states [28].

Second Stiefel-Whitney invariant — These are robust to boundary deformations, since the effect of the latter always cancels out modulo 2.

The classification results are summarized in Tab. V. They are consistent with the conclusions of Ref. [28], which considered the case $\Lambda_{x/y} = \mathbb{1}$, corresponding to all orbitals being at the same Wyckoff position. In the stable

limit, there are two $\mathbb{Z}_2$-valued level-1 invariants and one $\mathbb{Z}_2$-valued level-2 invariant.

C. $\mathrm{C}_2\mathrm{T}$ symmetry in three dimensions

In three dimensions, $\mathrm{C}_2\mathrm{T}$ symmetric Hamiltonians satisfy Eq. (26). The fundamental domain is a cuboid with the top/bottom faces (at $k_z = 0, \pi$) formed by copies of the 2d fundamental domain, and the side faces formed by copies of two distinct 2-cells.

1. Homotopic classification

The level-1 invariants are two independent copies of the invariants obtained for the 2d classification. As discussed in Sec. IV, there are no topological invariants at the 1-cells parallel to k_z.

The level-2 invariants for the $k_z = 0, \pi$ planes are copies of those obtained for the 2d classification. For the two distinct faces parallel to the k_z-axis, the parent topological invariants are the Chern numbers $\mathrm{C}_{x/y}$. There are two kinds of boundary deformations for these invariants: those along the 1-cells parallel to the k_z-axis and those perpendicular to it. The former cannot change the Chern number, since the two vertical boundaries of each face are copies of the the same 1-cell, so that a deformation with Chern number C on one copy of the 1-cell is exactly canceled by the other. The latter deformations cannot carry a Chern number, since the Hamiltonian is constrained to be real at the boundary. Thus, the Chern numbers $\mathrm{C}_{x/y}$ are robust topological invariants. There are no additional constraints on them from level-3 topology, since each of these 2-cells occurs twice in the boundary of the 3-cell, so that the total Chern number always vanishes.

The $\mathbb{Z}$-valued $\mathrm{C}_{x/y}$ can be combined with the $\mathbb{Z}_2$ valued difference between $\mathrm{SW}_{1,x/y}$ computed at $k_z = 0$ and π to get a $\mathbb{Z}$-valued invariant $\mathrm{C}_{x/y}^{\mathrm{full}}$, which is simply the Chern number computed on the k_x/k_y plane for the full range $k_z \in (-\pi, \pi)$. This is because the symmetry condition $H(k_x, k_y, k_z) = H^*(k_x, k_y, -k_z)$ implies that the Chern numbers for $k_z \in (-\pi, 0)$ and $(0, \pi)$ add up to give even integers. Furthermore, a difference between $\mathrm{SW}_{1,x/y}$ at $k_z = 0$ and π implies that the Wilson loop along k_x/k_y changes from 0 to π along k_z, which, combined with the symmetry of Wilson loops under time reversal, implies that the Chern number computed for $k_z \in (-\pi, \pi)$ is unity (see Appendix F 1 for a similar argument). Combining this with the even total Chern number yields two $\mathbb{Z}$-valued invariants $\mathrm{C}_{x/y}^{\mathrm{full}}$, which represent weak Chern insulator phases protected by discrete translation symmetry in the x and y direction, respectively.

At level-3, we get the Hopf invariant when $n_{\mathrm{o}} = n_{\mathrm{e}} = 1$. This is not affected by deformations, since the Bloch Hamiltonian is real for $k_z = 0, \pi$ and thus cannot carry a Chern number (see Sec. IV for details).

	Bands	Topological invariant
Level 1	—	Two copies of invariants from Tab. V
Level 2	—	C_x, $C_y \in \mathbb{Z}$ and two copies of invariants from Tab. V
Level-3	$n_o = n_e = 1$	$H \in \mathbb{Z}$
	$n_o + n_e > 2$	—

TABLE VI. Homotopic classification of gapped band structures with C_2T symmetry in three dimensions.

FIG. 8. (Left) The Wyckoff positions for a square lattice with C_2 symmetry. (Right) The fundamental domain $\mathbb{D}$ for two-dimensional band structures with C_2 symmetry.

The classification results are summarized in Tab. VI.

2. Anomalous boundary states

The presence of stable topological indices for a 3d band structure with C_2T symmetry implies the existence of anomalous boundary states on boundaries invariant under C_2, i.e., a surface parallel to the xy plane [34]. The stable topological invariants are the $\mathbb{Z}$-valued $C_{x,y}^{\mathrm{full}}$ associated with the vertical 2-cells and the $\mathbb{Z}_2$-valued difference between SW_2 associated with the planes $k_z = 0, \pi$ [75]. The former lead to anomalous chiral states at the surface that propagate along x and y, respectively, while the latter leads to a surface Dirac cone.

We now derive these anomalous states from the boundary perspective. Following the argument for symmetry class A (Sec. III C), a chiral state violates the level-0 compatibility condition as well as the gluing condition and is thus anomalous. To see that a surface Dirac cone is anomalous, one first observes that a closed path γ around a single Dirac cone has Berry phase π, so that $\det W^{\mathrm{o/e}}(\gamma) = -1$ [34]. On the other hand, for any set of $\mathbb{Z}_2$-valued level-1 invariants $SW_{1,x/y}$, the level-1 compatibility condition arising from the triviality of the Wilson loop $\det W^{\mathrm{o/e}}(\partial \mathbb{D}) = 1$ is trivially satisfied, since each 1-cell occurs twice in $\partial \mathbb{D}$ and the corresponding invariants add up to 0 mod 2. The two copies of a 1-cell have identical SW_1, since the Hamiltonians at them are related by a unitary transformation given by $\Lambda_{x,y}$. As a Dirac cone manifestly violates the level-1 compatibility condition, it can be realized only if SW_1 is different for the two copies of a 1-cell, i.e., if the the gluing condition is violated. This implies that a single surface Dirac cone must be anomalous.

VI. C_2 SYMMETRY

A classification of C_2-symmetric topological insulators in the stable limit was previously obtained in Refs. [22–25, 76]. A partial fragile classification, based on level-0 invariants only, was obtaied using the method of topological quantum chemistry [54]. Delicate topological invari-
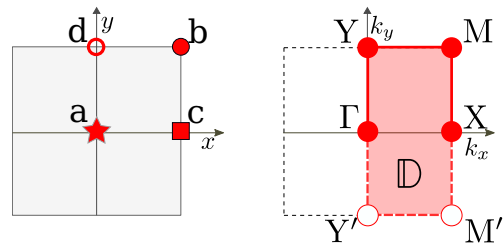
ants at levels 1 and 2 were constructed by Kobayashi and Furusaki [31], who also identified representation-protected phases. The full homotopic classification we present below rederives and completes these results from the literature in a consistent mathematical framework.

A. Wyckoff positions, basis orbitals, and symmetries

With twofold rotation symmetry and in two dimensions, there are four special Wyckoff positions "a", "b", "c", and "d" (shown in Fig. 8) and one pair of generic Wyckoff positions "g". At each special Wyckoff position, electron orbitals are even (+) or odd (−) under twofold rotation. Combining orbitals at the two generic Wyckoff positions, one even (+) and one odd (−) orbital may be obtained. Denoting the number of orbitals of parity $\pm$ by $n_\pm$, the total number of orbitals is

$$n = n_a + n_b + n_c + n_d + 2n_g = n_+ + n_-. \tag{37}$$

The reciprocal-space group G_Λ is generated by twofold rotation g_2 and two reciprocal-space translations g_x and g_y. We denote the corresponding representation matrices (see Eq. (4)) by C_2, Λ_x, and Λ_y, respectively. The Bloch Hamiltonian satisfies

$$H(k_x, k_y) = C_2 H(-k_x, -k_y) C_2^\dagger \tag{38}$$

as well as Eq. (5) for the reciprocal-space translations $g_{x,y}$. Since the matrices C_2, Λ_x, and Λ_y generate a representation of G_Λ, they satisfy

$$C_2 \Lambda_{x,y} = \Lambda_{x,y}^\dagger C_2. \tag{39}$$

We choose the over-all phase factor of the twofold rotation operator C_2 such that $C_2^2 = \mathbb{1}$. Hence, in its eigenbasis, it can be written explicitly as

$$C_2 = \mathrm{diag}\{\mathbb{1}_{n_+}, -\mathbb{1}_{n_-}\}. \tag{40}$$

Explicit expressions for $\Lambda_{x,y}$ are derived in Appendix B 1.

We take the fundamental domain $\mathbb{D}$ as the right half of the Brillouin zone, as shown in Fig. 8. It consists of four 0-cells, three 1-cells and one 2-cell. The 0-cells all

have a nontrivial little group $G_S = \{0, g_S\}$, with $g_\Gamma = g_2$ a twofold rotation, whereas g_X, g_Y, and g_M are combinations of a twofold rotation and a reciprocal lattice translation. The corresponding representation matrices $C_S \equiv C(g_S)$ are

$$
\begin{aligned}
C_\Gamma &= C_2, \\
C_{X,Y} &= \Lambda_{x,y}^\dagger C_2 = C_2 \Lambda_{x,y}, \\
C_M &= \Lambda_x^\dagger \Lambda_y^\dagger C_2 = C_2 \Lambda_x \Lambda_y.
\end{aligned}
\tag{41}
$$

These matrices all square to $\mathbb{1}$ and thus have eigenvalues ± 1. The eigenstates of H_S are thus labeled by the C_S-eigenvalue ± 1. The four matrices C_S are not independent, since they satisfy

$$
C_\Gamma C_X C_M C_Y = \mathbb{1}.
\tag{42}
$$

The eigenvalues of C_S for band structures with a minimal set of orbitals at a single Wyckoff position constitute the EBRs [54, 55, 77]. These are derived in Appendix B 2 and listed in Tab. XV.

The three 1-cells ΓY, YM, and MX each have two copies, which are related as

$$
\begin{aligned}
H(0, -k) &= C_\Gamma^\dagger H(0, k) C_\Gamma, \\
H(\pi, -k) &= C_X^\dagger H(\pi, k) C_X, \\
H(k, \pi) &= \Lambda_y^\dagger H(k, -\pi) \Lambda_y.
\end{aligned}
\tag{43}
$$

The last expression is independent of C_2, since the two copies of YM are related by a translation $2\pi \mathbf{e}_y$. There are no local-in-$\mathbf{k}$ constraints on the Hamiltonian at the 1-cells or the 2-cell. If time-reversal symmetry is present, we choose a basis where $C_2 T = \mathbb{1}$, so that the Hamiltonian satisfies the reality condition $H(\mathbf{k}) = H^*(\mathbf{k})$.

B. Homotopic classification in two dimensions

1. Without time-reversal (symmetry class A)

The level-0 invariants are given by the number of occupied/empty bands $n_{o/e,\pm}^S$ for each 0-cell S with even/odd parity under C_2. These satisfy a "level-0 compatibility relation" (see Eq. (7))

$$
n_{o/e} = \sum_{x=\pm} n_{o/e,x}^S.
\tag{44}
$$

Additionally, there are constraints on the level-0 invariants that follow from the restrictions imposed on the representation matrices C_S. In particular, from Eqn. (42), it follows that $\prod_S \det C_S = 1$, so that

$$
\sum_S \left(n_{o,-}^S + n_{e,-}^S \right) = 0 \mod 2.
\tag{45}
$$

This is sufficient to ensure that the level-0 invariants, summed over occupied and unoccupied bands, constitute a linear combination of the EBRs listed in Tab. XV.

For fixed level-0 invariants, the target spaces are

$$
\mathcal{X}_S = \mathrm{Gr}_\mathbb{C}(n_{o,+}^S, n_{e,+}^S) \times \mathrm{Gr}_\mathbb{C}(n_{o,-}^S, n_{e,-}^S).
\tag{46}
$$

for the 0-cells and $\mathcal{X} = \mathrm{Gr}_\mathbb{C}(n_o, n_e)$ for the 1- and the 2-cell. The corresponding parent invariants are identical to those obtained for class A (Sec. III), i.e., trivial at level-1 and a $\mathbb{Z}$-valued Chern invariant C at level-2. Proceeding as in Sec. III, one sees that the Chern invariant is robust to boundary deformations, because the Chern number of a boundary deformation along a 1-cell enters through both its copies at the boundary of the 2-cell, which precisely cancel each other. Thus, we obtain the Chern number $C \in \mathbb{Z}$ as the level-2 topological invariant.

These results are summarized in Tab. VII.

2. With time-reversal (symmetry class AI)

The level-0 topological invariants are identical to the time-reversal-broken case, but now subject to an additional constraint

$$
\sum_S n_{o,-}^S = 0 \mod 2,
\tag{47}
$$

which arises from the level-1 topology (as we show below) and thus constitutes a level-1 compatibility relation. Following Eq. (45), an identical constraint also applies to the unoccupied bands. The target spaces now consist of real Grassmannians, and are explicitly given for the 0-cells by

$$
\mathcal{X}_S = \mathrm{Gr}_\mathbb{R}(n_{o,+}^S, n_{e,+}^S) \times \mathrm{Gr}_\mathbb{R}(n_{o,-}^S, n_{e,-}^S)
\tag{48}
$$

and for the 1-cells and the 2-cell by $\mathcal{X} = \mathrm{Gr}_\mathbb{R}(n_o, n_e)$. Thus, the parent classification is similar to that of $C_2 T$ discussed in Sec. V. We summarize our classification results in Tab. VII and briefly discuss their derivation here.

Classification on 1-cells

At level-1, the parent invariants for the 1-cell SS' are the $\mathbb{Z}$-valued first Euler invariant $\mathrm{Eu}_1^{SS'} = -\mathrm{Eu}_1^{S'S}$ if $n_o = n_e = 1$ and the $\mathbb{Z}_2$-valued first Stiefel-Whitney number $\mathrm{SW}_1^{SS'}$ otherwise. The parent classification set for boundary deformations K_1^∂ consists of a factor $\pi_1[\mathcal{X}_S]$ for each 0-cell S. The boundary deformations at S do not have an effect on the level-1 invariants if $\pi_1[\mathcal{X}_S] = 0$, which happens if $\mathrm{Gr}_\mathbb{R}(n_{o,a}^S, n_{e,a}^S)$ degenerates to a point for both $a = \pm$. In terms of the level-0 invariants, this happens when

$$
\mathcal{Q}_1^S : \; n_{o,+}^S n_{e,+}^S = n_{o,-}^S n_{e,-}^S = 0.
\tag{49}
$$

We now discuss the effect of boundary deformations on the Euler and Stiefel-Whitney invariant separately.

First Euler invariant — A boundary deformation at the

0-cell S may add an integer simultaneously to $\mathrm{Eu}_1^{SS'}$ for all 1-cells with S as an end point if $\pi_1[\mathcal{X}_S] \neq 0$. Thus, $\mathrm{Eu}_1^{SS'}$ is robust to boundary deformations only if the conditions $\mathcal{Q}_1^S$ and $\mathcal{Q}_1^{S'}$ are satisfied, see Eq. (49). If $\mathcal{Q}_1^S$ is obeyed at all four 0-cells, then all three first Euler numbers Eu_1^{XM}, Eu_1^{MY}, and Eu_1^{YT} are well defined. If this condition is violated, then using $n_{\mathrm{o/e},\pm}^S \in \{0,1\}$ and Eq. (47), we conclude that it must be violated at either two or all four 0-cells. In these cases, upon taking into account the ambiguity from boundary deformations, we are left with one and no first Euler invariant, respectively.

The number of first Euler invariants are further reduced by the level-1 compatibility conditions. If $\mathcal{Q}_1^S$ is obeyed at all four 0-cells, then one has the symmetry relations $\mathrm{Eu}_1^{\Gamma Y'} = -\mathrm{Eu}_1^{\Gamma Y}$, $\mathrm{Eu}_1^{Y'M'} = -\mathrm{Eu}_1^{YM}$, and $\mathrm{Eu}_1^{M'X} = -\mathrm{Eu}_1^{XM}$. Triviality of the first Euler invariant computed for the boundary of the 2-cell then gives the constraint

$$\mathrm{Eu}_1^{XM} + \mathrm{Eu}_1^{MY} + \mathrm{Eu}_1^{YT} = 0, \qquad (50)$$

which effectively removes one level-1 invariant. There is a similar constraint if $\mathcal{Q}_1^S$ is obeyed only at two of the 0-cells, which removes the only level-1 invariant present in that case. Thus, there are two independent first Euler invariants if $\mathcal{Q}_1^S$ is obeyed at all 0-cells S, while there are none otherwise.

First Stiefel-Whitney invariant — If a boundary deformation flips the orientation at a 0-cell S, then it flips the sign of $\det W_{SS'}^{\mathrm{o/e}}$ for all 1-cells having S as their end point. Such a boundary deformation is allowed if $\mathcal{Q}_1^S$ is violated, thereby effectively "removing" one level-1 invariant.

The level-1 compatibility condition follows from triviality of the Wilson loop around the boundary of the 2-cell

$$W_{\partial \mathbb{D}} = W_{\Gamma Y'} W_{Y'M'} W_{M'X} W_{XM} W_{MY} W_{YT} = \mathbb{1}, \quad (51)$$

where we have skipped the superscript o/e to avoid notational clutter. The Wilson loops at the symmetry-related 1-cells satisfy

$$\begin{aligned} W_{\Gamma Y'}^{\mathrm{o/e}} &= C_\Gamma^{\mathrm{o/e}\dagger} W_{\Gamma Y}^{\mathrm{o/e}} C_Y^{\mathrm{o/e}}, \\ W_{Y'M'}^{\mathrm{o/e}} &= W_{YM}^{\mathrm{o/e}}, \\ W_{M'X}^{\mathrm{o/e}} &= C_M^{\mathrm{o/e}\dagger} W_{MX}^{\mathrm{o/e}} C_X^{\mathrm{o/e}}. \end{aligned} \qquad (52)$$

Using these and $\det W_{SS'} \in \{\pm 1\}$, we get

$$\det W_{\partial \mathbb{D}}^{\mathrm{o/e}} = \det \left(C_\Gamma^{\mathrm{o/e}\dagger} C_Y^{\mathrm{o/e}} C_M^{\mathrm{o/e}\dagger} C_X^{\mathrm{o/e}} \right), \qquad (53)$$

so that the compatibility condition becomes

$$1 = \prod_S \det C_S^{\mathrm{o/e}} = \prod_S (-1)^{n_{\mathrm{o/e},-}^S}, \qquad (54)$$

which is equivalent to Eq. (47). Thus, the compatibility condition does not constrain the level-1 invariants, but imposes a constraint on the level-0 invariants.

Classification on the 2-cell

At level-2, the the parent classification set is given by $K_2 = \pi_2[\mathcal{X}]$, with the corresponding invariants being the $\mathbb{Z}$-valued second Euler invariant or the $\mathbb{Z}_2$-valued second Stiefel-Whitney invariant, depending on $n_{\mathrm{o/e}}$ (see Table II). The parent classification set for boundary deformations K_2^∂ consists of a factor of $\pi_2[\mathcal{X}] \cong K_2$ for each 1-cell and of $\pi_1[\mathcal{X}_S]$ for each 0-cell, which consists of two factors corresponding to the two parity sectors (see Eq. (48)). We now discuss the effect of boundary deformations on the Euler and Stiefel-Whitney invariant separately.

Second Euler invariant — For the occupied/empty subspaces, $\mathrm{Eu}_2^{\mathrm{o/e}}$ is defined if $n_{\mathrm{o/e}} = 2$, whereby it is $\mathbb{Z}$-valued if $n_{\mathrm{e/o}} \geq 2$ and $2\mathbb{Z}$-valued if $n_{\mathrm{e/o}} = 1$. For the former case, boundary deformations that are nontrivial along a 1-cell (*i.e.*, in $\pi_2[\mathcal{X}] \cong K_2$) can add an arbitrary integer to $\mathrm{Eu}_2^{\mathrm{o/e}}$. However, as each 1-cell occurs twice in $\partial \mathbb{D}$, following the argument for C_2T (Sec. V), these individual contributions cancel out unless the orientation of the occupied/empty subspace is flipped between the two copies of the 1-cell. From Eq. (52), this can happen if $\det C_S^{\mathrm{o/e}} = -1$ for any of the 0-cells. Thus, the two boundary contributions cancel if $\det C_S^{\mathrm{o/e}} = 1$ for all S, or, equivalently, if

$$\mathcal{Q}_2^{\mathrm{o/e}} : \ n_{\mathrm{o/e},+}^S n_{\mathrm{o/e},-}^S = 0 \text{ for all } S. \qquad (55)$$

If this condition is violated, then the boundary deformations at the two copies of the 1-cell add up. For $n_{\mathrm{o/e}} = 2$ and $n_{\mathrm{e/o}} \geq 2$, such a boundary deformation may add an even integer to $\mathrm{Eu}^{\mathrm{o/e}}$, rendering the classification group $\mathbb{Z}/2\mathbb{Z} \cong \mathbb{Z}_2$. On the other hand, for $n_{\mathrm{o/e}} = 2$ and $n_{\mathrm{e/o}} = 1$, such boundary deformations may add an arbitrary multiple of four to $\mathrm{Eu}_2^{\mathrm{o/e}}$, so that the classification group becomes $2\mathbb{Z}/4\mathbb{Z} = \mathbb{Z}_2$.

Next, we consider boundary deformations that are nontrivial at a 0-cell S, which may be nontrivial in either one or both factors of $\pi_1[\mathcal{X}_S]$. In the former case, boundary deformations can flip the orientation of the basis of the occupied/empty subspace for one of the parity sectors at S, and hence of that subspace also away from S. By continuity, such a deformation must be nontrivial at each 0-cell, so that it cannot exist if $\pi_1[\mathcal{X}_S] = 0$ for at least one 0-cell, *i.e.*, if $\exists S$ for which $\mathcal{Q}_1^S$ holds. If that is not the case, then such a boundary deformation changes the sign of both Eu_2^o and Eu_2^e, replacing the level-2 classifying spaces $\mathbb{Z}$ by $\mathbb{N}$ and $\mathbb{Z}^2|_{\mathrm{p}}$ by $\mathbb{N} \times \mathbb{Z}|_{\mathrm{p}}$.

Boundary deformations with nontrivial topology in both factors of $\pi_1[\mathcal{X}_S]$ cannot change the orientation of the occupied/empty subspaces, so that they are trivial away from S. Such deformations may, however, change both Eu_2^o and Eu_2^e by arbitrary integers. (See App. F for an explicit construction of such a boundary deformation.) These deformations do not exist if either Grassmannian

	Bands	Additional condition(s)	Topological invariant
A, Level 1	$n_{\mathrm{o}}, n_{\mathrm{e}} \geq 1$		——
A, Level 2	$n_{\mathrm{o}}, n_{\mathrm{e}} \geq 1$	—	$C \in \mathbb{Z}$ [S]
AI, Level 1	$n_{\mathrm{o}} = n_{\mathrm{e}} = 1$	if $\mathcal{Q}_1^\wedge$	$\mathrm{Eu}_1^{\Gamma Y}, \mathrm{Eu}_1^{YM} \in \mathbb{Z}$
		if not $\mathcal{Q}_1^\wedge$	—
	$n_{\mathrm{o}} \geq 1,\, n_{\mathrm{e}} > 1$ or $n_{\mathrm{o}} > 1,\, n_{\mathrm{e}} \geq 1$	—	$\mathrm{SW}_1^{\Gamma Y}, \mathrm{SW}_1^{YM}, \mathrm{SW}_1^{MX} \in \mathbb{Z}_2$ one less for every violation of $\mathcal{Q}_1^S$
AI, Level 2	$n_{\mathrm{o}} = n_{\mathrm{e}} = 1$		——
	$n_{\mathrm{o}} = 1,\, n_{\mathrm{e}} = 2$	if $\mathcal{Q}_1^\vee$ and $\mathcal{Q}_2^{\mathrm{e}}$	$\mathrm{Eu}_2^{\mathrm{e}} \in 2\mathbb{Z}$
		if $\mathcal{Q}_2^{\mathrm{e}}$, but not $\mathcal{Q}_1^\vee$	$\mathrm{Eu}_2^{\mathrm{e}} \in 2\mathbb{N}$
		if not $\mathcal{Q}_2^{\mathrm{e}}$	$\mathrm{Eu}_2^{\mathrm{e}} \in \mathbb{Z}_2$
	$n_{\mathrm{o}} = 1,\, n_{\mathrm{e}} > 2$		——
	$n_{\mathrm{o}} = n_{\mathrm{e}} = 2$	if $\mathcal{Q}_1^\vee$ and $\mathcal{Q}_2^{\mathrm{e}}$ and $\mathcal{Q}_2^{\mathrm{o}}$	$(\mathrm{Eu}_2^{\mathrm{o}}, \mathrm{Eu}_2^{\mathrm{e}}) \in \mathbb{Z}^2|_{\mathrm{p}}$
		if $\mathcal{Q}_2^{\mathrm{e}}$ and $\mathcal{Q}_2^{\mathrm{o}}$, but not $\mathcal{Q}_1^\vee$	$(\mathrm{Eu}_2^{\mathrm{o}}, \mathrm{Eu}_2^{\mathrm{e}}) \in \mathbb{N} \times \mathbb{Z}|_{\mathrm{p}}$
		if $\mathcal{Q}_1^\vee$ and $\mathcal{Q}_2^{\mathrm{o}}$, but not $\mathcal{Q}_2^{\mathrm{e}}$	$\mathrm{Eu}_2^{\mathrm{o}} \in \mathbb{Z}$
		if $\mathcal{Q}_1^\vee$ and $\mathcal{Q}_2^{\mathrm{e}}$, but not $\mathcal{Q}_2^{\mathrm{o}}$	$\mathrm{Eu}_2^{\mathrm{e}} \in \mathbb{Z}$
		if $\mathcal{Q}_2^{\mathrm{o}}$, but not $\mathcal{Q}_1^\vee$ and not $\mathcal{Q}_2^{\mathrm{e}}$	$\mathrm{Eu}_2^{\mathrm{o}} \in \mathbb{N}$
		if $\mathcal{Q}_2^{\mathrm{e}}$, but not $\mathcal{Q}_1^\vee$ and not $\mathcal{Q}_2^{\mathrm{o}}$	$\mathrm{Eu}_2^{\mathrm{e}} \in \mathbb{N}$
		if $\mathcal{Q}_2^\wedge$, but not $\mathcal{Q}_2^{\mathrm{e}}$ and not $\mathcal{Q}_2^{\mathrm{o}}$	$\mathrm{SW}_2 \in \mathbb{Z}_2$
		if not $\mathcal{Q}_2^\wedge$	—
	$n_{\mathrm{o}} = 2,\, n_{\mathrm{e}} > 2$	if $\mathcal{Q}_1^\vee$ and $\mathcal{Q}_2^{\mathrm{o}}$	$\mathrm{Eu}_2^{\mathrm{o}} \in \mathbb{Z}$
		if $\mathcal{Q}_2^{\mathrm{o}}$, but not $\mathcal{Q}_1^\vee$	$\mathrm{Eu}_2^{\mathrm{o}} \in \mathbb{N}$ [F]
		if $\mathcal{Q}_2^\wedge$, but not $\mathcal{Q}_2^{\mathrm{o}}$	$\mathrm{SW}_2 \in \mathbb{Z}_2$
		if not $\mathcal{Q}_2^\wedge$	—
	$n_{\mathrm{o}}, n_{\mathrm{e}} > 2$	if $\mathcal{Q}_2^\wedge$	$\mathrm{SW}_2 \in \mathbb{Z}_2$ [F]
		if not $\mathcal{Q}_2^\wedge$	—

TABLE VII. Homotopic classification of gapped band structures with C_2 symmetry in two dimensions for various possible combinations of number of bands and level 0 invariants, the latter encoded in the $\mathcal{Q}$'s. In particular, $\mathcal{Q}_1^S$, $\mathcal{Q}_2^{\mathrm{o/e}}$, $\mathcal{Q}_2^S$, and $\mathcal{Q}_2^\wedge$ are defined by Eqs. (49), (55), (56), and (57), respectively. The condition $\mathcal{Q}_1^\wedge$ holds if $\mathcal{Q}_1^S\,\forall S$, while $\mathcal{Q}_1^\vee$ holds if $\exists S$ where $\mathcal{Q}_1^S$ is true. The set $\mathbb{Z}^2|_{\mathrm{p}}$ consists of all ordered integer pairs (p, q) with $p = q \mod 2$, while the set $\mathbb{N} \times \mathbb{Z}_{\mathrm{p}}$ consists of all ordered integer pairs (p, q) with $p \geq 0$ and $p = q \mod 2$. The table lists the cases $n_{\mathrm{o}} \leq n_{\mathrm{e}}$ only. The remaining classifications with $n_{\mathrm{o}} > n_{\mathrm{e}}$ can be obtained from the entries in the Table by exchanging the labels "o" and "e". The fragile and stable topological phases are marked by [F] and [S], respectively.

in $\mathcal{X}_S$ degenerates to a point, *i.e.*, if

$$\mathcal{Q}_2^S:\ n_{\mathrm{o},+}^S n_{\mathrm{o},-}^S n_{\mathrm{e},+}^S n_{\mathrm{e},-}^S = 0. \qquad (56)$$

We further define

$$\mathcal{Q}_2^\wedge:\ \mathcal{Q}_2^S \text{ for all } S. \qquad (57)$$

Thus, if $\mathcal{Q}_2^\wedge$ is violated, *i.e.*, if $\mathcal{Q}_2^S$ is violated at any S, then the boundary deformation around S can change both $\mathrm{Eu}_2^{\mathrm{o}}$ and $\mathrm{Eu}_2^{\mathrm{e}}$ by arbitrary integers, so that there are no topological invariants at level-2.

Second Stiefel-Whitney invariant — The boundary deformations at 1-cells do not affect $\mathbb{Z}_2$-valued SW_2, since the contributions from its two copies always cancel out. On the other hand, boundary deformations at the 0-cells with nontrivial topology in both factors of $\pi_1[\mathcal{X}_S]$, if they exist, can add arbitrary integers to SW_2, rendering the topology at level-2 trivial.

Summary

Table VII summarizes the classification for C_2-symmetric gapped band structures with time-reversal symmetry. To obtain the fragile and stable classifications, besides taking the limits $n_{\mathrm{e}} \gg 1$ or $n_{\mathrm{o}}, n_{\mathrm{e}} \gg 1$, one must also verify compatibility of the various conditions for the existence of these invariants with the rules of fragile and stable topology. In particular, the conditions $\mathcal{Q}_1^S$ and $\mathcal{Q}_2^{\mathrm{e}}$ are incompatible with fragile classification rules, since the latter allows for addition of unoccupied bands with arbitrary band representations. Furthermore, $\mathcal{Q}_2^\wedge$ and $\mathcal{Q}_2^{\mathrm{o}}$ become equivalent, since $n_{\mathrm{e},\pm} > 0$ after a possible addition of empty bands. Finally, all of these conditions are incompatible with the rules of stable classification, which allows for adding occupied/empty bands with arbitrary band representations. Thus, there are no

		Level 1	Level 2	Level 3
A	$n_{\mathrm{o}} = n_{\mathrm{e}} = 1$	—	C_z, $C^{\Gamma Y}$, C^{YM}, $C^{MX} \in \mathbb{Z}$, one less for every violation of $\mathcal{Q}_1^S$	if $C_z = 0$: $H \in \mathbb{Z}$
				if $C_z \neq 0$: $H \in \mathbb{Z}_{2C_z}$
	$n_{\mathrm{o}}, n_{\mathrm{e}} \geq 1,$ $n_{\mathrm{o}} + n_{\mathrm{e}} > 2$	—	$C \in \mathbb{Z}$ [S]; $C^{\Gamma Y}$, C^{YM}, $C^{MX} \in \mathbb{Z}$, one less for every violation of $\mathcal{Q}_1^S$	—
AI	$n_{\mathrm{o}} = n_{\mathrm{e}} = 1$	Two copies of invariants from Tab. VII	$C^{\Gamma Y}$, C^{YM}, $C^{MX} \in \mathbb{Z}$, one less for every violation of $\mathcal{Q}_1^S$	$H \in \mathbb{Z}$
	$n_{\mathrm{o}}, n_{\mathrm{e}} \geq 1,$ $n_{\mathrm{o}} + n_{\mathrm{e}} > 2$	Two copies of invariants from Tab. VII	two copies of invariants from Tab. VII [F]; $C^{\Gamma Y}$, C^{YM}, $C^{MX} \in \mathbb{Z}$, one less for every violation of $\mathcal{Q}_1^S$	—

TABLE VIII. Homotopic classification of gapped band structures with C_2 symmetry in three dimensions. The condition $\mathcal{Q}_1^S$ is given in Eq. (49). Nontrivial fragile and stable invariants are denoted with [F] and [S], respectively.
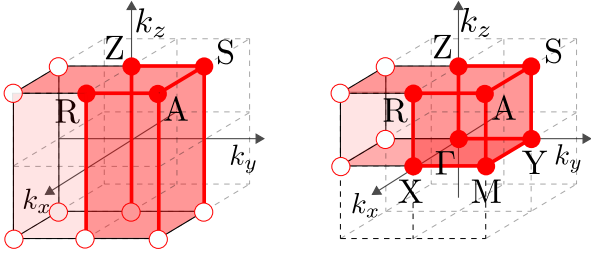

FIG. 9. Fundamental domains $\mathbb{D}$ for a three-dimensional band structure with twofold rotation symmetry without (left) and with (right) time-reversal symmetry.

C_2-symmetric stable topological phases. For $n_{\mathrm{e}} \gg 1$, we get the classification of fragile phases consistent with the fragile band structures identified via topological quantum chemistry [54]. The delicate topological invariants agree with those obtained by Kobayashi and Furusaki [31].

We also encounter our first example of *representation-protected stable topology*, whereby a stable topological phase exists if we constrain the band representations such that the condition $\mathcal{Q}_2^\wedge$ is always satisfied, without limiting the number of occupied and unoccupied bands. This can be ensured by demanding that all bands at each 0-cell must have the same parity. To ensure the representation constraint in real space, we turn to the EBRs [54, 55, 77] of a C_2-symmetric band structure, listed in Tab. XV. Since each EBR, labelled by a special Wyckoff position and a parity, corresponds to a fixed set of parities at each 0-cell, we can ensure a representation-protected stable phase only by allowing a *single* orbital type at a single Wyckoff position. Inspection of Tab. XV further shows that the presence of multiple EBRs always leads to the existence of different parity bands at at least one of the high-symmetry points, thereby violating the condition for representation-protected stable topology.

C. Classification in three dimensions

1. Without time-reversal symmetry

The fundamental domain is a cuboid as shown in Fig. 9(left). There are no level-1 invariants, as follows for horizontal and vertical 1-cells from the 2d classification and Sec. IV, respectively. At level-2, the parent invariants are Chern numbers for each 2-cell. For the horizontal 2-cell, C_z is robust to boundary deformations and can be computed for any fixed-k_z slice of $\mathbb{D}$. For the vertical 2-cells, boundary deformations at the vertical line through a 0-cell S can add arbitrary integers to all $C^{SS'} = -C^{S'S}$. Such deformations are allowed if $\pi_1[\mathcal{X}_S] \neq 0$, *i.e.*, if $\mathcal{Q}_1^S$ (Eq. (47)) is violated. Thus, the number of level-2 invariants associated with vertical faces is one less than the number of 0-cells satisfying $\mathcal{Q}_1^S$. These invariants were previously identified by Nelson *et al.* [78], who refer to them as "returning Thouless pump". At level-3, we get the $\mathbb{Z}$-valued Hopf invariant when $n_{\mathrm{o}} = n_{\mathrm{e}} = 1$. This reduces to a $\mathbb{Z}_{2C_z}$-valued invariant if $C_z \neq 0$.

2. With time-reversal symmetry

The fundamental domain is a cuboid as shown in Fig. 9(right). At level-0, level-1, and level-2, we get two independent sets of topological invariants as for the two-dimensional case, associated with the planes $k_z = 0$ and $k_z = \pi$. At level-2, we additionally get three Chern numbers as parent invariants, associated with the vertical faces of $\mathbb{D}$. The conditions for their robustness with respect to boundary deformations is the same as in the case of broken time-reversal symmetry. At level-3, we get the Hopf invariant if $n_{\mathrm{o}} = n_{\mathrm{e}} = 1$, which is always $\mathbb{Z}$-valued, since the Chern number associated to a cross section of $\mathbb{D}$ at constant k_z vanishes.

These classification results are summarized in Table VIII. Fragile and stable invariants in 3d derive entirely from those in 2d (see Sec. VI B).
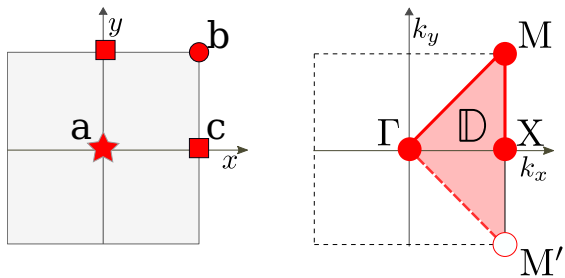
FIG. 10. (Left) The Wyckoff positions for a square lattice with C_4 symmetry. (Right) The fundamental domains $\mathbb{D}$ for two-dimensional band structures with C_4 symmetry.

3. Anomalous boundary states

In the absence of time-reversal symmetry, a nontrivial Chern number C_z for the horizontal 2-cell indicates a weak Chern-insulator phase, which is a stable topological phase with topologically protected chiral surface states on surfaces parallel to the rotation axis.

In the presence of time-reversal symmetry, we get a pair of surface Dirac cones related by C_2 [31], which are associated with a nontrivial representation-protected stable topology if the level-2 invariants at $k_z = 0, \pi$ are different. From the boundary perspective, following the C_2T-symmetric case (Sec. V C 2), a single Dirac node in the fundamental domain implies that $\det W^{o/e}(\partial\mathbb{D}) = -1$, which violates the level-1 compatibility constraint of Eq. (47). This condition cannot be satisfied for a lattice model with only orbitals of a single parity at a single Wyckoff position, as evident from the EBRs of Tab. XV. Hence, a surface band structure with a pair of Dirac cones (or an odd number of such pairs) is anomalous under the rules of representation-protected stable topology.

VII. C_4 SYMMETRY

A four-band lattice model of spinless electrons in three dimensions with C_4 and T symmetries was introduced by Fu, as an early example of topology protected by a crystalline symmetry [39]. Song, Elcoro, and Bernevig discuss a model of spinless electrons with C_4 symmetry in two dimensions and show that it is topologically inequivalent to a insulator with localized orbitals under the rules of fragile topology. Both of these are particularly instructive, because, depending on the precise constraints imposed, they exhibit nontrivial stable, fragile, or delicate topology. Previous theoretical analyses of these models have identified multiple topological invariants specific to delicate or fragile classifications [29–31, 35–37]. We now show how these invariants arise in the framework of a systematic homotopic classification.

A. Wyckoff positions and basis orbitals

With fourfold rotation symmetry, there are three special Wyckoff positions "a", "b", and "c", as well as one pair of generic Wyckoff positions "g", as shown in Fig. 10. The special Wyckoff positions "a" and "b" have fourfold rotation symmetry, whereas the special Wyckoff position "c" has twofold rotation symmetry only. Correspondingly, one may choose a basis of orbitals at the Wyckoff positions that transform under one of the irreducible representations of the fourfold or twofold rotation operation, respectively. For "a" and "b", this means that orbitals can be of s, d, or $p\pm$ type, corresponding to eigenvalue 1, -1, or $\pm i$ under fourfold rotation. With time-reversal symmetry the $p\pm$ orbitals must be combined into a doublet of p orbitals that transforms under a two-dimensional representation of a fourfold rotation. For the two "c" positions, orbitals are even $(+)$ or odd $(-)$ under twofold rotation. Combining orbitals at the two "c" positions, a pair of even-parity orbitals may be rearranged as one s orbital and one d orbital, whereas the pair of odd-parity orbitals may be arranged as a pair of p orbitals. Finally, at the generic Wyckoff position orbitals appear in quartets that can be arranged as one s orbital, one d orbital, and a pair of p orbitals. The parity of s and d orbitals under twofold rotation is even $(+)$; the parity of p orbitals under twofold rotation is odd $(-)$.

The reciprocal-space group G_Λ is generated by fourfold rotation g_4 and two reciprocal-space translations g_x and g_y. The corresponding representation matrices $C(g)$ (cf. Eq. (4)) are denoted C_4, Λ_x, and Λ_y, respectively. The Bloch Hamiltonian satisfies

$$H(k_x, k_y) = C_4 H(-k_y, k_x)C_4^\dagger \tag{58}$$

for a fourfold rotation, as well as Eq. (5) under $g_{x,y}$. Since the matrices C_4, Λ_x, and Λ_y generate a representation of G_Λ, they satisfy

$$C_4\Lambda_x = \Lambda_y C_4, \qquad C_4\Lambda_y = \Lambda_x^\dagger C_4. \tag{59}$$

We choose the overall phase factor of C_4 such that $C_4^4 = \mathbb{1}$. In its eigenbasis, it can be written explicitly as

$$C_4 = \mathrm{diag}\{\mathbb{1}_{n_s}, -\mathbb{1}_{n_d}, i\mathbb{1}_{n_{p+}}, -i\mathbb{1}_{n_{p-}}\}. \tag{60}$$

In the presence of time-reversal symmetry, the $p_\pm$ orbitals always come in pairs, and changing to a basis where C_4 is manifestly real, we can write

$$C_4 = \mathrm{diag}\{\mathbb{1}_{n_s}, -\mathbb{1}_{n_d}, i\sigma_2 \mathbb{1}_{n_p}\}. \tag{61}$$

Explicit expresions for $\Lambda_{x,y}$ are derived in Appendix B 2.

We take the fundamental domain $\mathbb{D}$ as the right quadrant of the Brillouin zone enclosed between the lines $k_y = \pm k_x$, as shown in Fig. 10. It consists of three 0-cells, two 1-cells and one 2-cell. The little groups of the 0-cells are $G_\Gamma \cong G_M \cong C_4$ and $G_X \cong \mathbb{Z}_2$, with G_Γ generated by the fourfold rotation $g_\Gamma = g_4$, G_M generated by

$g_{\mathrm{M}} = g_x^{-1} g_4$ and G_{X} by the twofold rotation followed by a reciprocal lattice translation $g_{\mathrm{X}} = g_x^{-1} g_4^2$. The corresponding matrices $C_S \equiv C(g_S)$ are thus given by

$$C_\Gamma = C_4,$$
$$C_{\mathrm{M}} = \Lambda_x^\dagger C_4 = C_4 \Lambda_y,$$
$$C_{\mathrm{X}} = \Lambda_x^\dagger C_4^2 = C_4^2 \Lambda_x \qquad (62)$$

and satisfy

$$C_{\mathrm{X}} C_{\mathrm{M}} C_\Gamma = \mathbb{1}. \qquad (63)$$

We can derive the spectrum of these matrices without knowing their explicit form. By definition, $C_\Gamma^4 = \mathbb{1}$, and furthermore, using Eq. (59), we get

$$C_{\mathrm{M}}^4 = \left(\Lambda_x^\dagger C_4 \right)^4 = \Lambda_x^\dagger \Lambda_y^\dagger C^4 \Lambda_x \Lambda_y = \mathbb{1}. \qquad (64)$$

Thus, the spectrum of $C_{\Gamma,\mathrm{M}}$ is $\{1, -1, \mathrm{i}, -\mathrm{i}\}$, corresponding to $\{s, d, p_+, p_-\}$-type orbitals. in the presence of time-reversal symmetry, the $p_\pm$-type orbitals always come in pairs. Finally,

$$C_{\mathrm{X}}^2 = (\Lambda_x^\dagger C_4^2)(C_4^2 \Lambda_x) = \Lambda_x^\dagger \Lambda_x = \mathbb{1}, \qquad (65)$$

so that the spectrum of C_{X} consists of ± 1, $i.e.$, an even and an odd orbital. The EBRs for a C_4-symmetric band structure are listed in the appendix, see Table XVII.

B. Homotopic classification in two dimensions

The homotopic classification for this case closely follows that for C_2-symmetric band structures described in Sec. VI B. We summarize these results in Tab. IX.

1. Without time-reversal symmetry

The level-0 invariants are given by $n_{\mathrm{o/e},\rho}^S$, the number of occupied/empty bands at S, with $\rho \in \{s, p_\pm, d\}$ for $S = \Gamma, \mathrm{M}$ and $\rho \in \{\pm\}$ for $S = \mathrm{X}$. The "level-0 compatibility relation" (Eq. (7)) reads

$$n_{\mathrm{o/e}} = \sum_{\rho \in \{s, p_\pm, d\}} n_{\mathrm{o/e},x}^S = \sum_{\rho = \pm} n_{\mathrm{o/e},\rho}^{\mathrm{X}}, \qquad (66)$$

where $S = \Gamma, \mathrm{M}$. Additionally, there are constraints on the level-0 invariants that follow from Eq. (63). The target spaces for the 0-cells are given by

$$\mathcal{X}_S = \prod_\rho \mathrm{Gr}_{\mathbb{C}} \left(n_{\mathrm{o},\rho}^S, n_{\mathrm{o},\rho}^S \right), \qquad (67)$$

where the direct product is over $\rho = s$, d, $p+$, and $p-$ for $S = \Gamma$, M and $\rho = \pm$ for $S = \mathrm{X}$. For the 1-cells and the 2-cell, the target space is $\mathcal{X} = \mathrm{Gr}_{\mathbb{C}}(n_{\mathrm{o}}, n_{\mathrm{e}})$.

At level-1, there are no topological invariants, while at level-2, we get a $\mathbb{Z}$-valued topological invariant, viz, the Chern number, irrespective of the level-0 invariants. The latter is robust to boundary deformations following an argument identical to Sec. VI.

2. With time-reversal symmetry

In the presence of time-reversal symmetry, the p bands always come in pairs at the high-symmetry points $S = \Gamma$, M. Denoting the number of these doublets by $n_{\mathrm{o/e},p}^S$, the level-0 invariants for the Γ and M point are $(n_{\mathrm{o/e},s}^S, n_{\mathrm{o/e},d}^S, n_{\mathrm{o/e},p}^S)$, while those at X are identical to the time-reversal broken case. The level-0 compatibility relation (7) takes the form

$$n_{\mathrm{o/e}} = n_{\mathrm{o/e},+}^{\mathrm{X}} + n_{\mathrm{o/e},-}^{\mathrm{X}}$$
$$= n_{\mathrm{o/e},s}^S + n_{\mathrm{o/e},d}^S + 2 n_{\mathrm{o/e},p}^S, \qquad (68)$$

where $S = \Gamma, M$. The level-0 invariants also satisfy the level-1 compatibility condition

$$n_{\mathrm{o/e},-}^{\mathrm{X}} = n_{\mathrm{o/e},d}^\Gamma + n_{\mathrm{o/e},d}^{\mathrm{M}} \quad \mathrm{mod} \ 2, \qquad (69)$$

which will be derived below. The target spaces for the high-symmetry points are given by

$$\mathcal{X}_S = \mathrm{Gr}_{\mathbb{R}}(n_{\mathrm{o},s}^S, n_{\mathrm{e},s}^S) \times \mathrm{Gr}_{\mathbb{R}}(n_{\mathrm{o},d}^S, n_{\mathrm{e},d}^S) \times \mathrm{Gr}_{\mathbb{C}}(n_{\mathrm{o},p}^S, n_{\mathrm{e},p}^S),$$
$$\mathcal{X}_{\mathrm{X}} = \mathrm{Gr}_{\mathbb{R}} \left(n_{\mathrm{o},+}^{\mathrm{X}}, n_{\mathrm{e},-}^{\mathrm{X}} \right) \times \mathrm{Gr}_{\mathbb{R}} \left(n_{\mathrm{o},-}^{\mathrm{X}}, n_{\mathrm{e},-}^{\mathrm{X}} \right), \qquad (70)$$

where $S = \Gamma, \mathrm{M}$. To see that the target space for p orbitals is a complex Grassmannian, we note that for p-orbitals, we can choose a basis where $C_S = \mathbb{1}_{n_p^S} \otimes \mathrm{i}\sigma^2$, where $n_p^S = n_{\mathrm{o},p}^S + n_{\mathrm{e},p}^S$. Any H_S that commutes with C_S can thus be written as

$$H_S = h_S \otimes \sigma^0 + \mathrm{i} h_S' \otimes \sigma^2,$$

where h_S amd $h_{S'}$ are n_p^S-dimensional real-valued symmetric and antisymmetric matrices, respectively. Hence, the $2 n_p^S$-dimensional real symmetric matrix H_S can equivalently be represented by the complex n_p^S-dimensional matrix $h_S + \mathrm{i} h_S'$.

Classification on 1- and 2-cells

The parent invariants at level-1 and -2 are identical to that of C_2-symmetric band structures described in Sec. VI. The effect of boundary deformations is also quite similar, so that we only describe the difference from the C_2-symmetric case. The condition of Eq. (49) for the triviality of $\pi_1[\mathcal{X}_S]$ now reads

$$\mathcal{Q}_1^S : \begin{cases} n_{\mathrm{os}}^S n_{\mathrm{es}}^S = n_{\mathrm{od}}^S n_{\mathrm{ed}}^S = 0, & S = \Gamma, \mathrm{M}, \\ n_{\mathrm{o}+}^S n_{\mathrm{e}+}^S = n_{\mathrm{o}-}^S n_{\mathrm{e}-}^S = 0, & S = \mathrm{X}. \end{cases} \qquad (71)$$

No condition is imposed on the level-0 invariants associated with the p-orbital, since the corresponding factor in $\mathcal{X}_S$ is a complex Grassmannian.

At level-1, the band structure is always trivial when $n_{\mathrm{o}} = n_{\mathrm{e}} = 1$, since the existence of a first Euler invariant requires that $\mathcal{Q}_1^S$ be satisfied $\forall S$, which is incompatible

	Bands	Additional condition(s)	Topological invariant
A, Level 1	$n_\mathrm{o}, n_\mathrm{e} \geq 1$		——
A, Level 2	$n_\mathrm{o}, n_\mathrm{e} \geq 1$	—	$C \in \mathbb{Z}$ [S]
AI, Level 1	$n_\mathrm{o} = n_\mathrm{e} = 1$		——
	$n_\mathrm{o} \geq 1, n_\mathrm{e} > 1$	—	$\mathrm{SW}_1^{\Gamma\mathrm{M}}, \mathrm{SW}_1^{\mathrm{MX}} \in \mathbb{Z}_2$
	or $n_\mathrm{o} > 1, n_\mathrm{e} \geq 1$		one less for every violation of $\mathcal{Q}_1^S$
AI, Level 2	$n_\mathrm{o} = n_\mathrm{e} = 1$		——
	$n_\mathrm{o} = 1, n_\mathrm{e} = 2$	if $\mathcal{Q}_1^\vee$ and $\mathcal{Q}_2^\mathrm{e}$	$\mathrm{Eu}_2^\mathrm{e} \in 2\mathbb{Z}$
		if $\mathcal{Q}_2^\mathrm{e}$, but not $\mathcal{Q}_1^\vee$	$\mathrm{Eu}_2^\mathrm{e} \in 2\mathbb{N}$
		if not $\mathcal{Q}_2^\mathrm{e}$	$\mathrm{Eu}_2^\mathrm{e} \in \mathbb{Z}_2$
	$n_\mathrm{o} = 1, n_\mathrm{e} > 2$		——
	$n_\mathrm{o} = n_\mathrm{e} = 2$	if $\mathcal{Q}_1^\vee$ and $\mathcal{Q}_2^\mathrm{e}$ and $\mathcal{Q}_2^\mathrm{o}$	$(\mathrm{Eu}_2^\mathrm{o}, \mathrm{Eu}_2^\mathrm{e}) \in \mathbb{Z}^2|_\mathrm{p}$
		if $\mathcal{Q}_2^\mathrm{e}$ and $\mathcal{Q}_2^\mathrm{o}$, but not $\mathcal{Q}_1^\vee$	$(\mathrm{Eu}_2^\mathrm{o}, \mathrm{Eu}_2^\mathrm{e}) \in \mathbb{N} \times \mathbb{Z}|_\mathrm{p}$
		if $\mathcal{Q}_1^\vee$ and $\mathcal{Q}_2^\mathrm{o}$, but not $\mathcal{Q}_2^\mathrm{e}$	$\mathrm{Eu}_2^\mathrm{o} \in \mathbb{Z}$
		if $\mathcal{Q}_1^\vee$ and $\mathcal{Q}_2^\mathrm{e}$, but not $\mathcal{Q}_2^\mathrm{o}$	$\mathrm{Eu}_2^\mathrm{e} \in \mathbb{Z}$
		if $\mathcal{Q}_2^\mathrm{o}$, but not $\mathcal{Q}_1^\vee$ and not $\mathcal{Q}_2^\mathrm{e}$	$\mathrm{Eu}_2^\mathrm{o} \in \mathbb{N}$
		if $\mathcal{Q}_2^\mathrm{e}$, but not $\mathcal{Q}_1^\vee$ and not $\mathcal{Q}_2^\mathrm{o}$	$\mathrm{Eu}_2^\mathrm{e} \in \mathbb{N}$
		if $\mathcal{Q}_2^\wedge$, but not $\mathcal{Q}_2^\mathrm{e}$ and not $\mathcal{Q}_2^\mathrm{o}$	$\mathrm{SW}_2 \in \mathbb{Z}_2$
		if not $\mathcal{Q}_2^\wedge$	—
	$n_\mathrm{o} = 2, n_\mathrm{e} > 2$	if $\mathcal{Q}_1^\vee$ and $\mathcal{Q}_2^\mathrm{o}$	$\mathrm{Eu}_2^\mathrm{o} \in \mathbb{Z}$
		if $\mathcal{Q}_2^\mathrm{o}$, but not $\mathcal{Q}_1^\vee$	$\mathrm{Eu}_2^\mathrm{o} \in \mathbb{N}$ [F]
		if $\mathcal{Q}_2^\wedge$, but not $\mathcal{Q}_2^\mathrm{o}$	$\mathrm{SW}_2 \in \mathbb{Z}_2$
		if not $\mathcal{Q}_2^\wedge$	—
	$n_\mathrm{o}, n_\mathrm{e} > 2$	if $\mathcal{Q}_2^\wedge$	$\mathrm{SW}_2 \in \mathbb{Z}_2$ [F]
		if not $\mathcal{Q}_2^\wedge$	—

TABLE IX. Homotopic classification of spinless gapped band structures with C_4 symmetry in two dimensions for various possible combinations of number of bands and level 0 invariants, the latter encoded in the $\mathcal{Q}$'s. In particular, $\mathcal{Q}_1^S$, $\mathcal{Q}_2^{\mathrm{o/e}}$, and $\mathcal{Q}_2^S$ are defined by Eqs. (71), (73), and (74), respectively. The condition $\mathcal{Q}_1^\wedge$ holds if $\mathcal{Q}_1^S \forall S$, $\mathcal{Q}_1^\vee$ holds if $\exists S$ where $\mathcal{Q}_1^S$ is true, and $\mathcal{Q}_2^\wedge$ holds if $\mathcal{Q}_2^S \forall S$. The set $\mathbb{Z}^2|_\mathrm{p}$ consists of all ordered integer pairs (p,q) with $p = q \mod 2$; the set $\mathbb{N} \times \mathbb{Z}_\mathrm{p}$ consists of all ordered integer pairs (p,q) with $p \geq 0$ and $p = q \mod 2$. The invariants are only specified for $n_\mathrm{o} \leq n_\mathrm{e}$, since the classification is symmetric under $n_\mathrm{o} \leftrightarrow n_\mathrm{e}$. The fragile and stable topological phases are marked by [F] and [S], respectively.

Allowed EBRs	Level 1	Level 2
$p_\mathrm{a}, p_\mathrm{b}$	$\mathbb{Z}_2$	$\mathbb{Z}_2$
$p_\mathrm{a} \oplus p_\mathrm{b}$	$\mathbb{Z}_2$	0
$s_\mathrm{a}, s_\mathrm{b}, d_\mathrm{a}, d_\mathrm{b}$	0	$\mathbb{Z}_2$

TABLE X. Representation-protected stable topology: Restrictions to certain EBRs (combinations of orbital types and Wyckoff positions) allow for a nontrivial stable representation-protected classification in the presence of time-reversal symmetry. The first row indicates that we can have either p_a or p_b *but not both*, while $p_\mathrm{a} \oplus p_\mathrm{b}$ means that p-orbitals are allowed simultaneously at Wyckoff positions a and b.

with Eq. (69). In the stable limit, there are up to two first Stiefel-Whitney invariants and every violation of $\mathcal{Q}_1^S$ effectively removes one of these. The level-1 compatibility condition, following from the triviality of the Wilson loop around the boundary of the 2-cell, reads

$$1 = \prod_S \det C_S^{\mathrm{o/e}} = (-1)^{n_{\mathrm{o/e},d}^{\Gamma} + n_{\mathrm{o/e},d}^{\mathrm{M}} + n_{\mathrm{o/e},-}^{\mathrm{X}}}, \quad (72)$$

which is equivalent to Eq. (69).

At level-2, the analogue of condition $\mathcal{Q}_2^{\mathrm{o/e}}$ (Eq. (55)) now reads

$$\mathcal{Q}_2^{\mathrm{o/e}}: \; n_{\mathrm{o/e},s}^S n_{\mathrm{o/e},d}^S = n_{\mathrm{o/e},+}^X n_{\mathrm{o/e},-}^X = 0, \quad (73)$$

with $S \in \{\Gamma, \mathrm{M}\}$, and $\mathcal{Q}_2^S$ (Eq. (55)) becomes

$$\mathcal{Q}_2^S: \begin{cases} n_{os}^S n_{es}^S n_{od}^S n_{ed}^S = 0, & S = \Gamma, \mathrm{M}, \\ n_{\mathrm{o}+}^S n_{\mathrm{e}+}^S n_{\mathrm{o}-}^S n_{\mathrm{e}-}^S = 0, & S = \mathrm{X}, \end{cases} \quad (74)$$

and we again define $\mathcal{Q}_2^\wedge$ as $\mathcal{Q}_2^S \forall S$. Thus, Eu_2 is $\mathbb{N}$-valued if $\mathcal{Q}_1^S$ is violated $\forall S$, $\mathbb{Z}_2$-valued if $\mathcal{Q}_2^{\mathrm{o/e}}$ are violated, and trivial if $\mathcal{Q}_2^S$ is violated for any S, while SW_2 is is $\mathbb{Z}_2$-valued if $\mathcal{Q}_2^\wedge$ holds and trivial otherwise.

		level 1	level 2	level 3
A	$n_{\mathrm{o}} = n_{\mathrm{e}} = 1$	—	C_z, $C^{\Gamma M}$, $C^{MX} \in \mathbb{Z}$, one less for every violation of $\mathcal{Q}_1^{Sz}$	if $C_z = 0$: $H \in \mathbb{Z}$ if $C_z \neq 0$: $H \in \mathbb{Z}_{2C_z}$
	$n_{\mathrm{o}}, n_{\mathrm{e}} \geq 1$, $n_{\mathrm{o}} + n_{\mathrm{e}} > 2$	—	$C_z \in \mathbb{Z}$ [S]; $C^{\Gamma M}$, $C^{MX} \in \mathbb{Z}$, one less for every violation of $\mathcal{Q}_1^{Sz}$	—
AI	$n_{\mathrm{o}} = n_{\mathrm{e}} = 1$	two copies of invariants from Tab. IX	$C^{\Gamma M}$, $C^{MX} \in \mathbb{Z}$, one less for every violation of $\mathcal{Q}_1^{Sz}$	$H \in \mathbb{Z}$
	$n_{\mathrm{o}}, n_{\mathrm{e}} \geq 1$, $n_{\mathrm{o}} + n_{\mathrm{e}} > 2$	two copies of invariants from Tab. VII	two copies of invariants from Tab. IX [F]; $C^{\Gamma M}$, $C^{MX} \in \mathbb{Z}$, one less for every violation of $\mathcal{Q}_1^{Sz}$	—

TABLE XI. Homotopic classification of spinless gapped band structures with C_4 in three dimensions. The condition $\mathcal{Q}_1^{Sz}$ is given in Eq. (76). Nontrivial fragile and stable invariants are marked with "[F]" and "[S]", respectively.
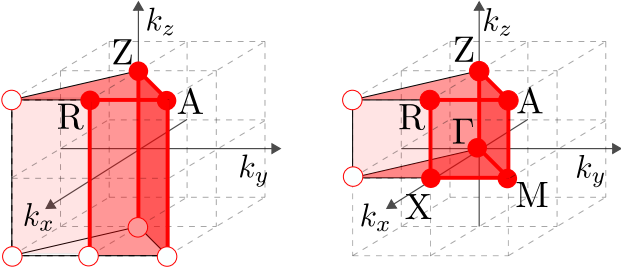
FIG. 11. Fundamental domains $\mathbb{D}$ for a three-dimensional band structure with fourfold rotation symmetry without (left) and with (right) time-reversal symmetry.

These results are summarized in Table IX.

Summary

To obtain the fragile and stable classification from the results listed in Table IX, we again need to check whether the various conditions for the existence of topologically nontrivial phases are compatible with the rules of the corresponding topology. For $n_{\mathrm{o,e}} \gg 1$, there are no stable topological phases, since the required conditions $\mathcal{Q}_1^S$ or $\mathcal{Q}_2^{\wedge}$ are both incompatible with the rules of stable topology. However, imposing either of these conditions, we get representation-protected stable topological phases. Unlike the case of C_2, these phases can have a nontrivial level-1 invariant, since $\mathcal{Q}_1^S$ for $S = \Gamma, M$ does not include the p-type orbitals, so that they are satisfied for arbitrary number of p-orbitals. In Table X, we list all possible EBRs (i.e., combinations of Wyckoff positions and allowed orbital types) for which such a phase exists.

C. Classification in three dimensions

The 3d classification is again analogous to those for C_2 symmetry discussed in Sec. VI C.

1. Without time-reversal symmetry

The fundamental domain is a triangular prism depicted in Fig. 11 (left). There are no level-1 invariants. At level-2, we get Chern numbers for each face of $\mathbb{D}$, where C_z for the horizontal face is robust. For the vertical faces, boundary deformations at vertical line through a 0-cell S can add arbitrary integers to all $C^{SS'}$ if $\pi_1[\mathcal{X}_S] \neq 0$, which happens if

$$\mathcal{Q}_1^{S,z}: \ n_{\mathrm{o},\rho}^S n_{\mathrm{e},\rho}^S = 0 \ \forall \rho \tag{75}$$

is violated, where ρ runs over the irreps of G_S, i.e., $\rho \in \{s, d, p_+, p_-\}$ for $S = \Gamma, M$ and $\rho \in \{+, -\}$ for $S = X$. At level-3, we get the $\mathbb{Z}$-valued Hopf invariant if $n_{\mathrm{o}} = n_{\mathrm{e}} = 1$, which reduces to a $\mathbb{Z}_{2C_z}$-valued if $C_z \neq 0$.

2. With time-reversal symmetry

The fundamental domain is a triangular prism based depicted in Fig. 11(right). We get two independent copies of the 2d classification problem (Sec. VII B) at levels 0, 1, and 2, as well as Chern numbers $C^{SS'}$ for each of the vertical faces of $\mathbb{D}$. Boundary deformations can add arbitrary integers to $C^{SS'}$ if

$$\mathcal{Q}_1^{S,z}: \ n_{\mathrm{o},\rho}^S n_{\mathrm{e},\rho}^S = 0 \ \forall \rho \tag{76}$$

is violated, where ρ now runs over the *real* irreps of G_S, i.e., $\rho \in \{s, d, p\}$ for $S = \Gamma, M$ and $\rho \in \{+, -\}$ for $S = X$. At level-3, we get the $\mathbb{Z}$-valued Hopf invariant.

These classification results are summarized in Tab. XI.

3. Anomalous boundary states

Without time-reversal symmetry, a nonzero Chern number at fixed k_z signals a weak Chern-insulator phase.

Irrep.	$\{\mathbb{1}\}$	$\{C_4, C_4^{-1}\}$	$\{C_2\}$	$\{M_x, M_y\}$	$\{M_d, M_{\bar{d}}\}$
A_1	1	1	1	1	1
A_2	1	1	1	-1	-1
A_3	1	-1	1	1	-1
A_4	1	-1	1	-1	1
B	2	0	-2	0	0

TABLE XII. The character table of D_4. The character corresponding to $\{\mathbb{1}\}$ is equal to the dimensionality of the representation.
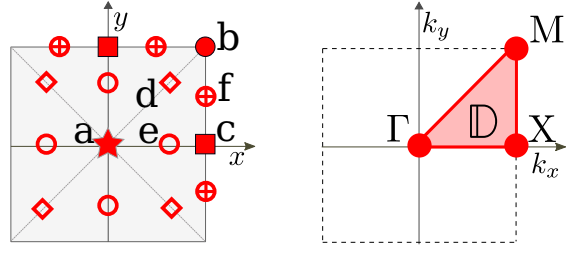

FIG. 12. (Left) The Wyckoff positions for a square lattice with D_4 symmetry. (Right) The fundamental domains $\mathbb{D}$ for two-dimensional band structures with D_4 symmetry.

With time-reversal symmetry, we get anomalous surface modes associated with the nontrivial representation-protected stable topology. A difference in the level-1 topological invariants between $k_z = 0$ and π leads to a protected quadratic band touching at the $\bar{\Gamma}$ and $\bar{M}$ points in the surface Brillouin zone, while a difference in level-2 invariants is associated with the presence of a set of four surface Dirac cones related by C_4 [31].

From the boundary perspective, an odd number of Dirac cones in the fundamental domain is anomalous when we restrict to a single orbital type at a single Wyckoff position. This follow from the violation of the level-1 compatibility condition (Eq. (69)), as in the case of the surface Dirac cones for C_2. On the other hand, a single quadratic band touching at $\bar{\Gamma}$ or $\bar{M}$ comes with an *odd* number of levels crossing the Fermi energy between $\bar{\Gamma}$ and $\bar{M}$. However, for band structures with only p-orbitals, the number of occupied bands at $\bar{\Gamma}$ and $\bar{M}$ must be even, rendering the quadratic band touching anomalous.

VIII. D_4 SYMMETRY

Dihedral groups D_n are the groups of symmetries of regular polygons, which includes rotation as well as reflections. The homotopic classification of D_4-symmetric band structures is instructive for two reasons: (i) D_4-symmetry in two dimensions allows for high-symmetry lines, in contrast to C_n, which only has high-symmetry points, and (ii) The group D_4 is nonabelian, so that not all of its irreps are one-dimensional. Explicitly, the group D_4 can be defined as

$$D_4 = \{\mathbb{1}, C_4, C_2, C_4^{-1}, M_x, M_y, M_d, M_{\bar{d}}\}, \quad (77)$$

where C_N denotes the N-fold rotation and $M_{x,y,d,\bar{d}}$ denote reflection in the x-axis, y-axis, the lines $y = \pm x$, respectively. The non-commutativity of D_4 can be seen, for instance, in $C_4 M_x = M_d$ while $M_x C_4 = M_{\bar{d}}$. The irreps of D_4 are listed in the its character table, which is shown in Table. XII. For the one-dimensional irreps, the characters are the eigenvalues of the corresponding symmetry operator. Thus, irreps A_1, A_3 and A_4 correspond to s, $d_{x^2-y^2}$, and d_{xy} orbitals, while the irrep A_2 requires angular momentum $\ell = 4$. For the two-dimensional irrep

B, we can choose the representation matrices as

$$C_4 = -\mathrm{i}\sigma^2, \qquad M_x = \sigma^3, \quad (78)$$

which act on a doublet formed by the p_x and p_y orbitals. These symmetry operators are also real-valued and thus compatible with time-reversal symmetry.

A. Wyckoff positions, basis orbitals and symmetries

A lattice with D_4 symmetry has six special Wyckoff positions (labelled "a"–"f") as well as the generic Wyckoff position("g"), as shown in Fig. 12. The Wyckoff position "a" and "b" are invariant under the full symmetry group D_4 and thus have a multiplicity of one. The Wyckoff position "c" with multiplicity two is invariant under M_x, M_y, and a C_2 rotation, so that its little group is isomorphic to $\mathbb{Z}_2^2$. The Wyckoff positions "d", "e" and "f" with multiplicity four are invariant under various mirror symmetries, making their little groups isomorphic to $\mathbb{Z}_2$.

The reciprocal space group G_Λ is generated by fourfold rotation g_4, reflection in the k_x-axis m_x, and the reciprocal space translations g_x and g_y. The Bloch Hamiltonian satisfies

$$H(k_x, k_y) = C_4^\dagger H(-k_y, k_x)C_4,$$
$$= M_x^\dagger H(k_x, -k_y)M_x, \quad (79)$$

as well as Eq. (5) for reciprocal space translations. Since the unitary matrices C_4 and M_x generate a representation of D_4, they satisfy

$$C_4^4 = M_x^2 = \mathbb{1}, \quad C_4 M_x C_4 = M_x. \quad (80)$$

The matrices C_4 and M_x cannot be diagonalized simultaneously. Together with Λ_x and Λ_y, they form a representation of G_Λ, so that

$$C_4 \Lambda_x = \Lambda_y C_4, \qquad C_4 \Lambda_y = \Lambda_x^\dagger C_4, \quad (81)$$
$$M_x \Lambda_x = \Lambda_x M_x, \qquad M_x \Lambda_y = \Lambda_y^\dagger M_x. \quad (82)$$

Explicit expressions for the representation matrices for various Wyckoff positions are derived in Appendix B 3.

In two dimensions, we take the fundamental domain $\mathbb{D}$ as the triangle ΓXM, as shown in Fig. 12. It consists of three 0-cells, three 1-cells and one 2-cell. The 0-cells Γ and M are invariant under D_4, while X is invariant under its subgroup $D_2 \cong \mathbb{Z}_2 \times \mathbb{Z}_2$ consisting of the mirror symmetries $M_{x,y}$ and their product $M_x M_y = C_2$. Thus, H_S commutes with two matrices C_S and M_S, which, using Eqs. (81) and (82), are given by

$$
\begin{aligned}
C_\Gamma &= C_4, & M_\Gamma &= M_x, \\
C_M &= \Lambda_x^\dagger C_4 = C_4 \Lambda_y, & M_M &= \Lambda_y^\dagger M_x = M_x \Lambda_y, \\
C_X &= \Lambda_x^\dagger C_4^2 = C_4^2 \Lambda_x, & M_X &= M_x.
\end{aligned} \tag{83}
$$

The matrices C_M and M_M generate a representation of D_4, since $C_M^4 = 1$, $M_M^2 = \Lambda_y^\dagger M_x^2 \Lambda_y = \mathbb{1}$, and

$$
C_M M_M C_M = C_4 M_x C_4 \Lambda_y = M_x \Lambda_y = M_M. \tag{84}
$$

Similarly, C_X and M_X satisfy $C_X^2 = M_X^2 = 1$. Thus, the eigenstates of H_S at $S = \Gamma$, M can be labeled by an irrep of D_4, while those of H_X can be labeled by $(\pm, \pm)$, the eigenvalues of C_X and M_X, respectively.

The 1-cells SS' are invariant under a reflection, so that $H_{SS'}$ satisfies

$$
H(\mathbf{k}) = M_{SS'}^\dagger H(\mathbf{k}) M_{SS'}, \quad \mathbf{k} \in \mathbb{D}_\alpha \tag{85}
$$

with

$$
M_{\Gamma X} = M_x, \quad M_{\Gamma M} = M_d, \quad M_{MX} = \Lambda_x^\dagger M_y. \tag{86}
$$

The bands can thus be labeled by a mirror parity at each 1-cell. There are no additional constraints on the 2-cell.

B. Homotopic classification in two dimensions

The homotopic classification for D_4-symmetric band structures exhibit two features that are distinct from the previously discussed cases:

- The 1-cells have nontrivial little groups, leading to additional level-0 constraints from the gluing of the 0-cells at the ends of the 1-cells.

- All 1-cells occur only once in the fundamental domain, so that we do not get the symmetry-based cancellations of boundary deformations, in contrast to the symmetries discussed previously.

1. Without time-reversal symmetry

The level-0 invariants $n_{o/e,\rho}^S$ count the number of occupied/empty copies of each irrep ρ of the little group G_S of the 0-cells S. Explicitly, for $S \in \{\Gamma, M\}$, $n_{o/e,A_j}^S$ is the number of orbitals transforming under irrep A_j, while $n_{o/e,B}^S$ is the number of *doublets* transforming under the
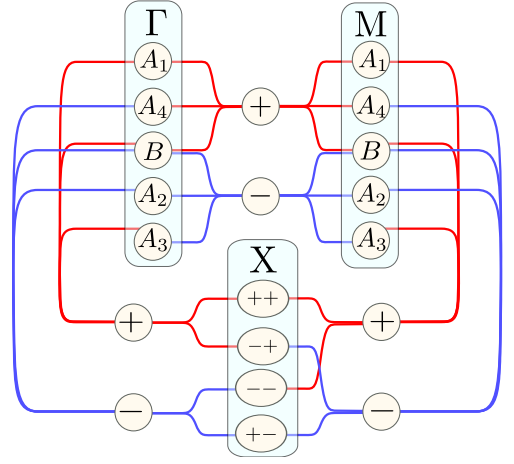

FIG. 13. Splitting rules for the band representations of D_4-symmetric lattices at high-symmetry points/lines. The irreps A_i for $i = 1, 2, 3, 4$ at the Γ and M point are one-dimensional, while the irrep B is two-dimensional.

irrep B. Similarly, numbers $n_{o/e,a}^{SS'}$ of occupied/empty copies of the irreps can also be defined for the 1-cells SS'. The level-0 compatibility relations (7) then read

$$
\begin{aligned}
n_{o/e} &= \sum_{j=1}^4 n_{o/e,A_j}^S + 2 n_{o/e,B}^S \\
&= n_{o/e,++}^X + n_{o/e,+-}^X + n_{o/e,-+}^X + n_{o/e,--}^X \\
&= n_{o/e,+}^{SS'} + n_{o/e,-}^{SS'},
\end{aligned} \tag{87}
$$

where $S = \Gamma$, M. Additional constraints on the level-0 invariants arise from the *splitting rules*, which describe how the two parities at the 1-cell SS' connect to various irreps of G_S as one approaches the end point. For the 1d irreps, the splitting rules can be read off directly from the character table of D_4, while the 2d irrep B connects to one odd and one even state on the 1-cells (see Fig. 13). The resulting constraints are identical at the 0-cells $S = \Gamma$, M, and read

$$
\begin{aligned}
n_{o/e,+}^{\Gamma M} &= n_{o/e,A_1}^S + n_{o/e,A_4}^S + n_{o/e,B}^S, \\
n_{o/e,-}^{\Gamma M} &= n_{o/e,A_2}^S + n_{o/e,A_3}^S + n_{o/e,B}^S, \\
n_{o/e,+}^{SX} &= n_{o/e,A_1}^S + n_{o/e,A_3}^S + n_{o/e,B}^S, \\
n_{o/e,-}^{SX} &= n_{o/e,A_2}^S + n_{o/e,A_4}^S + n_{o/e,B}
\end{aligned} \tag{88}
$$

For the 0-cell X, we get

$$
\begin{aligned}
n_{o/e,+}^{\Gamma X} &= n_{o/e,++}^X + n_{o/e,-+}^X, \\
n_{o/e,-}^{\Gamma X} &= n_{o/e,+-}^X + n_{o/e,--}^X, \\
n_{o/e,+}^{MX} &= n_{o/e,++}^X + n_{o/e,--}^X, \\
n_{o/e,-}^{MX} &= n_{o/e,+-}^X + n_{o/e,-+}^X.
\end{aligned} \tag{89}
$$

For fixed level-0 invariants, the target spaces for the p-cell α with $p = 0, 1$ are given by

$$\mathcal{X}_\alpha = \prod_\rho \mathrm{Gr}_{\mathbb{C}}(n_{\mathrm{o},\rho}^\alpha, n_{\mathrm{o},\rho}^\alpha), \tag{90}$$

where ρ runs over the irreps of the little group G_α. For the 2-cell, we have $\mathcal{X} = \mathrm{Gr}_{\mathbb{C}}(n_{\mathrm{o}}, n_{\mathrm{e}})$.

At level-1, there are no topological invariants, while at level-2, the parent invariant is the Chern number. The parent classification set for boundary deformations K_2^∂ consists of a copy of $\pi_1[\mathcal{X}_S]$ for each 0-cell S and of $\pi_2[\mathcal{X}_{SS'}]$ for each 1-cell SS'. The former are always trivial, while the latter are trivial only if $\mathrm{Gr}_{\mathbb{C}}(n_{\mathrm{o},\pm}^{SS'}, n_{\mathrm{e},\pm}^{SS'})$ degenerates to a point, i.e., if

$$\mathcal{Q}_{1,a}^{SS'} : \ n_{\mathrm{o},a}^{SS'} n_{\mathrm{e},a}^{SS'} = 0 \tag{91}$$

for $a = \pm$. If this condition is violated for either parity at any 1-cell, then boundary deformations can add an arbitrary integer to the level-2 invariant. Thus, there is a $\mathbb{Z}$-valued level-2 invariant if $\mathcal{Q}_{1,a}^{SS'}$ is obeyed for both parities at each 1-cell [79]. This condition also indirectly constraints the level-0 invariants because of the splitting rules. For instance, the presence of irrep B at $S = \Gamma, \mathrm{M}$ violates $\mathcal{Q}_{1,\pm}^{SS'}$, since B splits into an even and an odd orbitals on the adjoining 1-cell.

2. With time-reversal symmetry

The level-0 invariants and the corresponding compatibility conditions are identical to the time-reversal-broken case. The target spaces are now real Grassmannians:

$$\mathcal{X}_\alpha = \prod_\rho \mathrm{Gr}_{\mathbb{R}}(n_{\mathrm{o},\rho}^\alpha, n_{\mathrm{e},\rho}^\alpha) \tag{92}$$

for the p-cell α with $p = 0, 1$ and $\mathcal{X} = \mathrm{Gr}_{\mathbb{R}}(n_{\mathrm{o}}, n_{\mathrm{e}})$ for the 2-cell. In contrast to C_4, the presence of a two-dimensional irrep B at the Γ and M points does not lead to a complex Grassmannian. This is because if H_S transforms under the two-dimensional irrep B, it must commute with the representation matrices for all elements of D_4, i.e., with all matrices of the form $\mathbb{1}_{n_B^S} \otimes \sigma^j$ for $j = 1, 2, 3$. Such matrices can always be written as $H_S = h_S \otimes \sigma^0$, where h_S is a real symmetric matrix.

Classification on 1-cells

There are up to six parent level-1 invariants, since there are two parity sectors for each 1-cell. The type of the level-1 invariants depends on the number $n_{\mathrm{e},s}^{SS'}$ of occupied and empty bands per parity sector a at each 1-cell (in contrast to C_2 and C_4 symmetry, where the type of the level-1 invariants is completely determined by the total numbers of occupied/empty bands). The numbers $n_{\mathrm{o}/\mathrm{e},a}^{SS'}$ are determined by the level-0 invariants $n_{\mathrm{o}/\mathrm{e},\rho}^S$ via

the splitting rules. The level-1 invariant is a first Euler invariant $\mathrm{Eu}_{1,a}^{SS'} = -\mathrm{Eu}_{1,a}^{S'S}$ if $n_{\mathrm{o},a}^{SS'} = n_{\mathrm{e},a}^{SS'} = 1$, a first Stiefel-Whitney invariant $\mathrm{SW}_{1,a}^{SS'}$ if $n_{\mathrm{o},a}^{SS'} > 1$ and $n_{\mathrm{e},a}^{SS'} \geq 1$ or $n_{\mathrm{o},a}^{SS'} \geq 1$ and $n_{\mathrm{e},a}^{SS'} > 1$, whereas no nontrivial level-1 invariant exists if $n_{\mathrm{o},a}^{SS'} = 0$ or $n_{\mathrm{e},a}^{SS'} = 0$.

The classification set of boundary deformations K_1^∂ consists of a copy of $\pi_1[\mathcal{X}_S]$ for each 0-cell S. This means that there are no topologically nontrivial boundary deformations associated with the irrep ρ at S if

$$\mathcal{Q}_{1,\rho}^S : \ n_{\mathrm{o},\rho}^S n_{\mathrm{e},\rho}^S = 0. \tag{93}$$

Boundary deformations at S with irrep ρ only affect level-1 invariants on a 1-cell SS' in parity sector $a = \pm$ if ρ connects to the parity a under the splitting rules (see Fig. 13). For instance, at the Γ-point, the boundary deformation with $\rho = A_4$ only affects two level-1 invariants, viz, the positive parity sector on $\Gamma\mathrm{M}$ and the negative parity sector on $\Gamma\mathrm{X}$. Boundary deformations with $\rho = B$, however, affect both parity sectors on $\Gamma\mathrm{M}$ and $\Gamma\mathrm{X}$, i.e., four level-1 invariants in total. Provided the boundary deformations act independently on the parent level-1 invariants, each violation of $\mathcal{Q}_{1,\rho}^S$ effectively removes one level-1 invariant. (An example in which boundary deformations do not act independently is discussed below.)

The level-1 compatibility relation follows from demanding that the level-1 invariant corresponding to the full target space $\mathcal{X}$ be trivial when computed around $\partial\mathbb{D}$. Thus, for $n_{\mathrm{o}} = n_{\mathrm{e}} = 1$, the compatibility relation reads

$$\sum_{a=\pm} \left(\mathrm{Eu}_{1,a}^{\Gamma\mathrm{M}} + \mathrm{Eu}_{1,a}^{\mathrm{MX}} + \mathrm{Eu}_{1,a}^{\mathrm{X}\Gamma} \right) = 0, \tag{94}$$

while for $n_{\mathrm{o}} > 1$ or $n_{\mathrm{e}} > 1$, we get

$$\sum_{a=\pm} \left(\mathrm{SW}_{1,a}^{\Gamma\mathrm{M}} + \mathrm{SW}_{1,a}^{\mathrm{MX}} + \mathrm{SW}_{1,a}^{\mathrm{X}\Gamma} \right) = 0 \mod 2. \tag{95}$$

In both cases, $\mathrm{Eu}_{1,a}^{SS'} = \mathrm{SW}_{1,a}^{SS'} = 0$ if $n_{\mathrm{o},a}^{SS'} n_{\mathrm{e},a}^{SS'} = 0$. In Eq. (95), one has $\mathrm{SW}_{1,a}^{SS'} = \mathrm{Eu}_{1,a}^{SS'} \mod 2$ if $n_{\mathrm{o},a}^{SS'} = n_{\mathrm{e},a}^{SS'} = 1$. The integer constraint of Eq. (94) reduces the number of independent integer level-1 invariants by one. On the other hand, the parity constraint of Eq. (94) reduces the number of independent $\mathbb{Z}_2$ level-1 invariants by one, but if an integer invariant exists, then the compatibility relation only restricts its parity.

Classification on the 2-cell

At level-2, the parent invariants are one or two $\mathbb{Z}$-valued second Euler invariants or a $\mathbb{Z}_2$-valued second Stiefel-Whitney invariant, depending on $n_{\mathrm{o},\mathrm{e}}$ (see Sec. II D). The parent classification set for boundary deformations K_2^∂ contains a copy of $\pi_2[\mathcal{X}_{SS'}]$ for each 1-cell and of $\pi_1[\mathcal{X}_S]$ for each 0-cell. We now discuss their effect on $\mathrm{Eu}_2^{\mathrm{o}/\mathrm{e}}$ and SW_2 separately.

	Bands	Additional condition(s)	Topological invariant
A, Level 1	$n_\mathrm{o}, n_\mathrm{e} \geq 1$	See main text, Sec. VIII B 1	
A, Level 2	$n_\mathrm{o}, n_\mathrm{e} \geq 1$	if $\mathcal{Q}_1^\wedge$	$C \in \mathbb{Z}$
		if not $\mathcal{Q}_1^\wedge$	—
AI, Level 1	$n_\mathrm{o}, n_\mathrm{e} \geq 1$	See main text, Sec. VIII B 2	
AI, Level 2	$n_\mathrm{o} = n_\mathrm{e} = 1$	—	—
	$n_\mathrm{o} = 1, n_\mathrm{e} = 2$	if $\mathcal{Q}_1^\vee$ and $\mathcal{Q}_2^\mathrm{e}$	$\mathrm{Eu}_2^\mathrm{e} \in 2\mathbb{Z}$
		if $\mathcal{Q}_2^\mathrm{e}$, but not $\mathcal{Q}_1^\vee$	$\mathrm{Eu}_2^\mathrm{e} \in 2\mathbb{N}$
		if not $\mathcal{Q}_2^\mathrm{e}$	—
	$n_\mathrm{o} = 1, n_\mathrm{e} > 2$	—	—
	$n_\mathrm{o} = n_\mathrm{e} = 2$	if $\mathcal{Q}_1^\vee$ and $\mathcal{Q}_2^\mathrm{e}$ and $\mathcal{Q}_2^\mathrm{o}$	$(\mathrm{Eu}_2^\mathrm{o}, \mathrm{Eu}_2^\mathrm{e}) \in \mathbb{Z}^2|_\mathrm{p}$
		if $\mathcal{Q}_2^\mathrm{e}$ and $\mathcal{Q}_2^\mathrm{o}$, but not $\mathcal{Q}_1^\vee$	$(\mathrm{Eu}_2^\mathrm{o}, \mathrm{Eu}_2^\mathrm{e}) \in \mathbb{N} \times \mathbb{Z}|_\mathrm{p}$
		if $\mathcal{Q}_1^\vee$ and $\mathcal{Q}_2^\mathrm{o}$, but not $\mathcal{Q}_2^\mathrm{e}$	$\mathrm{Eu}_2^\mathrm{o} \in \mathbb{Z}$
		if $\mathcal{Q}_1^\vee$ and $\mathcal{Q}_2^\mathrm{e}$, but not $\mathcal{Q}_2^\mathrm{o}$	$\mathrm{Eu}_2^\mathrm{e} \in \mathbb{Z}$
		if $\mathcal{Q}_2^\mathrm{o}$, but not $\mathcal{Q}_1^\vee$ and not $\mathcal{Q}_2^\mathrm{e}$	$\mathrm{Eu}_2^\mathrm{o} \in \mathbb{N}$
		if $\mathcal{Q}_2^\mathrm{e}$, but not $\mathcal{Q}_1^\vee$ and not $\mathcal{Q}_2^\mathrm{o}$	$\mathrm{Eu}_2^\mathrm{e} \in \mathbb{N}$
		if $\mathcal{Q}_2^\wedge$, but not $\mathcal{Q}_2^\mathrm{e}$ and not $\mathcal{Q}_2^\mathrm{o}$	$\mathrm{SW}_2 \in \mathbb{Z}_2$
		if not $\mathcal{Q}_2^\wedge$	—
	$n_\mathrm{o} = 2, n_\mathrm{e} > 2$	if $\mathcal{Q}_1^\vee$ and $\mathcal{Q}_2^\mathrm{o}$	$\mathrm{Eu}_2^\mathrm{o} \in \mathbb{Z}$
		if $\mathcal{Q}_2^\mathrm{o}$, but not $\mathcal{Q}_1^\vee$	$\mathrm{Eu}_2^\mathrm{o} \in \mathbb{N}$ [F]
		if $\mathcal{Q}_2^\wedge$, but not $\mathcal{Q}_2^\mathrm{o}$	$\mathrm{SW}_2 \in \mathbb{Z}_2$
		if not $\mathcal{Q}_2^\wedge$	—
	$n_\mathrm{o}, n_\mathrm{e} > 2$	if $\mathcal{Q}_2^\wedge$	$\mathrm{SW}_2 \in \mathbb{Z}_2$
		if not $\mathcal{Q}_2^\wedge$	—

TABLE XIII. Homotopic classification of spinless gapped band structures with D_4 symmetry in two dimensions for various possible combinations of number of bands and level 0 invariants, the latter encoded in the $\mathcal{Q}$'s. In particular, $\mathcal{Q}_{1,a}^{SS'}$, $\mathcal{Q}_{1,\rho}^S$, $\mathcal{Q}_2^{\mathrm{o/e}}$, $\mathcal{Q}_2^\wedge$ are defined in Eqs. (91), (93), (96), and (97), respectively. The condition $\mathcal{Q}_1^\wedge$ holds if $\mathcal{Q}_{1,a}^{SS'} \, \forall \, SS', a$ and $\mathcal{Q}_1^\vee$ holds if $\exists S$ where $Q_{1,\rho}^S$ is true $\forall \, \rho \neq B$. The set $\mathbb{Z}^2|_\mathrm{p}$ consists of all ordered integer pairs (p, q) with $p = q \mod 2$; the set $\mathbb{N} \times \mathbb{Z}_\mathrm{p}$ consists of all ordered integer pairs (p, q) with $p \geq 0$ and $p = q \mod 2$. The invariants are only specified for $n_\mathrm{o} \leq n_\mathrm{e}$, since the classification is symmetric under $n_\mathrm{o} \leftrightarrow n_\mathrm{e}$. The fragile topological phases are marked by [F].

Second Euler invariant — The existence of the parent invariant $\mathrm{Eu}_2^{\mathrm{o/e}} \in \mathbb{Z}$ requires $n_\mathrm{o/e} = 2$, whereby $\mathrm{Eu}_2^{\mathrm{o/e}} \in 2\mathbb{Z}$ if $n_\mathrm{e/o} = 1$. Boundary deformations at an 1-cell SS' and parity sector a can add an arbitrary integer to $\mathrm{Eu}_2^{\mathrm{o/e}}$ if $n_{\mathrm{o/e},a}^{SS'} = 2$ and $n_{\mathrm{e/o},a}^{SS'} \geq 2$, whereas they can add an arbitrary even integer if $n_{\mathrm{o/e},a}^{SS'} = 2$ and $n_{\mathrm{e/o},a}^{SS'} = 1$. Hence, $\mathrm{Eu}_2^{\mathrm{o/e}}$ is robust to deformations at 1-cells if the constraint

$$\mathcal{Q}_2^{\mathrm{o/e}} : \left[n_{\mathrm{o/e},a}^{SS'} \leq 1 \vee n_{\mathrm{e/o},a}^{SS'} = 0 \right] \forall \, SS', a, \qquad (96)$$

holds, whereas its parity is robust to deformations at 1-cells if the condition

$$\mathcal{Q}_2^\wedge : \left[n_{\mathrm{o/e},a}^{SS'} \leq 1 \vee n_{\mathrm{e/o},a}^{SS'} \leq 1 \right] \forall \, SS', a, \qquad (97)$$

is satisfied. Nontrivial boundary deformations at a 0-cell S with irrep $\rho \neq B$ may flip the orientation of the occupied and empty bases, thereby changing the signs of $\mathrm{Eu}_2^{\mathrm{o/e}}$. The irrep B at the Γ or M point must be excluded, since it cannot change the orientation of a subspace owing to the twofold degeneracy. Such boundary deformations do not exist if $\mathcal{Q}_{1,\rho}^S$ (Eq. (93)) holds $\forall \, \rho \neq B$ at any 0-cell.

Second Stiefel-Whitney invariant — The $\mathbb{Z}_2$ parent invariant SW_2 is trivialized by boundary deformations if and only if there exists a 1-cell SS' and parity a such that $n_{\mathrm{o/e},a}^{SS'} \geq 2$ and $n_{\mathrm{e/o},a}^{SS'} \geq 2$. Such boundary deformations do not exist if $\mathcal{Q}_2^\wedge$ of Eq. (97) is satisfied.

These classification results are summarized in Tab. XIII.

Summary

In the absence of time-reversal symmetry, there are no stable or fragile topological band structures, since $\mathcal{Q}_{1,a}^{SS'}$ (Eq. (91)) is incompatible with the rules of fragile as well as stable topology. These conditions further preclude the existence of stable representation-protected topology.

in the presence of time-reversal symmetry, there are no stable topological band structures, since rules of stable topology violate $\mathcal{Q}^S_{1,\rho}$, $\mathcal{Q}^{o/e}_2$, and $\mathcal{Q}^\wedge_2$. There is a fragile topological phase with a level-2 invariant $\mathrm{Eu}^o_2 \in \mathbb{Z}$ if $n_o = 2$, if the occupied orbitals transform under the irrep B at the Γ and M points.

3. Representation-protected stable topology

A restriction to the irrep B at Γ and M implies that $n^S_{o/e,B} = n^{SS'}_{o/e,\pm} = \frac{1}{2} n_{o/e}$ for $S = \Gamma, M$ and for all 1-cells SS'. Thus, in the stable limit, each 1-cell has two $\mathbb{Z}_2$ invariants $\mathrm{SW}^{SS'}_{1,\pm}$, yielding a total of six invariants. The effect of boundary deformations depends on the Wyckoff positions occupied, as we now discuss.

If only the special Wyckoff position "a" is allowed, then $n^X_{o/e,++} = n^X_{o/e,+-} = \frac{1}{2} n_{o/e}$, whereas $n^X_{o/e,-+} = n^X_{o/e,--} = 0$ (see Table XIX). Thus, only two independent boundary deformations exist at X. These simultaneously add integers to $\mathrm{SW}^{\Gamma X}_{1,a}$ and $\mathrm{SW}^{MX}_{1,a}$, $a = \pm$ and thus do not affect the differences $\mathrm{SW}^{\Gamma XM}_{1,a} \equiv \mathrm{SW}^{\Gamma X}_{1,a} - \mathrm{SW}^{XM}_{1,a}$. Boundary deformations at Γ and M have identical effect on the remaining four $\mathbb{Z}_2$ invariants $\mathrm{SW}^{\Gamma M}_{1,\pm}$, $\mathrm{SW}^{\Gamma XM}_{1,\pm}$, so that together they can remove one invariant. Imposing the compatibility condition, we get two independent $\mathbb{Z}_2$-valued level-1 invariants, which can be written as

$$\mathrm{SW}^{\Gamma M}_1 \equiv \mathrm{SW}^{\Gamma M}_{1+} - \mathrm{SW}^{\Gamma M}_{1-},$$
$$\mathrm{SW}^+_1 \equiv \mathrm{SW}^{\Gamma M}_{1+} + \mathrm{SW}^{MX}_{1+} + \mathrm{SW}^{X\Gamma}_{1+}. \qquad (98)$$

On the other hand, if only Wyckoff position "b" is allowed, then $n^X_{o/e,-+} = n^X_{o/e,--} = \frac{1}{2} n_{o/e}$, whereas $n^X_{o/e,++} = n^X_{o/e,+-} = 0$ (see Table XIX), so that the parity labels are switched between ΓX and XM. This is analogous to the case discussed above, with the second invariant redefined as

$$\mathrm{SW}^+_1 \equiv \mathrm{SW}^{\Gamma M}_{1+} + \mathrm{SW}^{MX}_{1+} + \mathrm{SW}^{X\Gamma}_{1-}. \qquad (99)$$

If both Wyckoff positions "a" and "b" are allowed, then there are three independent boundary deformation at X [80], which remove the invariant SW^+_1, leaving us with a single $\mathbb{Z}_2$-valued invariant $\mathrm{SW}^{\Gamma M}_1$. In Appendix. G, we construct a minimal lattice model with nontrivial invariants $\mathrm{SW}^{\Gamma M}_1$ and SW^+_1.

There are no stable representation-protected level-2 invariants, since $\mathcal{Q}^{o/e}_2$ and $\mathcal{Q}^\wedge_2$ are incompatible with the rules of stable representation-protected topology.

C. Homotopic classification in three dimensions

1. Without time-reversal symmetry

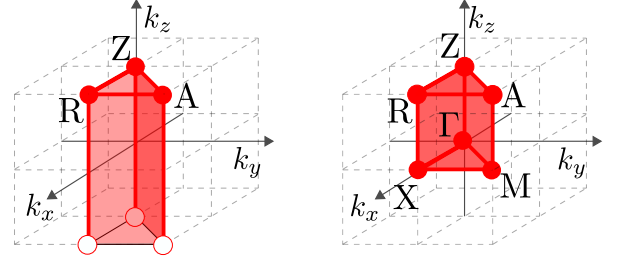Without time-reversal symmetry, the 3d fundamental domain is a triangular prism, as shown in Fig. 14 (left).

FIG. 14. Fundamental domains $\mathbb{D}$ for a three-dimensional band structure with D_4 symmetry without (left) and with (right) time-reversal symmetry.

There are no level-1 invariants, while at level-2, we get a Chern number C_z for the horizontal face as well as two Chern numbers $C^{SS'}_\pm$ for each vertical face. The former is robust only when the Hamiltonian is completely fixed at $\partial\mathbb{D}_2$, i.e., if $\mathcal{Q}^{SS'}_{1,\pm}$ (Eq. (91)) is satisfied for all 1-cells. For the latter, topologically nontrivial deformations along the vertical 1-cell passing through S can add arbitrary integers to $C^{SS'}_\pm$ on the adjacent 2-cells following the rules identical to those for the first Euler invariant for a 2d D_4-symmetric band structure with time-reversal symmetry. The Chern numbers on vertical faces further satisfy the level-2 compatibility condition

$$\sum_{a=\pm} \left(C^{\Gamma M}_a + C^{MX}_a + C^{X\Gamma}_a \right) = 0. \qquad (100)$$

At level-3 and $n_o = n_e = 1$, we get a $\mathbb{Z}$-valued invariant if the Chern number C_z for a fixed-k_z cross section of $\mathbb{D}$ vanishes, and a $\mathbb{Z}_{2C_z}$-valued invariant otherwise.

2. With time-reversal symmetry

In the presence of time-reversal symmetry, the 3d fundamental domain is a triangular prism, as shown in Fig. 14 (right). At levels 0, 1, and 2, we get two copies of the 2d classification problem discussed in Sec. VIII B. At level-2, we additionally get Chern numbers $C^{SS'}_\pm$ for the vertical 2-cells. The conditions for their robustness and the level-2 compatibility condition are identical to the time-reversal broken case. At level-3, we get the $\mathbb{Z}$-valued Hopf invariant if $n_o = n_e = 1$.

3. Representation-protected stable topology

A restriction to the two dimensional irrep B leads to representation-protected stable topology with nontrivial level-2 invariants. In the absence of time-reversal symmetry, the parent invariants are the six Chern numbers $C^{SS'}_\pm \in \mathbb{Z}$ computed on the vertical faces. In the presence of time-reversal symmetry, $C^{SS'}_\pm \in \mathbb{Z}$ can be combined with the difference between the $\mathbb{Z}_2$-valued invariants $\mathrm{SW}^{SS'}_{1,\pm}$ computed at $k_z = 0, \pi$ to yield a $\mathbb{Z}$-valued

Chern number computed for $k_z \in (-\pi, \pi]$. (The situation is analogous to the case of $C_2 T$-symmetry, see Sec. V C.) Time reversal symmetry thus plays no role in this case. In the following, we use $C_\pm^{SS'}$ to refer to the Chern number computed for $k_z \in (-\pi, \pi]$ both without and with time-reversal symmetry.

The effect of boundary deformations depends on whether one or both Wyckoff positions are allowed, as in the case of the 2d representation protected phase (see Sec. VIII B 3). Thus, if a single Wyckoff position is allowed, then we are left with two independent $\mathbb{Z}$-valued invariants. For the Wyckoff position "a", these can be written as (*cf.* Eq. (98))

$$
\begin{aligned}
C^{\Gamma M} &\equiv C_+^{\Gamma M} - C_-^{\Gamma M}, \\
C^+ &\equiv C_+^{\Gamma M} + C_+^{MX} + C_+^{X\Gamma}.
\end{aligned} \tag{101}
$$

For only the Wyckoff position "b", the latter is instead defined as

$$
C^+ \equiv C_+^{\Gamma M} + C_+^{MX} + C_+^{X\Gamma}. \tag{102}
$$

If both Wyckoff positions are allowed, then only $C^{\Gamma M}$ remains well-defined.

D. Anomalous boundary states

For the band structures with representation-protected topology, there are anomalous boundary modes at the D_4-symmetric surfaces at constant z. For the case that only orbitals at Wyckoff position "a" are allowed, we find it convenient to replace the integer invariant C^+ with

$$
\begin{aligned}
C^{MX\Gamma} &= C_+^{MX} + C_+^{X\Gamma} - C_-^{MX} - C_-^{X\Gamma} \\
&= 2C^+ - C^{\Gamma M},
\end{aligned} \tag{103}
$$

which, by definition, has the same parity as $C^{\Gamma M}$. The case that only orbitals at "b" are allowed proceeds analogously, whereas $C^{MX\Gamma}$ is not defined if both Wyckoff positions are allowed. To relate these invariants to boundary states, we note that, since $n_{o/e,+}^{SS'} = n_{o/e,-}^{SS'}$ for each 1-cell, we can glue the two parity sectors to define a Chern insulator on SS'. The Chern number $C^{\Gamma M}$ then equals the difference of the number of even-parity and odd-parity bands crossing the Fermi surface along ΓM, while $C^{MX\Gamma}$ (if defined) counts this difference along MX and $X\Gamma$. An odd parity of $C^{\Gamma M}$ (and also of $C^{MX\Gamma}$, if defined) implies protected band touchings at Γ and M, similar to the case of a C_4-symmetric band structure [29, 31, 39]. Even contributions to $C^{\Gamma M}$ and $C^{MX\Gamma}$ can be traced back to equal numbers of even-parity and odd-parity bands crossing the Fermi level in opposite directions. Since such crossings can be gapped out away from the high-symmetry lines, they imply Dirac cones protected by mirror symmetry along ΓM and, if applicable, along $MX\Gamma$. If $C^{\Gamma M}$ and $C^{MX\Gamma}$ are both defined, the numbers of such Dirac crossings along along ΓM and $MX\Gamma$, counted according to

parity, are independent signatures of the representation-protected topology.

From the boundary perspective, the presence of only B irreps at $\overline{\Gamma}$ and $\overline{M}$ implies that the number of states in the occupied/empty subspaces is even, and furthermore, on each high-symmetry lines, $n_{o,+}^{\overline{SS'}} = n_{o,-}^{\overline{SS'}}$. In this setup, we can get anomalous gapless modes in two ways:

- A single surface band crosses the Fermi level between $\overline{\Gamma}$ and $\overline{M}$, so that so that $n_{o/e}^{\overline{\Gamma}} \neq n_{o/e}^{\overline{M}} \mod 2$. This is incompatible with having only the irrep B at both the $\overline{\Gamma}$ and $\overline{M}$ points. Since $n_{o/e}$ is defined for any path connecting $\overline{\Gamma}$ to $\overline{M}$, all such paths must have a level crossing the Fermi level, so that we get a loop of zero crossings.

- A pair of surface bands with opposite parities cross the Fermi level on $\overline{\Gamma M}$ in opposite directions. This is compatible with having only irrep B at $\overline{\Gamma}$ and $\overline{M}$; however, the level-0 compatibility conditions at $\overline{\Gamma}$ and $\overline{M}$ cannot be satisfied simultaneously by only B irreps. Since $n_{o/e}$ stay unchanged under this crossing, it can be gapped away from $\overline{\Gamma M}$, leading to a Dirac cone on $\overline{\Gamma M}$ protected by a mirror symmetry.

These are precisely the two kinds of anomalous boundary states obtained from the bulk perspective.

IX. DISCUSSION

In this article, we presented a homotopic classification of band-structures with crystalline symmetries. The homotopic classification describes the delicate topology of gapped Bloch Hamiltonians with a fixed number of occupied/empty bands n_o/n_e and fixed numbers of orbitals for each orbital type at each Wyckoff position. A fragile classification, in which only the number of occupied bands is fixed and unoccupied bands may be added *ad libitum*, and a stable classification, in which both occupied and unoccupied bands may be added, can be obtained from the homotopic classification by taking the limits $n_e \to \infty$ and $n_{o/e} \to \infty$, respectively.

The central object in our scheme is the interpretation as a *CW-complex* of the fundamental domain of the point group, which is the minimal region in reciprocal space required to define the full Bloch Hamiltonian. A CW complex, fundamental in homotopy theory, is a topological space constructed from a collection of "cells" of dimension p with $p = 0, \ldots, d$ using a set of "gluing conditions." We classify the Bloch Hamiltonians restricted to the p-cells, starting with $p = 0$ and building up to higher p, imposing the constraints demanded from the CW-complex at each step. The structure of the classification over p-cells then depends on the concrete topological invariants over q-cells with $q < p$, thereby endowing the classification with a hierarchical structure. For a homotopic classification, the classifying space does not

have a group structure. However, in the stable limit, the invariants at different levels factorize, leading to the well-known result that the full classifying spaces are products of groups, with the group operation deriving from the direct sum of bands.

Two basic elements of our approach — bootstrapping the full classification from that of restrictions of the Hamiltonian to individual cells, and, for each cell, the reduction of a larger (but easier to compute) "parent" classification group to the actual classification set by removing ambiguity from boundary deformations — have previously been applied to the classification of gapped band structures. The former element is shared with the partial classifications based on topological quantum chemistry [54–56, 59–63, 81, 82], which consider topological invariants of 0-cells only. The latter was used previously for symmetry class AII by Moore and Balents [33] as well as for the classification of inversion-symmetric insulators in the stable limit [22] (see also Ref. [83]).

We have illustrated the homotopic classification scheme on point groups of increasing complexity, for both time-reversal-invariant and time-reversal-broken cases. Applications to band structure without crystalline symmetry in symmetry classes A, AI, AII make a connection to existing homotopic classification approaches for gapped band structures without crystalline symmetries [27, 33]. The other examples we consider elucidate various aspects of the homotopic classification and illustrate that it can be performed systematically. However, this process is involved enough that we have not been able to automate the generation of delicate classification tables, which would allow us to compute the topological invariants at all levels for all space groups, as it is done for the level-0 invariants in the framework of topological quantum chemistry and symmetry indicators [54–56, 60–63]. A quick look at the complexity of arguments required to produce the classification tables for a single crystalline symmetry in Secs. VI, VII, and VIII explains why such an automatized procedure may be too much to expect.

We find that a crucial aspect of a delicate classification is that restricting only the number of occupied/empty bands does not determine the classification uniquely. Instead, it is essential to also fix the (total) number of orbitals of each type at each Wyckoff position. Typically, the Wyckoff positions determine the level-0 invariants, and all subsequent restrictions on higher-level invariants can be expressed in terms of these, so that the Wyckoff positions and the representations of orbitals do no appear explicitly in the classification tables. For the examples we consider, this is the case for the point groups C_2, C_4, and D_4. However, the Wyckoff positions may also enter the homotopic classification directly, as is the case for $C_2 T$-symmetric band structures.

The existence of boundary states is a hallmark of stable topology — a topologically nontrivial insulator protected by a lattice symmetry exhibits anomalous boundary states at a boundary that respect the requisite symmetries. In the examples that we consider here, the lattice symmetries include a rotation, so that there are no invariant boundaries in two dimensions. However, in three dimensions, there is an invariant boundary normal to the rotation axis. We establish that such a boundary indeed hosts anomalous boundary modes if the stable topology is nontrivial. Anomalous boundary modes also exist for stable representation-protected topology, whereby one must not only constrain the types (but not the number) of orbitals in the bulk, but also at the at the invariant boundary.

In real systems, the anomalous boundary states protected by representation-protected stable topology may disappear if there is a surface reconstruction that violates the constraint on orbital types. Nevertheless, if this violation is sufficiently weak, non-anomalous boundary states may exist that can be traced back to the anomalous boundary states of representation-protected topology. A similar reasoning relating non-anomalous boundary states to anomalous boundary states protected by additional symmetries is used in the case of, *e.g.*, simplified models with a sublattice symmetry, which have zero-energy flat bands on edges or on surfaces (such as the "drumhead states" of nodal-line semimetals [84] and the flat bands at zig-zag edges of graphene [85, 86]), which do not remain flat and at zero energy once sublattice-symmetry-breaking perturbations are taken into account.

Even in absence of *individual* invariant boundaries, stable topology can lead to boundary signatures if the overall crystal is invariant under the symmetry. Such boundary signatures may be of higher-order type [87–92] — such as anomalous gapless states at crystal hinges — and they are guaranteed to exist if the band structure is not of atomic limit type [25, 93]. For band structures of atomic-limit type, more subtle boundary signatures, such as fractional corner charges or "twisted boundary signatures" may exist [29, 47, 90, 91, 94–105], but this is not guaranteed. We expect no such higher-order boundary signatures for representation-protected topology, because it is not possible to organize orbitals according to their representation under the crystalline symmetry operations on a surface that is not itself invariant.

In conclusion, we have presented analytical machinery that can be used to classify band structures with crystalline symmetry at the highest possible level of granularity. Whether the application of this methodology to other symmetry classes and more complicated point groups might yield further examples of representation-protected topology, remains a topic of future study.

Appendix A: Symmetries of the Bloch Hamiltonian

We briefly recapitulate the symmetry analysis of the Bloch Hamiltonians for general crystalline symmetries. (For a detailed analysis, see, e.g., the Supplementary Material of Ref. [35].)

1. Crystalline symmetries

We consider a symmetry of the lattice, derived from an isometry of the underlying space $g \colon \mathbb{R}^d \to \mathbb{R}^d$. The physical systems of interest consist of a set of n orbitals α located at positions $\mathbf{r}_\alpha \in (-\frac{1}{2}, \frac{1}{2}]^d$ within the unit cell, whose origin is labeled by $\mathbf{R} \in \mathbb{Z}^d$. Under the action of g, an arbitrary lattice point transforms as

$$g(\mathbf{R} + \mathbf{r}_\alpha) = g\mathbf{R} + \delta\mathbf{R}_\alpha + \mathbf{r}_{\alpha'} \equiv \mathbf{R}' + \mathbf{r}_{\alpha'}, \qquad \text{(A1)}$$

where, since $g\mathbf{r}_\alpha$ may not lie within the unit cell, we subtract off a lattice translation $\delta\mathbf{R}_\alpha$ to move it back within the unit cell at the new position $\mathbf{r}_{\alpha'}$. The symmetry generically maps a basis orbital at $\mathbf{r}_\alpha$ to a linear combination of basis orbitals at $\mathbf{r}_{\alpha'}$, so that its action on the position space basis state $|\mathbf{R}, \alpha\rangle$ can be written as

$$C(g) |\mathbf{R}, \alpha\rangle = \sum_{\alpha'=1}^{n} C^*_{\alpha\alpha'}(g) |\mathbf{R}', \alpha'\rangle. \qquad \text{(A2)}$$

The unitary matrices $C(g)$ for various $g \in G$ then constitute a representation of the point group G.

In Sec. II, we define the Bloch states as

$$|\mathbf{k}, \alpha\rangle = \sum_{\mathbf{R}} e^{i\mathbf{k}\cdot(\mathbf{R}+\mathbf{r}_\alpha)} |\mathbf{R}, \alpha\rangle. \qquad \text{(A3)}$$

Under the lattice symmetry g, these transform as

$$\begin{aligned}
C(g) |\mathbf{k}, \alpha\rangle &= \sum_{\mathbf{R}} e^{i\mathbf{k}\cdot(\mathbf{R}+\mathbf{r}_\alpha)} C(g) |\mathbf{R}, \alpha\rangle \\
&= \sum_{\alpha'=1}^{n} \sum_{\mathbf{R}} e^{i\mathbf{k}\cdot(\mathbf{R}+\mathbf{r}_\alpha)} C^*_{\alpha\alpha'}(g) |\mathbf{R}', \alpha'\rangle \\
&= \sum_{\alpha'=1}^{n} C^*_{\alpha\alpha'}(g) \left(\sum_{\mathbf{R}'} e^{i(g\mathbf{k})\cdot(\mathbf{R}'+\mathbf{r}_{\alpha'})} |\mathbf{R}', \alpha'\rangle \right) \\
&= \sum_{\alpha'=1}^{n} C^*_{\alpha\alpha'}(g) |g\mathbf{k}, \alpha'\rangle, \qquad \text{(A4)}
\end{aligned}$$

where we have used Eq. (A1) and $\mathbf{k} \cdot \mathbf{R} = (g\mathbf{k}) \cdot (g\mathbf{R})$. The symmetry operators are independent of $\mathbf{R}'$, so that we do not need to account for the change in unit cell that a site might undergo under the symmetry operation. On the other hand, under translation by a reciprocal lattice vector $\mathbf{G}$, these Bloch states pick up a phase $e^{i\mathbf{k}\cdot\mathbf{r}_\alpha}$, which can be written in form identical to Eq. (A4) as

$$C(g_\mathbf{G}) |\mathbf{k}, \alpha\rangle \equiv |\mathbf{k}+\mathbf{G}, \alpha\rangle = \sum_{\alpha'} \Lambda^*_{\alpha\alpha'}(\mathbf{G}) |\mathbf{k}, \alpha'\rangle, \quad \text{(A5)}$$

where $\Lambda_{\alpha\beta}(\mathbf{k}) = e^{-i\mathbf{k}\cdot\mathbf{r}_\alpha} \delta_{\alpha\beta}$. We thus consider the point group symmetries and reciprocal lattice translations together as elements of the reciprocal space group G_Λ, whose action on the Bloch states is given by Eq. (A4). The Bloch Hamiltonian then satisfies the constraint

$$H(g\mathbf{k}) = C^\dagger(g) H(\mathbf{k}) C(g) \qquad \text{(A6)}$$

for all $g \in G_\Lambda$.

We contrast this with the conventional definition of Bloch states (which does not contain the position of orbitals within the unit cell)

$$|\mathbf{k}, \alpha\rangle_c = \sum_{\mathbf{R}} e^{i\mathbf{k}\cdot\mathbf{R}} |\mathbf{R}, \alpha\rangle_c. \qquad \text{(A7)}$$

These states are periodic under reciprocal lattice transformations, while under a lattice symmetry, they transform as

$$\begin{aligned}
C(g) |\mathbf{k}, \alpha\rangle_c &= \sum_{\mathbf{R}} e^{i\mathbf{k}\cdot\mathbf{R}} C(g) |\mathbf{R}, \alpha\rangle_c \\
&= \sum_{\alpha'=1}^{n} \sum_{\mathbf{R}} e^{i\mathbf{k}\cdot\mathbf{R}} C^*_{\alpha\alpha'}(g) |\mathbf{R}', \alpha'\rangle_c \\
&= \sum_{\alpha'=1}^{n} C^*_{\alpha\alpha'}(g) e^{-i(g\mathbf{k})\cdot\delta\mathbf{R}_\alpha} |g\mathbf{k}, \alpha'\rangle_c \\
&\equiv \sum_{\alpha'=1}^{n} \widetilde{C}^*_{\alpha\alpha'}(g, \mathbf{k}) |g\mathbf{k}, \alpha'\rangle_c, \qquad \text{(A8)}
\end{aligned}$$

so that the unitary matrix $\widetilde{C}(g, \mathbf{k})$ now depends on $\mathbf{k}$. The matrices $\widetilde{C}(g, \mathbf{k})$ can be related to the $\mathbf{k}$-independent representation matrices $C(g)$ as $\widetilde{C}(g, \mathbf{k}) = \Lambda(g\mathbf{k})C(g)\Lambda(\mathbf{k})^\dagger$. The two definitions of Bloch states are related by

$$|\mathbf{k}, \alpha\rangle = e^{i\mathbf{k}\cdot\mathbf{r}_\alpha} |\mathbf{k}, \alpha\rangle_c = \sum_{\alpha'} \Lambda^*_{\alpha\alpha'}(\mathbf{k}) |\mathbf{k}, \alpha'\rangle_c, \qquad \text{(A9)}$$

so that the corrresponding Bloch Hamiltonians are related by

$$H(\mathbf{k}) = \Lambda(\mathbf{k}) \widetilde{H}(\mathbf{k}) \Lambda^\dagger(\mathbf{k}). \qquad \text{(A10)}$$

In the following sections, we work exclusively in the Bloch basis of Eq. (A3).

2. Time reversal symmetry

With the exception of Sec. III B 2, we consider a time-reversal symmetry with $\mathrm{T}^2 = +1$, and choose a basis of orbitals at lattice sites such that the Bloch Hamiltonian satisfies

$$H(\mathbf{k}) = H^*(-\mathbf{k}). \qquad \text{(A11)}$$

This is equivalent to $\widetilde{H}^*(-\mathbf{k}) = \widetilde{H}(\mathbf{k})$ in the conventional Bloch basis, since the unitary matrix relating the two bases (Eq. A10) satisfies

$$\Lambda^*_{\alpha\beta}(\mathbf{k}) = e^{i\mathbf{k}\cdot\mathbf{r}_\alpha}\delta_{\alpha\beta} = \Lambda_{\alpha\beta}(-\mathbf{k}), \qquad (A12)$$

so that

$$H^*(-\mathbf{k}) = \Lambda^*(-\mathbf{k})\widetilde{H}^*(-\mathbf{k})\Lambda^*(-\mathbf{k})$$
$$= \Lambda^\dagger(\mathbf{k})\widetilde{H}(\mathbf{k})\Lambda(\mathbf{k}) = H(\mathbf{k}). \qquad (A13)$$

Let the symmetries of the lattice include twofold rotation (in 2d) or inversion (in 3d) that squares to $+1$, so that the Hamiltonian satisfies

$$H(\mathbf{k}) = C^\dagger H(-\mathbf{k})C \qquad (A14)$$

for some unitary matrix C satisfying

$$C^2 = \mathbb{1} = CC^\dagger \implies C = C^\dagger. \qquad (A15)$$

Thus, the time-reversed version of Eq. (A14) becomes

$$H^*(\mathbf{k}) = CH(\mathbf{k})C, \qquad (A16)$$

Complex conjugating both sides, we get

$$H(\mathbf{k}) = C^*H^*(\mathbf{k})C^* = (C^*C)H(\mathbf{k})(C^*C)^\dagger, \qquad (A17)$$

so that $H(\mathbf{k})$ must commute with C^*C. This is trivially satisfied if $C^*C = \pm\mathbb{1}$, i.e., if C is purely real or purely imaginary.

The local-in-$\mathbf{k}$ condition of Eq. (A16) can be reduced to a reality condition on the Bloch Hamiltonian by defining a unitarily equivalent Hamiltonian

$$H'(\mathbf{k}) \equiv BH(\mathbf{k})B^\dagger, \qquad (A18)$$

where B is unitary. Eq. (A16) then becomes

$$H'^*(\mathbf{k}) = B^*\left(CH(\mathbf{k})C\right)B^T$$
$$= \left(B^*CB^\dagger\right)H'(\mathbf{k})\left(B^*CB^\dagger\right)^\dagger. \qquad (A19)$$

Thus, $H'(\mathbf{k})$ is real if

$$B^*CB^\dagger = \mathbb{1} \implies C = B^TB, \qquad (A20)$$

i.e., if B is a "square root" of C. We can readily define such a matrix B by working in the eigenbasis of C, where B is simply a diagonal matrix whose entries are square roots of the diagonal entries of C.

Appendix B: Explicit construction of the representation matrices

In this section, we compute the unitary matrices $C(g)$ and Λ_a representing the reciprocal space groups G_Λ for the lattice symmetries discussed in this article. Specifically, for all Wyckoff position and orbitals, we derive the explicit form of the rotation matrices C_n and, in the case of D_4, the reflection matrix M_x. For the translation component of G_Λ, we derive $\Lambda(\mathbf{k})$ defined in Eq. (A5), from which the translation matrices can be obtained as $\Lambda_a = \Lambda(2\pi\mathbf{e}_a)$ for $a = x, y$.

α	G_α	Location(s) within the unit cell
a		$(0,0)$
b	C_2	$(1/2, 1/2)$
c		$(1/2, 0)$
d		$(0, 1/2)$
g	—	(a_x, a_y), $(-a_x, -a_y)$

TABLE XIV. Wyckoff positions α at coordinate $\mathbf{r}_\alpha$(s) within the unit cell and the corresponding little groups G_α for a 2d C_2-symmetric lattice. For the generic Wyckoff position, we take $a_{x,y} \in (0, 1/2)$.

1. C_2 symmetry

For twofold rotation symmetry, there are four special Wyckoff positions as well as the generic Wyckoff position, as listed in Table XIV. For a system with n_α electrons at the Wyckoff position α, the total number of electrons in the unit cell is

$$n = \sum_\alpha \text{mult}(\alpha)n_\alpha$$
$$= n_a + n_b + n_c + n_d + 2n_g.$$

The reciprocal space translation matrix is block diagonal in Wyckoff positions, so that

$$\Lambda(\mathbf{k}) = \text{diag}\left\{\Lambda_a(\mathbf{k}), \Lambda_b(\mathbf{k}), \Lambda_c(\mathbf{k}), \Lambda_d(\mathbf{k}), \Lambda_g(\mathbf{k})\right\}, \quad (B1)$$

The translation matrices for individual Wyckoff positions can be computed using their definition in Eq. (A5) and the coordinates of various Wyckoff positions listed in Table XIV as

$$\Lambda_a(\mathbf{k}) = \mathbb{1}_{n_a},$$
$$\Lambda_b(\mathbf{k}) = \mathbb{1}_{n_b}e^{i(k_x+k_y)/2},$$
$$\Lambda_c(\mathbf{k}) = \mathbb{1}_{n_c}e^{ik_x/2},$$
$$\Lambda_d(\mathbf{k}) = \mathbb{1}_{n_d}e^{ik_y/2},$$
$$\Lambda_g(\mathbf{k}) = \mathbb{1}_{n_g}\text{diag}\left\{e^{i(k_xa_x+k_ya_y)}, e^{-i(k_xa_x+k_ya_y)}\right\}.$$

The twofold rotation operator is $\mathbf{k}$-independent and block diagonal in the Wyckoff positions, i.e.,

$$C_2 = \text{diag}\left\{C_a, C_b, C_c, C_d, C_g\right\}. \qquad (B2)$$

We now compute the matrices for each sector.

The special Wyckoff positions all have multiplicity one, and thus map back to themselves under twofold rotation. Furthermore, each of them have a little group C_2, so that the orbitals at these Wyckoff positions are labeled by the corresponding irreps ±1. Thus,

$$C_\alpha = \text{diag}\left\{\mathbb{1}_{n_{\alpha+}}, -\mathbb{1}_{n_{\alpha-}}\right\}; \quad \alpha \in \{\text{a,b,c,d}\}. \qquad (B3)$$

The generic Wyckoff position has multiplicity two and thus constitutes of two points "g1" and "g2", which transform into each other under C_2, so that

$$C_g = \mathbb{1}_{n_g} \otimes \sigma_1. \qquad (B4)$$

Label	Γ	M	X	Y
$+_a$	$+$	$+$	$+$	$+$
$-_a$	$-$	$-$	$-$	$-$
$+_b$	$+$	$+$	$-$	$-$
$-_b$	$-$	$-$	$+$	$+$
$+_c$	$+$	$-$	$-$	$+$
$-_c$	$-$	$+$	$+$	$-$
$+_d$	$+$	$-$	$+$	$-$
$-_d$	$-$	$+$	$-$	$+$
2_g	$+-$	$+-$	$+-$	$+-$

TABLE XV. Elementary band representations for twofold rotation symmetry.

α	G_α	Location(s) within the unit cell ($\mathbf{r}_\alpha$)
a	C_4	$(0,0)$
b		$(1/2, 1/2)$
c	C_2	$(1/2, 0)$, $(0, 1/2)$
g	—	(a_x, a_y), $(-a_y, a_x)$, $(-a_x, -a_y)$, $(a_y, -a_x)$

TABLE XVI. Wyckoff positions α at coordinate $\mathbf{r}_\alpha$(s) within the unit cell and the corresponding little groups G_α for a 2d C_4-symmetric lattice. We take $a_{x,y} \in (0, 1/2)$.

Using these definitions, we can compute the unitary matrices C_2, Λ_x and Λ_y for any given combination of Wyckoff positions and orbitals.

For symmetry class AI, we need an additional basis transformation by B to ensure that C_2T acts as a complex conjugation, as discussed in App. A 2. To this end, we first rotate the basis in the subspace of generic Wyckoff positions (if present) to achieve $C_g = \mathbb{1}_{n_g} \otimes \sigma_3$. The resulting representation matrix C_2 is a diagonal matrix with entries ± 1. A requisite basis transformation B can then be computed using Eq. (A20) by defining B as a diagonal matrix with an i wherever there is -1 in C_2.

A band representation for C_2 symmetry consists of the set of rotation eigenvalues ($\pm$) at the four high-symmetry points. The EBRs, corresponding to single orbital at a single Wyckoff position, are listed in Table XV.

2. C_4 symmetry

For fourfold rotation symmetry, there are three special Wyckoff positions as well as the generic Wyckoff position, as listed in Table XVI. For a system with n_α electrons at the Wyckoff position α, the total number of electrons in the unit cell is

$$n = n_a + n_b + 2n_c + 4n_g.$$

The reciprocal space translation matrix is

$$\Lambda(\mathbf{k}) = \text{diag}\left\{\Lambda_a(\mathbf{k}), \Lambda_b(\mathbf{k}), \Lambda_c(\mathbf{k}), \Lambda_g(\mathbf{k})\right\}, \quad \text{(B5)}$$

where

$$\Lambda_a(\mathbf{k}) = \mathbb{1}_{n_a},$$
$$\Lambda_b(\mathbf{k}) = \mathbb{1}_{n_b}e^{i(k_x + k_y)/2},$$
$$\Lambda_c(\mathbf{k}) = \mathbb{1}_{n_c}\text{diag}\left\{e^{ik_x/2}, e^{ik_y/2}\right\} \quad \text{(B6)}$$
$$\Lambda_g(\mathbf{k}) = \mathbb{1}_{n_g}\text{diag}\left\{e^{i(a_x k_x + a_y k_y)}, e^{i(-a_y k_x + a_x k_y)},\right.$$
$$\left. e^{i(-a_x k_x - a_y k_y)}, e^{i(a_y k_x - a_x k_y)}\right\}.$$

The fourfold rotation operator is block diagonal in the Wyckoff positions, i.e.,

$$C_4 = \text{diag}\left\{C_a, C_b, C_c, C_g\right\}. \quad \text{(B7)}$$

We now compute the matrices for each sector.

The Wyckoff positions "a" and "b" have multiplicity one, so that they map back onto themselves under C_4. The orbitals at these Wyckoff positions are of s, d or $p_\pm$ type, corresponding to a C_4 eigenvalue 1, -1 and $\pm i$. Thus, in absence of time-reversal symmetry,

$$C_\alpha = \text{diag}\left\{\mathbb{1}_{n_{s\alpha}}, -\mathbb{1}_{n_{d\alpha}}, i\mathbb{1}_{n_{p_+\alpha}}, -i\mathbb{1}_{n_{p_-\alpha}}\right\}, \quad \text{(B8)}$$

where $\alpha \in \{a, b\}$ and $n_\alpha = n_{s\alpha} + n_{d\alpha} + n_{p_+\alpha} + n_{p_-\alpha}$. In the presence of time-reversal symmetry, the $p_\pm$ orbitals come together, so that we can set $n_{p_+,\alpha} = n_{p_-,\alpha} \equiv n_{p,\alpha}$. We write them in the real basis as p_x, p_y, so that

$$C_\alpha = \text{diag}\left\{\mathbb{1}_{n_{s\alpha}}, -\mathbb{1}_{n_{d\alpha}}, i\sigma_y \otimes \mathbb{1}_{n_{p\alpha}}\right\}, \quad \text{(B9)}$$

with $n_\alpha = n_{s\alpha} + n_{d\alpha} + 2n_{p\alpha}$. The two points constituting Wyckoff position "c" are labeled by their inversion parity and transform into each other under C_4, so that

$$C_c^2 = \mathbb{1}_2 c_c; \quad c_c = \text{diag}\left\{\mathbb{1}_{n_{+c}}, -\mathbb{1}_{n_{-c}}\right\}, \quad \text{(B10)}$$

where $\mathbb{1}_2$ corresponds to the two sites of Wyckoff position "c." The C_4 operator, which is a square root of this matrix, depends on the relation between the basis states at "c1" and "c2". We choose the basis at "c1" as the eigenbasis of C_2, and define the basis states at "c2" as the images under C_4 of those at "c1". We can thus write

$$C_4 \begin{pmatrix} |\mathbf{R}, c1\rangle \\ |\mathbf{R}, c2\rangle \end{pmatrix} = \begin{pmatrix} |\mathbf{R}, c2\rangle \\ c_c |\mathbf{R} - \mathbf{e}_x, c1\rangle \end{pmatrix}, \quad \text{(B11)}$$

where $|\mathbf{R}, c1\rangle$ to denote a column vector consisting of n_c orbitals at "c1". The matrix multiplying the RHS can be identified as C_4^T, so that

$$C_c(\mathbf{k}) = \begin{pmatrix} 0 & c_c \\ \mathbb{1}_{n_c} & 0 \end{pmatrix}, \quad \text{(B12)}$$

squaring which yields Eq. B10.

Finally, the four points that constitute the generic Wyckoff position "g" transform under C_4 as

$$C_4\mathbf{r}_{g1} = \mathbf{r}_{g2}, \qquad C_4\mathbf{r}_{g2} = \mathbf{r}_{g3},$$
$$C_4\mathbf{r}_{g3} = \mathbf{r}_{g4}, \qquad C_4\mathbf{r}_{g4} = \mathbf{r}_{g1}, \quad \text{(B13)}$$

Label	Γ	M	X
s_{a}	s	s	$+$
d_{a}	d	d	$+$
$p_{\pm\mathrm{a}}$	$p_\pm$	$p_\pm$	$-$
$2p_{\mathrm{a}}$	p^2	p^2	$--$
s_{b}	s	d	$-$
d_{b}	d	s	$-$
$p_{\pm\mathrm{b}}$	$p_\pm$	$p_\mp$	$+$
$2p_{\mathrm{b}}$	p^2	p^2	$++$
$+_{\mathrm{c}}$	sd	p^2	$+-$
$-_{\mathrm{c}}$	p^2	sd	$+-$
4_{g}	sdp^2	sdp^2	$++--$

TABLE XVII. Elementary band representations for fourfold rotation symmetry. in the presence of time-reversal symmetry, the two p orbitals transform as a doublet, denoted by $2p_{\mathrm{a}}$.

so that

$$
C_{\mathrm{g}}(\mathbf{k}) = \begin{pmatrix} 0 & 0 & 0 & \mathbb{1}_{n_c} \\ \mathbb{1}_{n_c} & 0 & 0 & 0 \\ 0 & \mathbb{1}_{n_c} & 0 & 0 \\ 0 & 0 & \mathbb{1}_{n_c} & 0 \end{pmatrix}. \tag{B14}
$$

In the presence of time-reversal symmetry, we can again diagonalize the C_2 operator and perform a basis transformation, as described in App. B 1, to ensure that $C_2 T$ acts as a complex conjugation.

A band representation for C_4 symmetry consists of the C_4 eigenvalue, (i.e., the orbital type s, $p_\pm$, d) at the Γ and M points and the C_2 eigenvalue ($\pm$) at the X point. The EBRs for C_4 symmetry are listed in Table XVII.

3. D_4 symmetry

For the fourfold dihedral symmetry, there are five special Wyckoff positions as well as the generic Wyckoff position, as listed in Table XVIII. For a system with n_α electrons at the Wyckoff position α, the total number of electrons in the unit cell is

$$
n = n_{\mathrm{a}} + n_{\mathrm{b}} + 2n_{\mathrm{c}} + 4n_{\mathrm{d}} + 4n_{\mathrm{e}} + 8n_{\mathrm{g}}.
$$

The reciprocal space translation matrix is

$$
\Lambda(\mathbf{k}) = \mathrm{diag}\left\{\Lambda_{\mathrm{a}}(\mathbf{k}), \Lambda_{\mathrm{b}}(\mathbf{k}), \Lambda_{\mathrm{c}}(\mathbf{k}), \Lambda_{\mathrm{d}}(\mathbf{k}), \Lambda_{\mathrm{e}}(\mathbf{k}), \Lambda_{\mathrm{g}}(\mathbf{k})\right\}, \tag{B15}
$$

α	G_α	Location(s) within the unit cell ($\mathbf{r}_\alpha$)
a	D_4	$(0,0)$
b		$(1/2, 1/2)$
c	D_2	$(1/2, 0)$, $(0, 1/2)$
d	$\mathbb{Z}_2$	$(a, 0)$, $(0, a)$, $(-a, 0)$, $(0, -a)$
e		(a, a), $(-a, a)$, $(-a, -a)$, $(a, -a)$
g	—	(a_x, a_y), $(-a_y, a_x)$, $(-a_x, -a_y)$, $(a_y, -a_x)$, $(a_x, -a_y)$, (a_y, a_x), $(-a_x, a_y)$, $(-a_y, -a_x)$

TABLE XVIII. Wyckoff positions α at coordinate $\mathbf{r}_\alpha$(s) within the unit cell and the corresponding little groups G_α for a 2d D_4-symmetric lattice. Here, D_n denotes the group formed by n-fold rotation along with n reflections. We take $a, a_{x,y} \in (0, 1/2)$.

where

$$
\Lambda_{\mathrm{a}}(\mathbf{k}) = \mathbb{1}_{n_{\mathrm{a}}},
$$
$$
\Lambda_{\mathrm{b}}(\mathbf{k}) = \mathbb{1}_{n_{\mathrm{b}}} \mathrm{e}^{\mathrm{i}(k_x + k_y)/2},
$$
$$
\Lambda_{\mathrm{c}}(\mathbf{k}) = \mathbb{1}_{n_{\mathrm{c}}} \mathrm{diag}\left\{\mathrm{e}^{\mathrm{i}k_x/2}, \mathrm{e}^{\mathrm{i}k_y/2}\right\}
$$
$$
\Lambda_{\mathrm{d}}(\mathbf{k}) = \mathbb{1}_{n_{\mathrm{d}}} \mathrm{diag}\left\{\mathrm{e}^{\mathrm{i}ak_x}, \mathrm{e}^{\mathrm{i}ak_y}, \mathrm{e}^{-\mathrm{i}ak_x}, \mathrm{e}^{-\mathrm{i}ak_y}\right\}
$$
$$
\Lambda_{\mathrm{e}}(\mathbf{k}) = \mathbb{1}_{n_{\mathrm{e}}} \mathrm{diag}\left\{\mathrm{e}^{\mathrm{i}a(k_x+k_y)}, \mathrm{e}^{\mathrm{i}a(-k_x+k_y)}, \mathrm{e}^{\mathrm{i}a(-k_x-k_y)}, \right.
$$
$$
\left. \mathrm{e}^{\mathrm{i}a(k_x-k_y)}\right\},
$$
$$
\Lambda_{\mathrm{g}}(\mathbf{k}) = \mathbb{1}_{n_{\mathrm{g}}} \mathrm{diag}\left\{\mathrm{e}^{\mathrm{i}(a_x k_x + a_y k_y)}, \mathrm{e}^{\mathrm{i}(-a_x k_x + a_y k_y)}, \right.
$$
$$
\mathrm{e}^{\mathrm{i}(a_x k_x - a_y k_y)}, \mathrm{e}^{\mathrm{i}(-a_x k_x - a_y k_y)},
$$
$$
\mathrm{e}^{\mathrm{i}(a_y k_x + a_x k_y)}, \mathrm{e}^{\mathrm{i}(-a_y k_x + a_x k_y)},
$$
$$
\left. \mathrm{e}^{\mathrm{i}(a_y k_x - a_x k_y)}, \mathrm{e}^{\mathrm{i}(-a_y k_x - a_x k_y)}\right\}. \tag{B16}
$$

Since the group D_4 is generated by two operators, we need to compute a fourfold rotation operator C_4 and the mirror operator M_x, both of which are block diagonal in the Wyckoff positions, i.e.,

$$
C = \mathrm{diag}\left\{C_{\mathrm{a}}, C_{\mathrm{b}}, C_{\mathrm{c}}, C_{\mathrm{d}}, C_{\mathrm{e}}, C_{\mathrm{g}}\right\},
$$
$$
M = \mathrm{diag}\left\{M_{\mathrm{a}}, M_{\mathrm{b}}, M_{\mathrm{c}}, M_{\mathrm{d}}, M_{\mathrm{e}}, M_{\mathrm{g}}\right\}. \tag{B17}
$$

We now compute the matrices for each sector.

The Wyckoff positions "a" and "b" have multiplicity one and thus map to themselves under both C_4 and M_x. The orbitals at Wyckoff positions "a" and "b" are labeled by the irreps of D_4 (see Table XII). Thus, for $\alpha \in \{\mathrm{a}, \mathrm{b}\}$,

$$
C_\alpha = \mathrm{diag}\left\{\mathbb{1}_{n_{A_1\alpha}}, \mathbb{1}_{n_{A_2\alpha}}, -\mathbb{1}_{n_{A_3\alpha}}, -\mathbb{1}_{n_{A_4\alpha}}, \mathrm{i}\sigma_2 \mathbb{1}_{n_{B\alpha}}\right\},
$$
$$
M_\alpha = \mathrm{diag}\left\{\mathbb{1}_{n_{A_1\alpha}}, -\mathbb{1}_{n_{A_2\alpha}}, \mathbb{1}_{n_{A_3\alpha}}, -\mathbb{1}_{n_{A_4\alpha}}, \sigma_3 \mathbb{1}_{n_{B\alpha}}\right\}, \tag{B18}
$$

with $n_\alpha = n_{A_1\alpha} + n_{A_2\alpha} + n_{A_3\alpha} + n_{A_4\alpha} + 2n_{B\alpha}$, and we have chosen the explicit matrices for irrep B as in Eq. (78).

The two points constituting the Wyckoff position "c" transform into each other under C_4 but into themselves

under M_x. The orbitals at these points are labeled by $(\pm\pm)$, their parity under C_2 and M_x, respectively. Thus, in the simultaneous eigenbasis of C_2 and M_x, we get

$$c_{\rm c} = {\rm diag}\left\{ \mathbb{1}_{n_{++\rm c}}, \mathbb{1}_{n_{+-\rm c}}, -\mathbb{1}_{n_{-+\rm c}}, -\mathbb{1}_{n_{--\rm c}} \right\},$$
$$m_{\rm c} = {\rm diag}\left\{ \mathbb{1}_{n_{++\rm c}}, -\mathbb{1}_{n_{+-\rm c}}, \mathbb{1}_{n_{-+\rm c}}, -\mathbb{1}_{n_{--\rm c}} \right\}, \quad (B19)$$

with $n_{\rm c} = n_{++\rm c} + n_{+-\rm c} + n_{-+\rm c} + n_{--\rm c}$. As for C_4, we choose the basis at "c2" as the images of those at "c1" under a rotation, so that the rotation and mirror operators are explicitly given by

$$C_{\rm c} = \begin{pmatrix} 0 & c_{\rm c} \\ \mathbb{1}_{n_{\rm c}} & 0 \end{pmatrix}, \quad M_{\rm c} = \begin{pmatrix} m_{\rm c} & 0 \\ 0 & m_{\rm c}c_{\rm c} \end{pmatrix}. \quad (B20)$$

where in the latter case, m_c denotes the mirror eigenvalues of $M_y = M_x C_2$.

The four points constituting the Wyckoff position "d" transform as

$$\begin{aligned}
C_4\mathbf{r}_{\rm d1} &= \mathbf{r}_{\rm d2}, & M_x\mathbf{r}_{\rm d1} &= \mathbf{r}_{\rm d1}, \\
C_4\mathbf{r}_{\rm d2} &= \mathbf{r}_{\rm d3}, & M_x\mathbf{r}_{\rm d2} &= \mathbf{r}_{\rm d4}, \\
C_4\mathbf{r}_{\rm d3} &= \mathbf{r}_{\rm d4}, & M_x\mathbf{r}_{\rm d3} &= \mathbf{r}_{\rm d3}, \\
C_4\mathbf{r}_{\rm d4} &= \mathbf{r}_{\rm d1}, & M_x\mathbf{r}_{\rm d4} &= \mathbf{r}_{\rm d2}. \quad (B21)
\end{aligned}$$

The orbitals at Wyckoff position "d" are labeled by $\pm$, corresponding to the eigenvalue under reflection by the x (resp. y) axis. Thus,

$$m_{\rm d} = {\rm diag}\left\{ \mathbb{1}_{n_{+\rm d}}, -\mathbb{1}_{n_{-\rm d}} \right\}, \quad (B22)$$

with $n_{\rm d} = n_{+\rm d} + n_{-\rm d}$. We choose the rotated version of the orbitals at "d1" as the orbitals at the remaining three points constituting the Wyckoff position "d". Thus,

$$C_{\rm d} = \begin{pmatrix} 0 & 0 & 0 & \mathbb{1}_{n_{\rm d}} \\ \mathbb{1}_{n_{\rm d}} & 0 & 0 & 0 \\ 0 & \mathbb{1}_{n_{\rm d}} & 0 & 0 \\ 0 & 0 & \mathbb{1}_{n_{\rm d}} & 0 \end{pmatrix} \quad (B23)$$

and

$$M_{\rm d} = \begin{pmatrix} m_{\rm d} & 0 & 0 & 0 \\ 0 & 0 & 0 & m_{\rm d} \\ 0 & 0 & m_{\rm d} & 0 \\ 0 & m_{\rm d} & 0 & 0 \end{pmatrix}. \quad (B24)$$

The four points constituting the Wyckoff position "e" transform as

$$\begin{aligned}
C_4\mathbf{r}_{\rm e1} &= \mathbf{r}_{\rm e2}, & M_x\mathbf{r}_{\rm e1} &= \mathbf{r}_{\rm e4}, \\
C_4\mathbf{r}_{\rm e2} &= \mathbf{r}_{\rm e3}, & M_x\mathbf{r}_{\rm e2} &= \mathbf{r}_{\rm e3}, \\
C_4\mathbf{r}_{\rm e3} &= \mathbf{r}_{\rm e4}, & M_x\mathbf{r}_{\rm e3} &= \mathbf{r}_{\rm e2}, \\
C_4\mathbf{r}_{\rm e4} &= \mathbf{r}_{\rm e1}, & M_x\mathbf{r}_{\rm e4} &= \mathbf{r}_{\rm e1}. \quad (B25)
\end{aligned}$$

with $n_{\rm e} = n_{+\rm e} + n_{-\rm e}$. We again choose the rotated version of the orbitals at "e1" as the orbitals at the remaining three points constituting the Wyckoff position "e". Thus,

$$C_{\rm e} = \begin{pmatrix} 0 & 0 & 0 & \mathbb{1}_{n_{\rm e}} \\ \mathbb{1}_{n_{\rm e}} & 0 & 0 & 0 \\ 0 & \mathbb{1}_{n_{\rm e}} & 0 & 0 \\ 0 & 0 & \mathbb{1}_{n_{\rm e}} & 0 \end{pmatrix} \quad (B26)$$

and

$$M_{\rm e} = \begin{pmatrix} 0 & 0 & 0 & m_{\rm e} \\ 0 & 0 & m_{\rm e} & 0 \\ 0 & m_{\rm e} & 0 & 0 \\ m_{\rm e} & 0 & 0 & 0 \end{pmatrix}. \quad (B27)$$

Finally, the eight points constituting the generic Wyckoff position transform as

$$\begin{aligned}
C_4\mathbf{r}_{\rm g1} &= \mathbf{r}_{\rm g2}, & M_x\mathbf{r}_{\rm g1} &= \mathbf{r}_{\rm g5}, \\
C_4\mathbf{r}_{\rm g2} &= \mathbf{r}_{\rm g3}, & M_x\mathbf{r}_{\rm g2} &= \mathbf{r}_{\rm g8}, \\
C_4\mathbf{r}_{\rm g3} &= \mathbf{r}_{\rm g4}, & M_x\mathbf{r}_{\rm g3} &= \mathbf{r}_{\rm g7}, \\
C_4\mathbf{r}_{\rm g4} &= \mathbf{r}_{\rm g1}, & M_x\mathbf{r}_{\rm g4} &= \mathbf{r}_{\rm g6}, \\
C_4\mathbf{r}_{\rm g5} &= \mathbf{r}_{\rm g6}, & M_x\mathbf{r}_{\rm g5} &= \mathbf{r}_{\rm g1}, \\
C_4\mathbf{r}_{\rm g6} &= \mathbf{r}_{\rm g7}, & M_x\mathbf{r}_{\rm g6} &= \mathbf{r}_{\rm g4}, \\
C_4\mathbf{r}_{\rm g7} &= \mathbf{r}_{\rm g8}, & M_x\mathbf{r}_{\rm g7} &= \mathbf{r}_{\rm g3}, \\
C_4\mathbf{r}_{\rm g8} &= \mathbf{r}_{\rm g5}, & M_x\mathbf{r}_{\rm g8} &= \mathbf{r}_{\rm g2}, \quad (B28)
\end{aligned}$$

so that

$$C_{\rm g} = \begin{pmatrix} 0 & 0 & 0 & \mathbb{1}_{n_{\rm g}} & 0 & 0 & 0 & 0 \\ \mathbb{1}_{n_{\rm g}} & 0 & 0 & 0 & 0 & 0 & 0 & 0 \\ 0 & \mathbb{1}_{n_{\rm g}} & 0 & 0 & 0 & 0 & 0 & 0 \\ 0 & 0 & \mathbb{1}_{n_{\rm g}} & 0 & 0 & 0 & 0 & 0 \\ 0 & 0 & 0 & 0 & 0 & 0 & 0 & \mathbb{1}_{n_{\rm g}} \\ 0 & 0 & 0 & 0 & \mathbb{1}_{n_{\rm g}} & 0 & 0 & 0 \\ 0 & 0 & 0 & 0 & 0 & \mathbb{1}_{n_{\rm g}} & 0 & 0 \\ 0 & 0 & 0 & 0 & 0 & 0 & \mathbb{1}_{n_{\rm g}} & 0 \end{pmatrix}$$

and

$$M_{\rm g} = \begin{pmatrix} 0 & 0 & 0 & 0 & \mathbb{1}_{n_{\rm g}} & 0 & 0 & 0 \\ 0 & 0 & 0 & 0 & 0 & 0 & 0 & \mathbb{1}_{n_{\rm g}} \\ 0 & 0 & 0 & 0 & 0 & 0 & \mathbb{1}_{n_{\rm g}} & 0 \\ 0 & 0 & 0 & 0 & 0 & \mathbb{1}_{n_{\rm g}} & 0 & 0 \\ \mathbb{1}_{n_{\rm g}} & 0 & 0 & 0 & 0 & 0 & 0 & 0 \\ 0 & 0 & 0 & \mathbb{1}_{n_{\rm g}} & 0 & 0 & 0 & 0 \\ 0 & 0 & \mathbb{1}_{n_{\rm g}} & 0 & 0 & 0 & 0 & 0 \\ 0 & \mathbb{1}_{n_{\rm g}} & 0 & 0 & 0 & 0 & 0 & 0 \end{pmatrix}.$$

A band representation for a D_4 symmetric lattice thus consists of the irrep label at the Γ and M points,

Label	Γ	M	X	ΓM	MX	ΓX
$(A_1)_\mathrm{a}$	A_1	A_1	$(++)$	$+$	$+$	$+$
$(A_2)_\mathrm{a}$	A_2	A_2	$(+-)$	$-$	$-$	$-$
$(A_3)_\mathrm{a}$	A_3	A_3	$(++)$	$-$	$+$	$+$
$(A_4)_\mathrm{a}$	A_4	A_4	$(+-)$	$+$	$-$	$-$
$(B)_\mathrm{a}$	B	B	$(++)(+-)$	$+-$	$+-$	$+-$
$(A_1)_\mathrm{b}$	A_1	A_4	$(-+)$	$+$	$+$	$+$
$(A_2)_\mathrm{b}$	A_2	A_3	$(--)$	$-$	$-$	$-$
$(A_3)_\mathrm{b}$	A_3	A_2	$(-+)$	$-$	$+$	$+$
$(A_4)_\mathrm{b}$	A_4	A_1	$(--)$	$+$	$-$	$-$
$(B)_\mathrm{b}$	B	B	$(-+)(--)$	$+-$	$+-$	$+-$
$(++)_\mathrm{c}$	A_1A_3	B	$(++)(-+)$	$+-$	$++$	$++$
$(+-)_\mathrm{c}$	A_2A_4	B	$(+-)(--)$	$+-$	$--$	$--$
$(-+)_\mathrm{c}$	B	A_1A_3	$(++)(--)$	$+-$	$+-$	$+-$
$(--)_\mathrm{c}$	B	A_2A_4	$(+-)(-+)$	$+-$	$+-$	$+-$
$(+)_\mathrm{d}$	A_1A_3B	A_1A_3B	$(++)(++)(-+)(--)$	$+\,+\,-\,-$	$+\,+\,+\,-$	$+\,+\,+\,-$
$(+)_\mathrm{d}$	A_2A_4B	A_2A_4B	$(+-)(+-)(-+)(--)$	$+\,+\,-\,-$	$+\,-\,-\,-$	$+\,-\,-\,-$
$(+)_\mathrm{e}$	A_1A_4B	A_1A_4B	$(++)(+-)(-+)(--)$	$+\,+\,+\,-$	$+\,+\,-\,-$	$+\,+\,-\,-$
$(+)_\mathrm{e}$	A_2A_3B	A_2A_3B	$(++)(+-)(-+)(--)$	$+\,-\,-\,-$	$+\,+\,-\,-$	$+\,+\,-\,-$
8_g	$A_1A_2A_3A_4B^2$	$A_1A_2A_3A_4B^2$	$(++)(++)(-+)(-+)$ $(+-)(+-)(--)(--)$	$+\,+\,+\,+$ $-\,-\,-\,-$	$+\,+\,+\,+$ $-\,-\,-\,-$	$+\,+\,+\,+$ $-\,-\,-\,-$

TABLE XIX. Elementary band representations of the square lattice with D$_4$ symmetry. The representations of the little groups G_Γ and G_M are labeled by the irrep labels of D$_4$ (see Tab. XII), while representations of G_X are labeled by the eigenvalue of C_2 and M_x.

the twofold rotation and mirror eigenvalues ($\pm$) at the X point, and the eigenvalues $\pm$ of M_α for the 1-cells $\alpha = \Gamma\mathrm{X}, \mathrm{MX}, \Gamma\mathrm{M}$. The EBRs for D$_4$-symmetric band structures are listed in Table XIX.

Appendix C: Homotopic classification of maps defined on CW complexes

In this Section, we describe the classification procedure outlined in Sec. II C more rigorously.

CW-complex — The fundamental domain of the d-dimensional Brillouin zone has the structure of a CW-complex $\mathbb{D}$. Formally, $\mathbb{D}$ is a collection of "p-cells" with $0 \leq p \leq d$, each of which is homotopic to $(0,1)^p$, or, equivalently, to a p-ball. The CW-complex structure further includes a gluing map, which, given a p-cell α, assigns to its boundary $\partial\alpha$ — homotopically equivalent to the $(p-1)$-sphere S^{p-1} — a collection of q-cells with $q < p$. Note that a given q-cell β may be glued multiple times to the boundary $\partial\alpha$. We define the boundary $\partial\mathbb{D}$ of the CW complex as the union of boundaries of individual d-cells. Note that for a d-dimensional CW-complex $\mathbb{D}$ with multiple d-cells, lower-dimensional cells at the boundary between two d-cells are also considered to be part of $\partial\mathbb{D}$.

Bloch Hamiltonians and loop spaces — A Bloch Hamiltonian is defined as a map $h\colon \mathbb{D} \to \mathcal{X}$, which constitutes of a set of continuous maps $\alpha \to \mathcal{X}_\alpha$ for each p-cell α, so that h is compatible with the CW-complex structure of $\mathbb{D}$. We denote the space of such maps by $\Omega^0(\mathbb{D}, \mathcal{X})$.

For the classification procedure, we also need m-parameter families or "m-loops" of Bloch Hamiltonians. We recursively define such an m-loop h^m as a map $h^m\colon \mathbb{D} \times [0,1]^m \to \mathcal{X}$ that is compatible with the CW-complex structure of $\mathbb{D}$ for each fixed $(t_1, \ldots, t_m) \in [0,1]^m$ and which for $m \geq 1$ satisfies the condition

$$h^m(\mathbf{k}; t_1, \ldots, t_{m-1}, t_m) = h_\mathrm{ref}^{m-1}(\mathbf{k}; t_1, \ldots, t_{m-1}), \quad \text{(C1)}$$

with a h_ref^{m-1} a reference $(m-1)$-loop if $m > 1$ and a reference Bloch Hamiltonian $h_\mathrm{ref}^0 \equiv h_\mathrm{ref}$ if $m = 1$. With this notation, a Bloch Hamiltonian can be considered a "0-loop". The space of such m-loops is denoted $\Omega^m(\mathbb{D}, \mathcal{X})$. We can similarly define the loop spaces for $\partial\mathbb{D}$ and any other subcomplex of $\mathbb{D}$. Our end goal is the computation of the homotopy set $\pi_0[\Omega^0(\mathbb{D}, \mathcal{X})]$ enumerating homotopy classes of Bloch Hamiltonians. However, we will need homotopy sets of m-loops as an intermediate step.

Classification on $\partial\mathbb{D}$ — The computation of $\pi_0[\Omega^m(\mathbb{D}, \mathcal{X})]$ is simplified by the observation that two maps $g^m, h^m \in \Omega^m(\mathbb{D}, \mathcal{X})$ cannot be topologically equivalent if the restrictions $g^m|_{\partial\mathbb{D}}, h^m|_{\partial\mathbb{D}} \in \Omega^m(\partial\mathbb{D}, \mathcal{X})$

are topologically inequivalent. Furthermore, not all $h_\partial^m \in \Omega^m(\partial\mathbb{D}, \mathcal{X})$ can occur as the boundary restriction of some $h^m \in \Omega^m(\mathbb{D}, \mathcal{X})$. To see this, consider a d-cell α. Since α is homotopically isomorphic to the d-ball, $\partial\alpha$ is homtopically equivalent to S^{d-1}, so that the restriction $h^m|_{\partial\alpha}$ defines a map $S^{d-1} \to \Omega^m(\mathcal{X}_\alpha)$. Since α is contractible, $h^m|_{\partial\alpha}$ must be trivial in $\pi_{d-1}[\Omega^m(\mathcal{X}_\alpha)]$ if there exists a $h^m \in \Omega^m(\mathbb{D}, \mathcal{X})$ such that h_∂^m is the boundary restriction h^m. We refer to this restriction as a *compatibility condition*. We denote the subspace of $\Omega^m(\partial\mathbb{D}, \mathcal{X})$ that satisfies the compatibility condition for all d-cells by $\Omega^m(\partial\mathbb{D}, \mathcal{X})|_0$.

Being in $\Omega^m(\partial\mathbb{D}, \mathcal{X})|_0$ is not only *necessary*, but also a *sufficient* condition for a $h_\partial^m \in \Omega^m(\partial\mathbb{D}, \mathcal{X})$ to be the boundary restriction of some $h^m \in \Omega^m(\mathbb{D}, \mathcal{X})$. This is because satisfying the compatibility condition implies that for each d-cell $\alpha \in \mathbb{D}$ there exists a homotopy $H_\partial^m : \partial\alpha \times [0,1] \to \mathcal{X}$ that interpolates between h_∂^m and the trivial (*i.e.*, constant) map. Using the homotopic equivalence of α and the p-ball, we can interpret H_∂^m as an extension of h_∂^m to the full d-cell α. Continuing this for each α, we can thus define an extension of h_∂^m to $\Omega^m(\mathbb{D}, \mathcal{X})$.

We next compute the equivalence classes of $\Omega^m(\mathbb{D}, \mathcal{X})$ for a fixed homotopic class on $\partial\mathbb{D}$, *i.e.*, for a fixed element of $\pi_0[\Omega^m(\partial\mathbb{D}, \mathcal{X})|_0]$. We denote the corresponding subspaces of $\Omega^m(\mathbb{D}, \mathcal{X})$ and $\Omega^m(\partial\mathbb{D}, \mathcal{X})|_0$ by $\overline{\Omega}^m(\mathbb{D}, \mathcal{X})$ and $\overline{\Omega}^m(\partial\mathbb{D}, \mathcal{X})$, respectively. Hence, by construction $\overline{\Omega}^m(\partial\mathbb{D}, \mathcal{X})$ is a connected space. The remaining classification problem amounts to the computation of $\pi_0[\overline{\Omega}^m(\mathbb{D}, \mathcal{X})]$, which enumerates the connected components of $\overline{\Omega}^m(\mathbb{D}, \mathcal{X})$.

Classification on $\mathbb{D}$ — We choose a reference m-loop $h_{\partial,\mathrm{ref}}^m \in \overline{\Omega}^m(\partial\mathbb{D}, \mathcal{X})$ and define $\overline{\Omega}_{\mathrm{ref}}^m(\mathbb{D}, \mathcal{X})$ as the set of maps h^m satisfying $h^m|_{\partial\mathbb{D}} = h_{\partial,\mathrm{ref}}^m \forall (t_1, \ldots, t_m) \in [0,1]^m$. If we further fix a reference m-loop $h_{\mathrm{ref}}^m \in \overline{\Omega}_{\mathrm{ref}}^m(\mathbb{D}, \mathcal{X})$, then for any $h^m \in \overline{\Omega}_{\mathrm{ref}}^m(\mathbb{D}, \mathcal{X})$ and any d-cell α, the pair $(h^m, h_{\mathrm{ref}}^m)$ defines a map from $(\alpha \times \alpha) \times [0,1]^m \to \mathcal{X}_\alpha$. Since h^m and h_{ref}^m agree on the boundary of α, we can identify them on $\partial\alpha$, thereby forming an m-loop defined on the d-sphere S^d. Such m-loops can be classified by

$$\pi_d[\Omega^m(\mathcal{X}_\alpha)] \cong \pi_{m+d}[\mathcal{X}_\alpha], \qquad (C2)$$

where we have used the Freudenthal suspension theorem [32, Corollary 4.24]. Combining classification spaces from all d-cells in $\mathbb{D}$, we get

$$\pi_0[\overline{\Omega}_{\mathrm{ref}}^m(\mathbb{D}, \mathcal{X})] = \prod_{d-\mathrm{cells}\,\alpha\in\mathbb{D}} \pi_{m+d}[\mathcal{X}_\alpha]. \qquad (C3)$$

To compute $\pi_0[\overline{\Omega}^m(\mathbb{D}, \mathcal{X})]$, we use that the natural inclusion $i: \overline{\Omega}_{\mathrm{ref}}^m(\mathbb{D}, \mathcal{X}) \hookrightarrow \overline{\Omega}^m(\mathbb{D}, \mathcal{X})$ induces a map

$$\pi_0\left[\overline{\Omega}_{\mathrm{ref}}^m(\mathbb{D}, \mathcal{X})\right] \xrightarrow{i_*} \pi_0\left[\overline{\Omega}^m(\mathbb{D}, \mathcal{X})\right]. \qquad (C4)$$

This map is surjective, because, by construction, the restriction $h^m|_{\partial\mathbb{D}}$ of any m-loop $h^m \in \overline{\Omega}^m(\mathbb{D}, \mathcal{X})$ can always
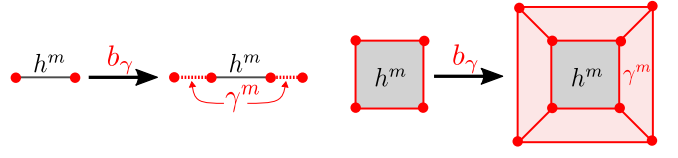

FIG. 15. Graphical representation of the bijection $b_{\gamma*}$ on $\pi_0[\Omega_{\mathrm{ref}}^m(\mathbb{D}, \mathcal{X})]$ induced by an element a loop γ on $\Omega^m(\partial\mathbb{D}, \mathcal{X})$ for a 1-cell (left) and a 2-cell(right).

be continuously deformed to $h_{\partial,\mathrm{ref}}^m$ and ths deformation can be extended to a homotopy between the full m-loop h^m and an m-loop in $\overline{\Omega}_{\mathrm{ref}}^m(\mathbb{D}, \mathcal{X})$ using the construction of Fig. 3. Since i_* is surjective, it follows that

$$\pi_0\left[\overline{\Omega}^m(\mathbb{D}, \mathcal{X})\right] \cong \pi_0\left[\overline{\Omega}_{\mathrm{ref}}^m(\mathbb{D}, \mathcal{X})\right] / \sim, \qquad (C5)$$

where $\sim$ denotes the equivalence classes of elements of $\pi_0[\overline{\Omega}_{\mathrm{ref}}^m(\mathbb{D}, \mathcal{X})]$ whose images under i_* are identical.

Quotienting out the boundary deformations — To characterize the equivalence classes defined in Eq. (C5), we first consider a pointed loop γ^m in $\overline{\Omega}^{m+1}(\partial\mathbb{D}, \mathcal{X})$ with the reference $h_{\partial,\mathrm{ref}}^m$, *i.e.*, a family of m-loops $\gamma^m(t) \in \Omega^m(\partial\mathbb{D}, \mathcal{X})$ parameterized by $t \in [0,1]$, such that $\gamma^m(0) = \gamma^m(1) = h_{\partial,\mathrm{ref}}^m$. Given $h^m \in \overline{\Omega}_{\mathrm{ref}}^m(\mathbb{D}, \mathcal{X})$, we can "attach" γ^m to h^m as shown graphically in Fig. 15 for one- and two-dimensional CW-complexes. We term this process a *boundary deformation* of h^m.

More formally, boundary deformation corresponding to the pointed loop $\gamma^m \in \overline{\Omega}^{m+1}(\partial\mathbb{D}, \mathcal{X})$ induces the map

$$\overline{\Omega}_{\mathrm{ref}}^m(\mathbb{D}, \mathcal{X}) \xrightarrow{b_\gamma} \overline{\Omega}_{\mathrm{ref}}^m(\mathbb{D}, \mathcal{X}). \qquad (C6)$$

This further induces a map between the homotopy sets

$$\pi_0\left[\overline{\Omega}_{\mathrm{ref}}^m(\mathbb{D}, \mathcal{X})\right] \xrightarrow{b_{\gamma*}} \pi_0\left[\overline{\Omega}_{\mathrm{ref}}^m(\mathbb{D}, \mathcal{X})\right]. \qquad (C7)$$

This map is well defined, since if $g^m, h^m \in \overline{\Omega}_{\mathrm{ref}}^m(\mathbb{D}, \mathcal{X})$ are homotopically equivalent, they remain so after identical boundary deformations. Since any loop γ^m has an inverse obtained by traversing it in the opposite direction, $b_{\gamma*}$ is a bijection.

We now show that for $g^m, h^m \in \overline{\Omega}_{\mathrm{ref}}^m(\mathbb{D}, \mathcal{X})$, the topological equivalence classes $[g^m] \sim [h^m]$ under the equivalence relation of Eq. (C5) *if and only if* there exists a pointed loop $\gamma^m \in \overline{\Omega}^{m+1}(\partial\mathbb{D}, \mathcal{X})$ such that $b_{\gamma*}([g^m]) = [h^m]$. To this end, we first note that attaching the loop γ^m to $h^m \in \overline{\Omega}_{\mathrm{ref}}^m(\mathbb{D}, \mathcal{X})$ naturally provides a homotopy between h^m and $b_\gamma(h^m)$ in $\overline{\Omega}^m(\mathbb{D}, \mathcal{X})$ (but not necessarily in $\overline{\Omega}_{\mathrm{ref}}^m(\mathbb{D}, \mathcal{X})$), so that the images in $\pi_0[\overline{\Omega}_{\mathrm{ref}}^m(\mathbb{D}, \mathcal{X})]$ of the topological equivalence classes $[h^m]$ and $b_{\gamma*}[h^m]$ under i_* are identical. To show that the converse is also true, we consider $g^m, h^m \in \overline{\Omega}_{\mathrm{ref}}^m(\mathbb{D}, \mathcal{X})$ such that $i_*[g^m] = i_*[h^m]$, *i.e.*, g^m and h^m are homotopically equivalent in $\overline{\Omega}^m(\mathbb{D}, \mathcal{X})$. Thus, there exists a homotopy $I^m(t)$

such that

$$I^m(\,\cdot\,,0) = g^m, \qquad I^m(\,\cdot\,,1) = h^m.$$

Since the boundary restrictions of g^m and h^m both equal $h_{\partial,\mathrm{ref}}^m$, the restriction $I^m|_{\partial\mathbb{D}}$ defines a boundary deformation in $\overline{\Omega}^{m+1}(\partial\mathbb{D}, \mathcal{X})$. Setting $\gamma^m \equiv I^m|_{\partial\mathbb{D}}$, the existence of I implies that h^m can be homotopically deformed into $b_\gamma(g^m)$, i.e., $b_{\gamma*}\colon [g^m] \mapsto [h^m]$.

From the definition of $b_{\gamma*}$ we note that $b_{\gamma*}$ depends only on the homotopic equivalence class of γ^m. These homotopic equivalence classes are classified by

$$\pi_1\!\left[\overline{\Omega}^m(\partial\mathbb{D}, \mathcal{X})\right] \cong \pi_0\!\left[\overline{\Omega}^{m+1}(\partial\mathbb{D}, \mathcal{X})\right]. \qquad \text{(C8)}$$

Hence, to compute the equivalence class under $\sim$, it is sufficient to consider the induced map $b_{\gamma*}$ for one boundary deformation γ^m of each equivalence class in $\pi_0[\overline{\Omega}^{m+1}(\partial\mathbb{D}, \mathcal{X})]$.

The full classification — We can complete the classification by computing $\pi_0[\overline{\Omega}^0(\mathbb{D}, \mathcal{X})]$ using Eqns. (C3) and (C5) for each element of $\pi_0[\Omega^0(\partial\mathbb{D}, \mathcal{X})|_0]$, i.e., for each possible lower-dimensional invariant. This requires knowledge of $\pi_0\big[\Omega^0(\partial\mathbb{D}, \mathcal{X})|_0\big]$, i.e.., of the homotopic classification on boundary $\partial\mathbb{D}$. Further, as discussed above, to evaluate the quotient in Eq. (C5), we need to know $\pi_0\big[\Omega^1(\partial\mathbb{D}, \mathcal{X})\big]$. Since $\partial\mathbb{D}$ is itself a $(d-1)$-dimensional CW complex, both $\pi_0\big[\Omega^0(\partial\mathbb{D}, \mathcal{X})|_0\big]$ and $\pi_0[\Omega^1(\partial\mathbb{D}, \mathcal{X})]$ can be calculated using the procedure described above. Proceeding recursively, we get classification sets with increasing loop order m, while lowering the dimension of the CW-complexes. We eventually end up with a 0-dimensional CW-complex, i.e., a disjoint set of points, the classification on which can be performed by elementary means.

This recursive procedure is greatly simplified by noting that it is not necessary to precisely determine $\pi_0\big[\Omega^{m+1}(\partial\mathbb{D}, \mathcal{X})\big]$ in order to obtain $\pi_0[\Omega^m(\mathbb{D}, \mathcal{X})]$ from Eq. (C5). Instead, it suffices to use the easier-to-compute classification sets $\pi_0[\overline{\Omega}_{\mathrm{ref}}^{m+1}(\partial\mathbb{D}, \mathcal{X})]$, thereby terminating the recursive procedure after one step. This simplification is possible because i_* is surjective and it is sufficient to consider a collection of boundary deformations $\gamma^m \in \overline{\Omega}^{m+1}(\partial\mathbb{D}, \mathcal{X})$ that is large enough to include *at least one* boundary deformation in each topological equivalence class.

Appendix D: Homotopy groups of Grassmannians

The Grassmannian $\mathrm{Gr}_\mathbb{F}(m, n)$ is a manifold that parameterize the n-dimenional linear subspaces of a $(m+n)$-dimensional vector space over the field $\mathbb{F} = \mathbb{R}, \mathbb{C}, \mathbb{H}$. They can be explicitly written as a quotient of groups as

$$\mathrm{Gr}_F(m, n) = \frac{G(m+n)}{G(m) \times G(n)}, \qquad \text{(D1)}$$

where G denotes the orthogonal, unitary or symplectic group for $F = \mathbb{R}, \mathbb{C}, \mathbb{H}$, respectively. The homotopy spaces of the Grassmannians can thus be computed by starting with the short exact sequence of groups

$$1 \to G(m) \times G(n) \to G(m+n) \to \mathrm{Gr}_\mathbb{F}(m, n) \to 1.$$

This defines the long exact sequence of homotopy spaces [32, Sec 4.2]

$$\begin{aligned}
\ldots &\to \pi_p[G(m)] \times \pi_p[G(n)] \to \pi_p[G(m+n)] \\
&\to \pi_p[\mathrm{Gr}_F(m, n)] \to \pi_{p-1}[G(m)] \times \pi_{p-1}[G(n)] \to \ldots
\end{aligned}$$

The homotopy groups of $G(n)$ for $G = \mathrm{O}, \mathrm{U}$, and Sp are well-known. They can all be computed in terms of the known homotopy groups of spheres using the short exact sequence [32, Sec 4.2, Example 4.55]

$$1 \to G(n) \to G(n+1) \to S^{r(n)} \to 1, \qquad \text{(D2)}$$

where $r(n) = n, 2n+1$, and $4n+3$ for $G = \mathrm{O}, \mathrm{U}$, and Sp, respectively. This leads to a long-exact sequence of homotopies

$$\cdots \to \pi_p[G(n)] \to \pi_p[G(n+1)] \to \pi_p[S^{r(n)}] \to \ldots$$

But since $\pi_p[S^k] = 0$ for $k > p$, this long exact sequence splits into

$$0 \to \pi_p[G(n)] \to \pi_p[G(n+1)] \to 0.$$

for $p > r(n)$. Thus, $\pi_p[G(n)] \cong \pi_p[G(n+1)]$ for $p > r(n)$, which is the stabilization of the homotopy groups of $G(n)$ for $n \to \infty$.

Appendix E: The Hopf invariant

The continuous maps from the 3-sphere S^3 to the complex Grassmannian $\mathrm{Gr}_\mathbb{C}(1, 1) \cong \mathbb{CP}^1 \cong S^2$ are classified by the third homotopy group

$$\pi_3[\mathrm{Gr}_\mathbb{C}(1, 1)] = \pi_3[S^2] = \mathbb{Z}. \qquad \text{(E1)}$$

The corresponding topological invariant is termed the *Hopf invariant* H. For a given map $h\colon S^3 \to S^2$, it can be calculated as the linking number of the preimages under h of two distinct points in S^2.

More explicitly, given a point $x \in S^2$, the preimage $\gamma = h^{-1}(x)$ defines a (single or multiple) closed loop(s). We take two distinct points x' and x'' infinitesimally close to x and denote their preimages under h by γ' and γ'', respectively. We then assign a directionality to γ for each point on it by computing the cross product of the vectors pointing towards γ' and γ''. The same direction may be assigned to γ' and γ'', as these curves are (infinitesimally) close to γ. The Hopf number H is then given by the linking number of the directed curves γ and γ'. Note that γ'' only serves to define the direction along γ and
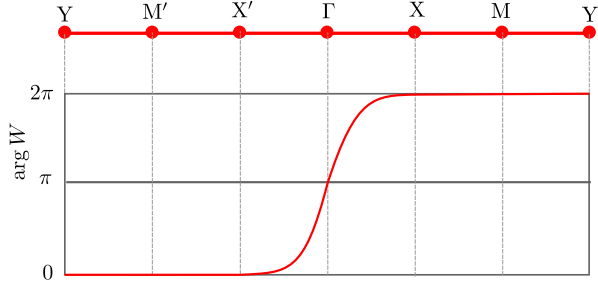
FIG. 16. The winding of the Wilson loop for a boundary deformation with nontrivial topology at Γ. Since $\arg W$ is pinned to π at Γ and time-reversal requires antisymmetry about it, the total winding must be odd. (see Fig. 4 for the definition of the high-symmetry points)

γ', but is otherwise not involved in the the calculation of the linking number.

An example of a map with H = 1 can be constructed by taking S^3 as the 3-ball $B^3 = \{\mathbf{r}|\,|\mathbf{r}| \leq 1\}$ with its surface identified to a single point. On B^3, we then consider the "band structure"

$$h(\mathbf{r}) = \mathrm{e}^{-\mathrm{i}\pi\mathbf{r}\cdot\boldsymbol{\tau}} h_0 \mathrm{e}^{\mathrm{i}\pi\mathbf{r}\cdot\boldsymbol{\tau}}, \quad (E2)$$

where the τ_α, $\alpha = 1,2,3$ are the Pauli matrices and $h_0 = \mathbf{h}_0 \cdot \boldsymbol{\tau}$ is a fixed gapped Hamiltonian. More explicitly,

$$h(\mathbf{r}) = \cos(2\pi r)h_0 - \sin(2\pi r)\mathbf{h}_0 \times \mathbf{r} \quad (E3)$$

Setting $h_0 = \tau_3$ in the following, the preimages γ, γ', and γ'' of $h = -\tau_3$, $h' = -\tau_3 + \pi^2\eta\tau_2$, and $h'' = -\tau_3 + \pi^2\eta\tau_1$, with $\eta \downarrow 0$ a positive infinitesimal are the curves parameterized by

$$\begin{aligned}
\mathbf{r}(\phi) &= (1/2)(\cos\phi, \sin\phi, 0),\\
\mathbf{r}'(\phi) &= (1 + \eta\cos\phi)\mathbf{r}(\phi) + \eta\sin\phi(0,0,1),\\
\mathbf{r}''(\phi) &= (1 - \eta\sin\phi)\mathbf{r}(\phi) + \eta\cos\phi(0,0,1), \quad (E4)
\end{aligned}$$

with $0 \leq \phi < 2\pi$. The curves are directed in the positive ϕ direction. The Hopf invariant H = 1 is the linking number of the curves γ and γ'.

Appendix F: Boundary deformations

This Appendix contains details on boundary deformations that may change the parent topological invariants at level-p. We thus consider families of Hamiltonians $H_\partial(\mathbf{k}_\partial, t)$, where $t \in [0,1]$ and $\mathbf{k}_\partial$ the coordinate along the boundary of a p-cell α, such that for any fixed t, H_∂ satisfies the symmetry constraints at the q-cells constituting $\partial\alpha$.

1. The Chern number

The $\mathbb{Z}$-valued Chern number is the level-2 parent invariant when the Hamiltonian is complex-valued. In the

following, we consider the Chern number over the 2-cell for a two-dimensional system with spinless time-reversal symmetry (symmetry class AI). We first present general arguments that a boundary deformation may change the parent Chern number C by an arbitrary integer and then construct an explicit deformation that changes C by one.

Consider a general boundary deformation $H_\partial(\mathbf{k}_\partial, t)$, where $\mathbf{k}_\partial$ denotes the momentum along the boundary and t is the homotopy parameter. Time-reversal symmetry implies that $H_\partial(\mathbf{k}_\partial, t) = \mathcal{U}_\mathrm{T} H_\partial^*(-\mathbf{k}_\partial, t)\mathcal{U}_\mathrm{T}^\dagger$ for some unitary $\mathcal{U}_\mathrm{T}$, where $-\mathbf{k}_\partial$ is the time-reversed momentum of $\mathbf{k}_\partial$, up to a translation by a reciprocal lattice vector. Thus, the Wilson loops $W_\partial(\mathbf{k}_\partial)$ describing parallel transport along t at fixed $\mathbf{k}_\partial \in \partial\mathbb{D}$ are related to those at $-\mathbf{k}_\partial$ as $W_\partial(\mathbf{k}_\partial) = W_\partial^*(-\mathbf{k}_\partial)$, so that

$$\arg\det W_\partial(\mathbf{k}_\partial) = -\arg\det W_\partial(-\mathbf{k}_\partial) \mod 2\pi. \quad (F1)$$

Thus, the windings from boundary segments related by time-reversal *add up*. This observation immediately allows one to construct boundary deformations with even Chern numbers.

To construct a boundary deformation with odd Chern numbers, we choose a basis where $\mathcal{U}_\mathrm{T} = \mathbb{1}$, so that the Hamiltonian is real at the high-symmetry points S. The corresponding Wilson loops are orthogonal, so that $\det W_\partial(\mathbf{k}_S) \in \{\pm 1\}$. If $\det W(\mathbf{k}_S) = -1$ at an odd number of 0-cells, then $W(\mathbf{k}_\perp)$ must have an odd winding number. This is illustrated in Fig. 16 for a minimal boundary transformation, which has winding number 1.

The existence of such a deformation can be traced back to nontrivial topology at one of the 0-cells, since $\pi_1[\mathcal{X}_S] = \pi_1[\mathrm{Gr}_\mathbb{R}(n_\mathrm{o}, n_\mathrm{e})] \cong \mathbb{Z}_2$ in the stable limit. Thus, we can construct a boundary deformation carrying a nonzero Chern number that is constant everywhere except in a neighborhood of a single high-symmetry point S. We denote the 1d coordinate along the boundary near S by θ such that S lies at $\theta = 0$, and define a deformation $H_\partial(\theta, t)$ as τ_3 (independent of t) for $|\theta| \geq \pi$ and

$$H_\partial(\theta, t) = \mathrm{e}^{\mathrm{i}\pi t\Gamma(\theta/2)}\tau_3\mathrm{e}^{-\mathrm{i}\pi t\Gamma(\theta/2)}, \quad (F2)$$

for $\theta \in (-\pi, \pi)$, where $\Gamma(\theta) = \tau_2\cos\theta - \tau_3\sin\theta$. We can verify that

$$H_\partial(\pm\pi, t) = H_\partial(\theta, 0) = H_\partial(\theta, 1) = \tau_3$$

and $H_\partial^*(\theta, t) = H_\partial(-\theta, t)$, so that the boundary constraint and the time-reversal symmetry are satisfied. The wavefunction for the occupied band is given by

$$\psi_\mathrm{o}(\theta, t) = \mathrm{e}^{\mathrm{i}\pi t\Gamma(\theta/2)}\begin{pmatrix}0\\1\end{pmatrix}$$

$$= \mathrm{e}^{\mathrm{i}\pi t\sin(\theta/2)}\mathrm{e}^{\mathrm{i}\pi t\cos(\theta/2)\tau_2}\begin{pmatrix}0\\1\end{pmatrix}.$$

The corresponding Wilson loop is

$$W^\mathrm{o}(\theta) = -\mathrm{e}^{\mathrm{i}\pi\sin(\theta/2)}. \quad (F3)$$

Thus, at the high symmetry point $\theta = 0$, we have $W^{\mathrm{o}}(0) = -1$. Upon taking θ over the interval $[-\pi, \pi]$, the phase of $W^o(\theta)$ winds once, corresponding to a Chern number $+1$.

2. The second Euler/Stiefel-Whitney number

The $\mathbb{Z}$-valued second Euler invariants $\mathrm{Eu}_2^{\mathrm{o/e}}$ are the level-2 parent invariants when the Hamiltonian is real-valued and the occupied/empty subspace consists of exactly two bands. In the following, we construct a boundary deformation that is nontrivial only in the neighborhood a high-symmetry point and carries a nonzero second Euler invariant. Such a deformation thus adds integers of the same parity to $\mathrm{Eu}_2^{\mathrm{o/e}}$. This boundary deformation is relevant for C_2 and C_4 symmetric band structure, whereby the rotation symmetry relates the two 1-cells adjacent to the high-symmetry point.

Explicitly, we assume that the rotation operator at the high symmetry point C_S, restricted to the subspace of interest $C_S'^{\mathrm{o/e}}$, contains one one positive and one negative eigenvalue. We work in the eigenbasis of the rotation operator, so that $C_S = \rho_3 \otimes \tau_0$, where ρ_μ and τ_μ are Pauli matrices. We again choose the 1d coordinate along the 1-cells near S by θ, with S located at $\theta = 0$. We then consider a boundary deformation

$$H_t^\pm(\theta) = e^{-i(\pi/4)\sin(\theta/2)\Sigma_{12}} h_t^\pm(\theta)\, e^{i(\pi/4)\sin(\theta/2)\Sigma_{12}}, \quad (\mathrm{F4})$$

where $\Sigma_{12} = \rho_1 \otimes \tau_2 - \rho_2 \otimes \tau_1$ and

$$h_t'^\pm(\theta) = e^{i\pi t\Gamma_\pm(\theta)}(\rho_0 \otimes \tau_3)e^{-i\pi t\Gamma_\pm(\theta)} \quad (\mathrm{F5})$$

with

$$\Gamma_-(\theta) = \rho_2 \otimes \tau_0 \sin(\theta/2) + \rho_3 \otimes \tau_2 \cos(\theta/2),$$
$$\Gamma_+(\theta) = \rho_2 \otimes \tau_3 \sin(\theta/2) + \rho_0 \otimes \tau_2 \cos(\theta/2). \quad (\mathrm{F6})$$

One verifies that $H_t^\pm(\theta) = \rho_3 H_t(-\theta)\rho_3$ and that $H_0^\pm(\theta) = H_1^\pm(\theta)$. At the high-symmetry point $\theta = 0$, $H_t^\pm(\theta)$ satisfies the symmetry constraints and has one occupied and one unoccupied band of each symmetry type. At $\theta = \pm\pi$, one has $H_t^\pm(\pi) = \rho_3 \otimes \tau_0$, independent of t. As a function of t, the two blocks of $H^\pm$ at $\theta = 0$ have winding numbers 1 and ± 1. To find the Wilson loops at fixed θ, we note that they are the same for $H^\pm$ and $h^\pm$, since $H^\pm$ and $h^\pm$ differ only by a t-independent basis transformation. Hence,

$$W_\pm^{\mathrm{o}}(\theta) = -e^{\mp i\pi\rho_2 \sin(\theta/2)},$$
$$W_\pm^{\mathrm{e}}(\theta) = -e^{i\pi\rho_2 \sin(\theta/2)}. \quad (\mathrm{F7})$$

At $\theta = 0$, all Wilson loops are equal to $-\rho_0$, which is topologically nontrivial and consistent with the winding numbers of $h^\pm$ being odd. Looking at the full family of Wilson loops $W^{\mathrm{o/e}}(\theta)$ for $-\pi \le \theta \le \pi$, we see that $H^\pm$ generates winding number pairs $(1,1)$ and $(-1,1)$ for occupied and unoccupied orbitals, thereby yielding the desired result.
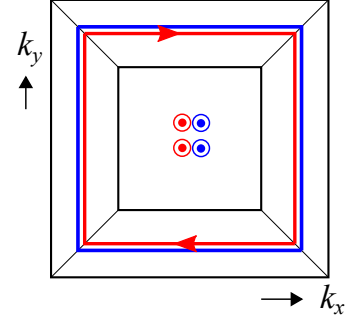

FIG. 17. Boundary deformation to change the Hopf invariant for a nonzero Chern number $C_z = 2$. The square represents a fixed-k_z cut of the 3-cell. The Chern number implies the existence of two directed segment pairs (shown red and blue) along the k_z-axis. The deformation nucleates a closed curve pair at the boundary, which encircles two curve pair segments running in the z direction, thereby changing the linking number — and hence the Hopf invariant — by $2C_z = 4$.

3. The Hopf invariant

The $\mathbb{Z}$-valued Hopf invariant is the parent invariant at level-3 when the Hamiltonian is complex-valued on the 3-cell and $n_{\mathrm{o}} = n_{\mathrm{e}} = 1$. In the following, we describe boundary deformations that may affect H.

No additional symmetries — In this case, the effect of boundary deformations on H depends on the level-2 invariants, *i.e.*, the Chern numbers $C_{x,y,z}$. To describe a general deformations, we first note that while the preimages of points for the Hopf map $S^3 \to S^2$ are closed curves in S^3, those for a 3-cell may start and end at the boundaries of $\mathbb{D}$. The difference between the number of times a component of a preimage γ starts and ends at the 2-cell perpendicular to the coordinate direction $\alpha = x, y, z$ is equal to the Chern number C_α. Since H is given by the linking number of a pair of preimages, we must construct a deformation that changes this linking number.

In Fig. 17, we depict such a deformation for the case of $C_x = C_y = 0$, $C_z = 2$, which implies the existence of two pairs of directed segments along z. We can then define a boundary deformation of the vertical faces, so that the deformation of each 1-cell carries a Chern number $+1$. This necessitates the existence of a pair of closed preimage curves, along the boundary. These curves encircle the two curve pairs running along z, thereby changing the linking number by $2C_z$. A similar deformation can be defined for Chern numbers in the other directions, so that the Hopf invariant can be changed by $n = 2\gcd(C_x, C_y, C_z)$.

With time-reversal symmetry — We explicitly construct a boundary deformation that changes H by one and is nontrivial only in the vicinity of a high symmetry point S at $\mathbf{k}_S = (0, 0, \pi)$. We introduce polar coordinates (ρ, ϕ) in the k_x-k_y plane with the origin at S and define a de-

formation $H_t(\rho, \phi)$ that is independent of t for $\rho > 1$. Explicitly, we take

$$H_t(\rho, \phi) = e^{i\pi\Gamma(t,\rho,\phi)}\tau_3 e^{-i\pi\Gamma(t,\rho,\phi)}, \qquad (F8)$$

with

$$\Gamma(t, \rho, \phi) = \cos(\pi t)\tau_2 + \rho\sin(\pi t)(\tau_1\cos\phi + \tau_3\sin\phi), \quad (F9)$$

This deformation then meets all required constraints, $H_t(\rho, \phi) = \tau_3$ for $t = 0, 1$ and for $\rho = 1$ and $H_t(\rho, \phi) = H_t(\rho, \phi + \pi)^*$. The boundary deformation $H_t(\rho, \phi)$ is a continuous deformation of the band structure h of Eq. (E2). Hence, it has unit Hopf number. This can be seen by noting that $H_t(\rho, \phi)$ is a deformation of the matrix-valued function $h(\mathbf{r}) = e^{i\pi\mathbf{r}\cdot\boldsymbol{\tau}}\tau_3 e^{-i\pi\mathbf{r}\cdot\boldsymbol{\tau}}$, which is defined on the 3-ball $|\mathbf{r}| \leq 1$ and which the paradigmatic example of a map with unit Hopf number.

With C_2T symmetry — In this case, the Hamiltonian is real for $k_z = 0$ and $k_z = \pi$. On the one hand, this implies that the Chern number $C_z = 0$, so that boundary deformations along the xz and yz faces of the fundamental domain do not change the Hopf number. On the other hand, this prohibits a boundary deformation along the xy and xz faces or along the xy and yz faces to nucleate a closed curve pair that encloses the fundamental domain. Hence, neither boundary deformations can change the Hopf number, so that Hopf number is a robust topological index if $n_o = n_e = 1$.

With C_2 or C_4 symmetry — In this case, there can be a curve pair penetrating the fundamental domain in the k_z direction only, so that boundary deformations associated with faces parallel to the k_z axis cannot change the parent Hopf number. Hence, with broken time-reversal symmetry the Hopf number is defined modulo 2C, C being the Chern number associated with a plane at constant k_z. With time-reversal symmetry, the Hamiltonian is real for $k_z = 0$ and $k_z = \pi$, which also rules out curve pairs penetrating the fundamental domain in the k_z direction. Hence, in this case the Hopf invariant is an integer.

Appendix G: Lattice model for the D_4-symmetric representation protected stable topological insulator

In this section, we construct lattice models that exhibit the D_4-symmetric representation protected stable topological phase described in Sec. VIII.

1. Two dimensions

Consider a system with two atoms at the Wyckoff position "a", each with a doublet that transforms under the 2d irrep B of D_4. The symmetry operators are thus

$$C_4 = i\sigma^2\tau^0, \qquad M_x = \sigma^3\tau^0, \qquad (G1)$$

where the Pauli matrices σ^μ and τ^μ denote the orbital and site degrees of freedom, respectively. The most general 4-band Bloch Hamiltonian can be written as

$$H(\mathbf{k}) = h_{\mu\nu}(\mathbf{k})\sigma^\mu\tau^\nu, \quad \mu, \nu \in \{0, 1, 2, 3\}, \qquad (G2)$$

where the functions $h_{\mu\nu}(\mathbf{k})$ are real-valued and periodic in $\mathbf{k}$, since we only consider the Wyckoff position "a" (see Appendix B 3). Next, as $C_2 \propto \mathbb{1}_4$, C_2T that $H(\mathbf{k})$ be real-valued, restricting the allowed matrices in Eq. (G2) to $\sigma^a\tau^b$, $a, b \in \{0, 1, 3\}$ and $\sigma^2\tau^2$. Finally, under C_4 and M_x, $\sigma^\mu\tau^\nu$ transform up to a sign, so that the functions $h_{\mu\nu}(\mathbf{k})$ must have the same behavior. A convenient set of such functions is given by:

$$f_{p,q}^\pm(\mathbf{k}) \equiv \cos(pk_x)\cos(qk_y) \pm \cos(qk_x)\cos(pk_y),$$
$$g_{p,q}^\pm(\mathbf{k}) \equiv \sin(pk_x)\sin(qk_y) \pm \sin(qk_x)\sin(pk_y), \quad (G3)$$

where $0 \leq p \leq q \in \mathbb{Z}$. Under M_x, $f_{p,q}^\pm$ remain invariant while $g_{p,q}^\pm$ change sign, and under C_4, $f_{p,q}^+$ and $g_{p,q}^-$ remain invariant while $f_{p,q}^-$ and $g_{p,q}^+$ change sign. Taking these into account, we can write $h_{\mu\nu}(\mathbf{k})$ as a linear combination of only one kind of functions defined in Eq. (G3).

Accounting for the constraints described above, we set

$$\begin{aligned} H(\mathbf{k}) &= \left[m - f_{0,1}^+(\mathbf{k})\right]\sigma^0\tau^1 + tg_{1,2}^+(\mathbf{k})\sigma^1\tau^3 \\ &\quad + t' f_{0,2}^-(\mathbf{k})\sigma^3\tau^3 \\ &= (\cos k_x + \cos k_y)\left[-\sigma^0\tau^1 + 2t\sin k_x\sin k_y\sigma^1\tau^3\right. \\ &\quad \left. -2t'(\cos k_x - \cos k_y)\sigma^3\tau^3\right] + m\sigma^0\tau^1. \quad (G4) \end{aligned}$$

We now show that $H(\mathbf{k})$ has two nontrivial level-1 invariants defined by Eq. (98). These can be computed from the two parity sectors of $H(\mathbf{k})$ at the high-symmetry lines, which correspond to eigenvalues ± 1 of the mirror operators (see Eq. (86)) given by

$$M_{\Gamma M} = \sigma^1\tau^0, \quad M_{\Gamma X} = \sigma^3\tau^0, \quad M_{XM} = -\sigma^3\tau^0.$$

The two parity sectors can be explicitly written as

$$\begin{aligned} h_{\Gamma M}^\pm(k) &= (m - 2\cos k)\tau^1 \pm 4t\sin^2 k\cos k\,\tau^3, \\ h_{\Gamma X}^\pm(k) &= (m - 1 - \cos k)\tau^1 \pm 2t'\sin^2 k\,\tau^3, \\ h_{XM}^\pm(k) &= (m + 1 - \cos k)\tau^1 \pm 2t'\sin^2 k\,\tau^3, \qquad (G5) \end{aligned}$$

where the argument $k \in [0, \pi]$ of $h_{SS'}^\pm$ denotes the coordinate along SS'. For $t, t' \neq 0$, all of these are gapless when $m = 0, \pm 2$ and trivial for $m \to \pm\infty$, so that we may get a topological phase for $0 < |m| < 2$.

The level-1 invariants are defined in terms of the Wilson loops on the 1-cells, which we can compute as the parity of the winding numbers associated with the 2×2 Hamiltonians $h_{SS'}^\pm(k)$ in the τ^1-τ^3 plane. Thus, to compute the invariant $\mathrm{SW}_1^{\Gamma M} = \mathrm{SW}_{1,+}^{\Gamma M} - \mathrm{SW}_{1,-}^{\Gamma M}$, we consider the difference of the winding numbers for $h_{SS'}^+$ and $h_{SS'}^-$, which is well defined, because $h_{SS'}^+(k) = h_{SS'}^-(k)$ for $k = 0, \pi$, *i.e.*, for the Γ and M points. For $0 < |m| < 2$, this winding number is given by $\mathrm{sgn}(mt)$. To compute
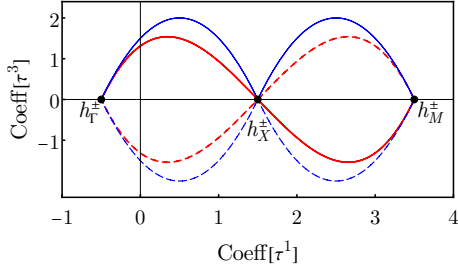
FIG. 18. The windings of $h_{\Gamma M}^{\pm}(k)$ for $m = 1.5$ for the positive (solid) and negative (dashed) subspaces along the ΓM (red) and ΓXM (blue). The two parities on ΓM taken together have a winding number -1, while the positive parities taken together have a winding number 0.
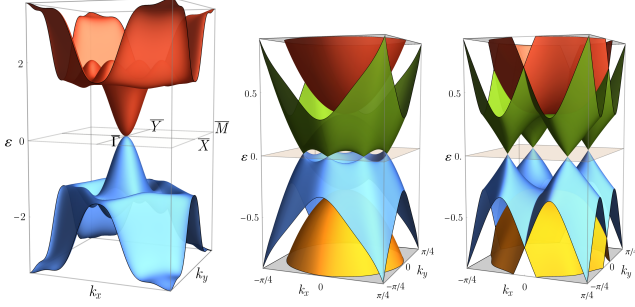

FIG. 19. (Left) Surface spectrum showing a quadratic band touching at the $\overline{\Gamma}$ point for the model defined in Eq. (G7) with parameters $t = t' = 1$ and $m = 2.5$. The remaining plots show the surface spectrum near the $\overline{\Gamma}$-point for two copies of this model with $t' = 1$ on both copies (center) and $t' = \pm 1$ for the two copies (right). The two copies are coupled by the Hamiltonian defined in Eq. (G13) with $\lambda_1 = 0.3$ and $\lambda_2 = 1.0$. The two cases show eight and four Dirac nodes in the surface Brillouin zone.

SW$_1^+$, we need the winding number of the positive parity sectors for the full loop $\Gamma M X \Gamma$, which is $\mathrm{sgn}(mt')$ if tt' is negative and zero otherwise (see Fig. 18). Thus, for $0 < |m| < 2$

$$\mathrm{SW}_1^{\Gamma M} = 1, \qquad \mathrm{SW}_1^+ = \Theta(-tt'), \qquad (G6)$$

while both invariants are trivial for $|m| > 2$.

2. Three dimensions

We consider the 3d Bloch Hamiltonian

$$H_{3d}(\mathbf{k}) = H(\mathbf{k}_\perp) + \sigma^0 \otimes \left[\cos k_z \tau^1 + \sin k_z \tau^2 \right], \quad (G7)$$

where $\mathbf{k}_\perp = (k_x, k_y)$. For $1 < |m| < 3$, the restriction of $H_{3d}(\mathbf{k})$ to $k_z = 0$ and $k_z = \pi$ are in different topological phases, so that $H_{3d}(\mathbf{k})$ has nontrivial level-2 invariants

$$C^{\Gamma M} = \mathrm{sgn}(mt), \qquad C^+ = \mathrm{sgn}(mt')\Theta(-tt'). \quad (G8)$$

For this model, we only get $C^{\Gamma M} = C^{M X \Gamma} = \pm 1$, so that we expect a quadratic band touching at a surface normal to k_z for $t, t' \neq 0$ for any $1 < |m| < 3$ (see the discussion

in Sec. VIII C). This is indeed what we see in numerical exact diagonalization, as shown in Fig. 19(left).

The boundary modes can be computed analytically following the generalized transfer matrix approach [106]. We follow the notation of Sec. V of Ref. [106] and identify the hopping and on-site matrices as [see 106, Eq. (124)]

$$J = \begin{pmatrix} 0 & \mathbb{1}_2 \\ 0 & 0 \end{pmatrix}, \qquad M(\mathbf{k}_\perp) = \begin{pmatrix} \mathbf{b} \cdot \boldsymbol{\sigma} & \mu \sigma^0 \\ \mu \sigma^0 & -\mathbf{b} \cdot \boldsymbol{\sigma} \end{pmatrix}, \quad (G9)$$

where $\mu(\mathbf{k}_\perp) = m - \cos k_x - \cos k_y$ and

$$\mathbf{b}(\mathbf{k}_\perp) = 2(\cos k_x + \cos k_y) \begin{pmatrix} t \sin k_x \sin k_y \\ 0 \\ t'(\cos k_y - \cos k_x) \end{pmatrix}.$$

The transfer matrix is given by [106, Eq. (131)]

$$T(\mathbf{k}_\perp) = \frac{1}{\mu} \begin{pmatrix} \left(\varepsilon^2 - b^2 - \mu^2 \right) \sigma^0 & -\varepsilon \sigma^0 + \mathbf{b} \cdot \boldsymbol{\sigma} \\ \varepsilon \sigma^0 + \mathbf{b} \cdot \boldsymbol{\sigma} & -\sigma^0 \end{pmatrix}. \quad (G10)$$

The modes localized at the surface satisfy

$$\varepsilon_{\mathrm{bdry}}(\mathbf{k}_\perp) = \pm \left| \mathbf{b}(\mathbf{k}_\perp) \right|, \qquad |\mu(\mathbf{k}_\perp)| < 1. \quad (G11)$$

The first equation is obtained by imposing the Dirichlet boundary condition at the surface, while the inequality follows from demanding that the states decay into the bulk. Near the $\overline{\Gamma}$ and $\overline{M}$ points, to lowest order, $\varepsilon_{\mathrm{bdry}}(\mathbf{k}_\perp) = 2 |\delta\mathbf{k}_\perp|^2$, where $\delta\mathbf{k}_\perp$ is measured from the gapless point. Since $\mu = m \mp 2$ for the $\overline{\Gamma}$ and $\overline{M}$ points, we get quadratic band touching at $\overline{\Gamma}$ for $1 < m < 3$ and at $\overline{M}$ for $-3 < m < -1$.

The nature of the anomalous boundary modes is independent of C^+ so far. However, we can see its effect by taking two copies of this model. From the transfer matrix, the surface Hamiltonian near the $\overline{\Gamma}$ point to the quadratic order in $\mathbf{k}_\perp$ is given by

$$H_{\mathrm{surf}}(\mathbf{k}_\perp) \approx 2tk_xk_y\sigma^1 - 2t'(k_x^2 - k_y^2)\sigma^3. \quad (G12)$$

Assuming $m, t > 0$, we get $C^{\Gamma M} = 1$ and $C^+ = \Theta(-t')$. We now consider the doubled Hamiltonian with the symmetry allowed mixing term

$$\delta H(\mathbf{k}_\perp) = \lambda_0 \sigma^0 \rho^1 + \lambda_2 k_x k_y (k_x^2 - k_y^2)\sigma^2 \rho^2, \quad (G13)$$

where ρ^μ are Pauli matrices in the space of the two copies. For two identical copies of $H_{\mathrm{surf}}(\mathbf{k}_\perp)$ with $t' = 1$,

$$C^{\Gamma M} = 2, \ C^+ = 0 \implies C^{\Gamma X M} = 2C^+ - C^{\Gamma M} = -2.$$

Thus, we get one Dirac cone on both ΓM and $\Gamma X M$, leading to eight Dirac cones in the surface Brillouin zone, as shown in Fig. 19(center). On the other hand, for two distinct copies of $H_{\mathrm{surf}}(\mathbf{k}_\perp)$ with $t' = \pm 1$,

$$C^{\Gamma M} = 2, \ C^+ = 1 \implies C^{\Gamma X M} = 2C^+ - C^{\Gamma M} = 0.$$

Thus, we get four Dirac cones in the surface Brillouin zone, as shown in Fig. 19(right).

[1] M. Z. Hasan and C. L. Kane, Colloquium: Topological insulators, Rev. Mod. Phys. **82**, 3045 (2010).

[2] X.-L. Qi and S.-C. Zhang, Topological insulators and superconductors, Rev. Mod. Phys. **83**, 1057 (2011).

[3] B. A. Bernevig and T. L. Hughes, *Topological Insulators and Topological Superconductors* (Princeton University Press, 2013).

[4] Y. Ando and L. Fu, Topological crystalline insulators and topological superconductors: From concepts to materials, Ann. Rev. Condensed Matter Physics **6**, 361 (2015).

[5] A. Kitaev, Periodic table for topological insulators and superconductors, AIP Conference Proceedings **1134**, 22 (2009).

[6] R. Kennedy and C. Guggenheim, Homotopy theory of strong and weak topological insulators, Phys. Rev. B **91**, 245148 (2015).

[7] A. Nelson, T. Neupert, T. c. v. Bzdušek, and A. Alexandradinata, Multicellularity of delicate topological insulators, Phys. Rev. Lett. **126**, 216404 (2021).

[8] J. E. Moore, Y. Ran, and X.-G. Wen, Topological surface states in three-dimensional magnetic insulators, Phys. Rev. Lett. **101**, 186805 (2008).

[9] D.-L. Deng, S.-T. Wang, C. Shen, and L.-M. Duan, Hopf insulators and their topologically protected surface states, Phys. Rev. B **88**, 201105(R) (2013).

[10] R. Kennedy, Topological Hopf-Chern insulators and the Hopf superconductor, Phys. Rev. B **94**, 035137 (2016).

[11] B. Bradlyn, Z. Wang, J. Cano, and B. A. Bernevig, Disconnected elementary band representations, fragile topology, and Wilson loops as topological indices: An example on the triangular lattice, Phys. Rev. B **99**, 045140 (2019).

[12] H. C. Po, H. Watanabe, and A. Vishwanath, Fragile topology and Wannier obstructions, Phys. Rev. Lett. **121**, 126402 (2018).

[13] Y. Hwang, J. Ahn, and B.-J. Yang, Fragile topology protected by inversion symmetry: Diagnosis, bulk-boundary correspondence, and Wilson loop, Phys. Rev. B **100**, 205126 (2019).

[14] S. Liu, A. Vishwanath, and E. Khalaf, Shift insulators: Rotation-protected two-dimensional topological crystalline insulators, Phys. Rev. X **9**, 031003 (2019).

[15] L. Zou, H. C. Po, A. Vishwanath, and T. Senthil, Band structure of twisted bilayer graphene: Emergent symmetries, commensurate approximants, and Wannier obstructions, Phys. Rev. B **98**, 085435 (2018).

[16] Z. Song, Z. Wang, W. Shi, G. Li, C. Fang, and B. A. Bernevig, All magic angles in twisted bilayer graphene are topological, Phys. Rev. Lett. **123**, 036401 (2019).

[17] H. C. Po, L. Zou, T. Senthil, and A. Vishwanath, Faithful tight-binding models and fragile topology of magic-angle bilayer graphene, Phys. Rev. B **99**, 195455 (2019).

[18] J. Ahn, S. Park, and B.-J. Yang, Failure of Nielsen-Ninomiya theorem and fragile topology in two-dimensional systems with space-time inversion symmetry: Application to twisted bilayer graphene at magic angle, Phys. Rev. X **9**, 021013 (2019).

[19] M. P. Zelatel and J. Y. Khoo, The gate-tunable strong and fragile topology of multilayer-graphene on a transition metal dichalcogenide, arXiv:1901.01294 (2019).

[20] A. P. Schnyder, S. Ryu, A. Furusaki, and A. W. W. Ludwig, Classification of topological insulators and superconductors in three spatial dimensions, Phys. Rev. B **78**, 195125 (2008).

[21] A. P. Schnyder, S. Ryu, A. Furusaki, and A. W. W. Ludwig, Classification of topological insulators and superconductors, AIP Conference Proceedings **1134**, 10 (2009).

[22] A. M. Turner, Y. Zhang, R. S. K. Mong, and A. Vishwanath, Quantized response and topology of magnetic insulators with inversion symmetry, Phys. Rev. B **85**, 165120 (2012).

[23] C.-K. Chiu, H. Yao, and S. Ryu, Classification of topological insulators and superconductors in the presence of reflection symmetry, Phys. Rev. B **88**, 075142 (2013).

[24] K. Shiozaki and M. Sato, Topology of crystalline insulators and superconductors, Phys. Rev. B **90**, 165114 (2014).

[25] L. Trifunovic and P. W. Brouwer, Higher-order bulk-boundary correspondence for topological crystalline phases, Phys. Rev. X **9**, 011012 (2019).

[26] E. Cornfeld and A. Chapman, Classification of crystalline topological insulators and superconductors with point group symmetries, Phys. Rev. B **99**, 075105 (2019).

[27] R. Kennedy and M. R. Zirnbauer, Bott periodicity for $\mathbb{Z}_2$ symmetric ground states of gapped free-fermion systems, Communications in Mathematical Physics **342**, 909 (2016).

[28] A. Bouhon, T. c. v. Bzdušek, and R.-J. Slager, Geometric approach to fragile topology beyond symmetry indicators, Phys. Rev. B **102**, 115135 (2020).

[29] Z.-D. Song, L. Elcoro, and B. A. Bernevig, Twisted bulk-boundary correspondence of fragile topology, Science **367**, 794 (2020).

[30] Z.-D. Song, L. Elcoro, Y.-F. Xu, N. Regnault, and B. A. Bernevig, Fragile phases as affine monoids: Classification and material examples, Phys. Rev. X **10**, 031001 (2020).

[31] S. Kobayashi and A. Furusaki, Fragile topological insulators protected by rotation symmetry without spin-orbit coupling, Phys. Rev. B **104**, 195114 (2021).

[32] A. Hatcher, *Algebraic topology* (Cambridge University Press, 2002).

[33] J. E. Moore and L. Balents, Topological invariants of time-reversal-invariant band structures, Phys. Rev. B **75**, 121306(R) (2007).

[34] C. Fang and L. Fu, New classes of three-dimensional topological crystalline insulators: Nonsymmorphic and magnetic, Phys. Rev. B **91**, 161105(R) (2015).

[35] A. Alexandradinata, C. Fang, M. J. Gilbert, and B. A. Bernevig, Spin-orbit-free topological insulators without time-reversal symmetry, Phys. Rev. Lett. **113**, 116403 (2014).

[36] A. Alexandradinata and B. A. Bernevig, Berry-phase description of topological crystalline insulators, Phys. Rev. B **93**, 205104 (2016).

[37] A. Alexandradinata, J. Höller, C. Wang, H. Cheng, and L. Lu, Crystallographic splitting theorem for band representations and fragile topological photonic crystals, Phys. Rev. B **102**, 115117 (2020).

[38] Anomalous boundary states also exist for the so-called *weak* [72] topology, whereby the topological invariant for a d-dimensional system is protected by discrete translation symmetry in less than d dimensions. The anomalous boundary modes occur only at boundaries that respect the discrete translation symmetry.

[39] L. Fu, Topological crystalline insulators, Phys. Rev. Lett. **106**, 106802 (2011).

[40] J. Höller and A. Alexandradinata, Topological Bloch oscillations, Phys. Rev. B **98**, 024310 (2018).

[41] B. Lian, F. Xie, and B. A. Bernevig, Landau level of fragile topology, Phys. Rev. B **102**, 041402(R) (2020).

[42] J. Liu, J. Liu, and X. Dai, Pseudo landau level representation of twisted bilayer graphene: Band topology and implications on the correlated insulating phase, Phys. Rev. B **99**, 155415 (2019).

[43] X. Lu, B. Lian, G. Chaudhary, B. A. Piot, G. Romagnoli, K. Watanabe, T. Taniguchi, M. Poggio, A. H. MacDonald, B. A. Bernevig, and D. K. Efetov, Multiple flat bands and topological Hofstadter butterfly in twisted bilayer graphene close to the second magic angle, PNAS **118**, e2100006118 (2021).

[44] Some of these signatures can be interpreted as manifestations of various other forms of stable topology, *viz*, that of topologically localized insulators [107] for Hopf insulators and that of obstructed atomic limits for the twisted boundary signature and the fractional corner charges.

[45] A. Alexandradinata, A. Nelson, and A. A. Soluyanov, Teleportation of berry curvature on the surface of a hopf insulator, Phys. Rev. B **103**, 045107 (2021).

[46] B. Lapierre, T. Neupert, and L. Trifunovic, n-band Hopf insulator, Phys. Rev. Research **3**, 033045 (2021).

[47] V. Peri, Z.-D. Song, M. Serra-Garcia, P. Engeler, R. Queiroz, X. Huang, W. Deng, Z. Liu, B. A. Bernevig, and S. D. Huber, Experimental characterization of fragile topology in an acoustic metamaterial, Science **367**, 797 (2020).

[48] W. A. Benalcazar, T. Li, and T. L. Hughes, Quantization of fractional corner charge in C_n-symmetric higher-order topological crystalline insulators, Phys. Rev. B **99**, 245151 (2019).

[49] A. Altland and M. R. Zirnbauer, Nonstandard symmetry classes in mesoscopic normal-superconducting hybrid structures, Phys. Rev. B **55**, 1142 (1997).

[50] This definition requires that $H_{1,2}$ have equal number of conduction and valence bands. However, if the symmetries allow for the definition of a canonical "trivial" band, then this definition can be further relaxed to allow comparison of systems with different number of bands by adding the trivial bands.

[51] G. D. Nittis and K. Gomi, Classification of "real" Bloch-bundles: Topological insulators of type AI, J. Geom. Phys. **86**, 303 (2014).

[52] G. D. Nittis and K. Gomi, Classification of "quaternionic" Bloch-bundles: topological quantum systems of type AII, Commun. Math. Phys. **339**, 1 (2015).

[53] Strictly speaking, defining the trivial element for the group operation does not require the identification of a trivial band structure, but, instead, proceeds via the Grothendieck construction, which considers topological equivalence of *pairs* (H, H') of gapped band structures. Two pairs (H_1, H_1') and (H_2, H_2') are then considered topologically equivalent if $H_1 \oplus H_2'$ can be smoothly deformed into $H_2 \oplus H_1'$, without closing the excitation gap and without violating the symmetry constraints.

[54] B. Bradlyn, L. Elcoro, J. Cano, M. G. Vergniory, Z. Wang, C. Felser, M. I. Aroyo, and B. A. Bernevig, Topological quantum chemistry, Nature **547**, 298 (2017).

[55] H. C. Po, A. Vishwanath, and H. Watanabe, Symmetry-based indicators of band topology in the 230 space groups, Nature Communications **8**, 50 (2017).

[56] Z. Song, T. Zhang, Z. Fang, and C. Fang, Quantitative mappings between symmetry and topology in solids, Nature Communications **9**, 3530 (2018).

[57] Mathematically, the fundamental domain can be defined as the closure of the largest open set in the BZ on which the group action of G is free (*i.e.*, no point maps onto itself under the action of any non-identity element of the G).

[58] A similar construction, but in position space, appears in the construction of a "topological crystal" in Ref. [108].

[59] J. Kruthoff, J. de Boer, J. van Wezel, C. L. Kane, and R.-J. Slager, Topological classification of crystalline insulators through band structure combinatorics, Phys. Rev. X **7**, 041069 (2017).

[60] F. Tang, H. C. Po, A. Vishwanath, and X. Wan, Topological materials discovery by large-order symmetry indicators, Sci Adv **5**, eaau8725 (2019).

[61] F. Tang, H. C. Po, A. Vishwanath, and X. Wan, Comprehensive search for topological materials using symmetry indicators, Nature **566**, 486 (2019).

[62] T. Zhang, Y. Jiang, Z. Song, H. Huang, Y. He, Z. Fang, H. Weng, and C. Fang, Catalogue of topological electronic materials, Nature **566**, 475 (2019).

[63] F. Tang, H. C. Po, A. Vishwanath, and X. Wan, Efficient topological materials discovery using symmetry indicators, Nature Physics **15**, 470 (2019).

[64] J. Cano, B. Bradlyn, Z. Wang, L. Elcoro, M. G. Vergniory, C. Felser, M. I. Aroyo, and B. A. Bernevig, Topology of disconnected elementary band representations, Phys. Rev. Lett. **120**, 266401 (2018).

[65] J. Cano and B. Bradlyn, Band representations and topological quantum chemistry, Annual Review of Condensed Matter Physics **12**, 225 (2021).

[66] M. Vergniory, L. Elcoro, C. Felser, N. Regnault, B. A. Bernevig, and Z. Wang, A complete catalogue of high-quality topological materials, Nature **566**, 480 (2019).

[67] A. Alexandradinata, X. Dai, and B. A. Bernevig, Wilson-loop characterization of inversion-symmetric topological insulators, Phys. Rev. B **89**, 155114 (2014).

[68] A. Bouhon, A. M. Black-Schaffer, and R.-J. Slager, Wilson loop approach to fragile topology of split elementary band representations and topological crystalline insulators with time-reversal symmetry, Phys. Rev. B **100**, 195135 (2019).

[69] J. Ahn, S. Park, D. Kim, Y. Kim, and B.-J. Yang, Stiefel–Whitney classes and topological phases in band theory, Chinese Physics B **28**, 117101 (2019).

[70] C. L. Kane and E. J. Mele, Quantum spin Hall effect in graphene, Phys. Rev. Lett. **95**, 226801 (2005).

[71] C. L. Kane and E. J. Mele, Z_2 topological order and the quantum spin Hall effect, Phys. Rev. Lett. **95**, 146802 (2005).

[72] L. Fu, C. L. Kane, and E. J. Mele, Topological insulators in three dimensions, Phys. Rev. Lett. **98**, 106803 (2007).

[73] R. Roy, Topological phases and the quantum spin Hall

effect in three dimensions, Phys. Rev. B **79**, 195322 (2009).

[74] If H has a zero energy mode at $\overline{\text{M}}$, then we shift the Hamiltonian by an infinitesimal constant to ensure that $n_{\text{o/e}}^{\overline{\text{M}}}$ is well-defined.

[75] A band structure with identical invariants for $k_z = 0, \pi$ and $\text{C}_x^{\text{full}} = \text{C}_y^{\text{full}} = 0$ is a weak topological phase that is protected by the discrete translation symmetry in the z direction. As a surface parallel to the xy plane breaks this symmetry, we do not generically get surface modes.

[76] T. Morimoto and A. Furusaki, Topological classification with additional symmetries from Clifford algebras, Phys. Rev. B **88**, 125129 (2013).

[77] J. Cano, B. Bradlyn, Z. Wang, L. Elcoro, M. G. Vergniory, C. Felser, M. I. Aroyo, and B. A. Bernevig, Building blocks of topological quantum chemistry: Elementary band representations, Phys. Rev. B **97**, 035139 (2018).

[78] A. Nelson, T. Neupert, A. Alexandradinata, and T. c. v. Bzdušek, Delicate topology protected by rotation symmetry: Crystalline Hopf insulators and beyond, Phys. Rev. B **106**, 075124 (2022).

[79] A similar phase for C_6-symmetry has previously been studied by Nelson *et al.* [7].

[80] Although there are four possible boundary deformations at X only three are independent, since the effect of simultaneous deformations at irreps $++$ and $--$ is identical to that of deformations at $+-$ and $-+$.

[81] L. Fu and C. L. Kane, Topological insulators with inversion symmetry, Phys. Rev. B **76**, 045302 (2007).

[82] C. Fang, M. J. Gilbert, and B. A. Bernevig, Bulk topological invariants in noninteracting point group symmetric insulators, Phys. Rev. B **86**, 115112 (2012).

[83] L. Trifunovic and P. Brouwer, Bott periodicity for the topological classification of gapped states of matter with reflection symmetry, Phys. Rev. B **96**, 195109 (2017).

[84] A. A. Burkov, M. D. Hook, and L. Balents, Topological nodal semimetals, Phys. Rev. B **84**, 235126 (2011).

[85] D. Klein, Graphitic polymer strips with edge states, Chemical Physics Letters **217**, 261 (1994).

[86] M. Fujita, K. Wakabayashi, K. Nakada, and K. Kusakabe, Peculiar localized state at zigzag graphite edge, Journal of the Physical Society of Japan **65**, 1920 (1996).

[87] F. Schindler, A. M. Cook, M. G. Vergniory, Z. Wang, S. S. P. Parkin, B. A. Bernevig, and T. Neupert, Higher-order topological insulators, Sci Adv **4**, eaat0346 (2018).

[88] J. Langbehn, Y. Peng, L. Trifunovic, F. von Oppen, and P. W. Brouwer, Reflection-symmetric second-order topological insulators and superconductors, Phys. Rev. Lett. **119**, 246401 (2017).

[89] Z. Song, Z. Fang, and C. Fang, $(d-2)$-dimensional edge states of rotation symmetry protected topological states, Phys. Rev. Lett. **119**, 246402 (2017).

[90] W. A. Benalcazar, B. A. Bernevig, and T. L. Hughes, Quantized electric multipole insulators, Science **357**, 61 (2017).

[91] W. A. Benalcazar, B. A. Bernevig, and T. L. Hughes, Electric multipole moments, topological multipole moment pumping, and chiral hinge states in crystalline insulators, Phys. Rev. B **96**, 245115 (2017).

[92] C. Fang and L. Fu, New classes of topological crystalline insulators having surface rotation anomaly, Science Advances **5**, 10.1126/sciadv.aat2374 (2019).

[93] L. Trifunovic and P. W. Brouwer, Higher-order topological band structures, Physica Stat. Solidi B **258** (2020).

[94] A. Lau, J. van den Brink, and C. Ortix, Topological mirror insulators in one dimension, Phys. Rev. B **94**, 165164 (2016).

[95] G. van Miert and C. Ortix, Higher-order topological insulators protected by inversion and rotoinversion symmetries, Phys. Rev. B **98**, 081110(R) (2018).

[96] F. Schindler, M. Brzezińska, W. A. Benalcazar, M. Iraola, A. Bouhon, S. S. Tsirkin, M. G. Vergniory, and T. Neupert, Fractional corner charges in spin-orbit coupled crystals, Phys. Rev. Res. **1**, 033074 (2019).

[97] S. Ono, L. Trifunovic, and H. Watanabe, Difficulties in operator-based formulation of the bulk quadrupole moment, Phys. Rev. B **100**, 245133 (2019).

[98] L. Trifunovic, Bulk-and-edge to corner correspondence, Phys. Rev. Res. **2**, 043012 (2020).

[99] H. Watanabe and S. Ono, Corner charge and bulk multipole moment in periodic systems, Phys. Rev. B **102**, 165120 (2020).

[100] S. Ren, I. Souza, and D. Vanderbilt, Quadrupole moments, edge polarizations, and corner charges in the Wannier representation, Phys. Rev. B **103**, 035147 (2021).

[101] H. Watanabe and H. C. Po, Fractional corner charge of sodium chloride, Phys. Rev. X **11**, 041064 (2021).

[102] S. Kooi, G. van Miert, and C. Ortix, The bulk-corner correspondence of time-reversal symmetric insulators, npj Quantum Mater. **6**, 1 (2021).

[103] Y. Fang and J. Cano, Filling anomaly for general two- and three-dimensional C_4 symmetric lattices, Phys. Rev. B **103**, 165109 (2021).

[104] R. Takahashi, T. Zhang, and S. Murakami, General corner charge formula in two-dimensional C_n-symmetric higher-order topological insulators, Phys. Rev. B **103**, 205123 (2021).

[105] K. Naito, R. Takahashi, H. Watanabe, and S. Murakami, Fractional hinge and corner charges in various crystal shapes with cubic symmetry, Phys. Rev. B **105**, 045126 (2022).

[106] V. Dwivedi and V. Chua, Of bulk and boundaries: Generalized transfer matrices for tight-binding models, Phys. Rev. B **93**, 134304 (2016).

[107] B. Lapierre, T. Neupert, and L. Trifunovic, Topologically localized insulators, Phys. Rev. Lett. **129**, 256401 (2022).

[108] Z. Song, S.-J. Huang, Y. Qi, C. Fang, and M. Hermele, Topological states from topological crystals, Science Advances **5**, eaax2007 (2019).